2014

Contribution To The Development Of A New Integrated Zonal Modeling Approach In Building Environment

Yao Yu
North Carolina Agricultural and Technical State University

CONTRIBUTION TO THE DEVELOPMENT OF A NEW INTEGRATED ZONAL MODELING APPROACH IN BUILDING ENVIRONMENT

Yao Yu

North Carolina A&T State University

A dissertation submitted to the graduate faculty

in partial fulfillment of the requirements for the degree of

DOCTOR OF PHILOSOPHY

Department: Computational Science and Engineering

Major: Computational Science and Engineering

Major Professor: Dr. Ahmed Cherif Megri

Greensboro, North Carolina

2014

The Graduate School
North Carolina Agricultural and Technical State University
This is to certify that the Doctoral Dissertation of

Yao Yu

has met the dissertation requirements of
North Carolina Agricultural and Technical State University

Greensboro, North Carolina
2014

Approved by:

Dr. AHMED CHERIF MEGRI
Major Professor

Dr. SAMEER HAMOUSH
Committee Member

Dr. NABIL NASSIF
Committee Member

Dr. DUKKA KC
Committee Member

Dr. MARWAN BIKDASH
Committee Member & Department Chair

Dr. ILKI KIM
Graduate Faculty Representative

Dr. SANJIV SARIN
Dean, The Graduate School

Biographical Sketch

Yao Yu was born in Shenyang, China, on October 26th, 1981. He earned his Bachelor degree in Building Environment and Equipment Engineering from Dalian University of Technology at Dalian, China, in 2004. He received his Mater degrees in Architectural Engineering in 2008 from Illinois Institute of Technology at Chicago, IL, US, and in Civil Engineering in 2012 from University of Wyoming at Laramie, WY, US. In 2013, he joined the doctoral program in Computational Science and Engineering at North Carolina A&T State University at Greensboro, NC, US.

SELECTED PUBLICATIONS

Megri, A.C., & Yu, Y. (2010). New calibrated zonal model for temperature, pressure and airflow predictions. 10th REHVA WORLD CONGRESS Sustainable Energy Use in Buildings (Clima 2010), May 9-12, Antalya, Turkey.

Yu, Y. & Megri, A.C. (2011). Development and Application of a new Dynamic Zonal model (POMA+). 12th International conference on air distribution in rooms (ROOMVENT 2011), June 19-22, Trondheim, Norway.

Megri, A.C., & Yu, Y. (2011). Prediction of Water Temperature of a Mantle Tank for Solar Domestic Hot Water Systems Using a New Zonal Model. 12th International conference on air distribution in rooms (ROOMVENT 2011), June 19-22, 2011, Trondheim, Norway.

Megri, A.C., Yu, Y., Zhang, Q., Denzer, A., & Puckett, J. (2011). Thermal comfort and energy analysis for the slab-on-grade floor and basement of a building. 12th International conference on air distribution in rooms (ROOMVENT 2011), June 19-22, 2011, Trondheim, Norway.

Megri, A.C., & Yu, Y. (2014). Energy Prediction of Electric Floor Radiation Systems Using a New Integrated Modeling Approach. ASHRAE Transactions, 120(1).

Dedication

To my wife Xiaoli Wang, son Winston Yu, and parents Wei Yu and Jiayuan Wang

Acknowledgements

First and foremost, I am heartily thankful to my supervisor, Dr. Ahmed Cherif Megri, whose encouragement, guidance and support from the initial to the final level enabled me to develop an understanding of the subject. He has been a role model of professionalism and integrity, as well as a good friend. His flexible working style inspires me to think and work independently. He also decisively guided me through the difficult moments when I was frustrated and confused.

I would like to express my gratitude to my dissertation committee: Professor Marwan Bikdash, Sameer Hamoush, Nabil Nassif, and Dukka KC, as well as the graduate school representative, Dr. ILki Kim. Thank you for your willingness to serve on my committee and your comments, patience, advice and help.

Many thanks are also expressed to my parents, Wei Yu and Jiayuan Wang, and my wife, Xiaoli Wang, for supporting and encouraging me to pursue this degree. Without their encouragements, I would not have finished the degree.

Lastly, I offer my regards and blessings to all of those who supported me in any respect during the completion of the degree.

Table of Contents

List of Figures

Chapter 1

Chapter 3

Chapter 4

Chapter 5

List of Tables

Chapter 3

Chapter 4

Chapter 5

Abstract

Various modeling approaches have been developed and applied to predict the heat and mass transfer phenomena within buildings. In consideration of the complexity of the phenomena observed, the results expected, the parameters investigated, and the degree of accuracy required, these modeling approaches can be categorized into three groups: Single-zone (and multi-zone) models, Zonal models, and Computational Fluid Dynamics (CFD) models. Zonal models, which combine the simplicity of single/multi-zone models with the comprehensiveness of CFD models, become better substitutes to predict detailed indoor thermal and airflow behaviors. Based on a geometrical partition of a room into a number of subzones, zonal models can provide more accurate and detailed results than single/multi-zone models and use less computer resources than CFD models. In this work, firstly, a comprehensive building thermal modeling approach has been developed by integrating the zonal model, Pressurized zOnal Model with the Air diffuser (POMA), with a building multi-zone thermal model, in order to improve the prediction aptitudes of the model used in building environment, in terms of accuracy and comprehensiveness. Secondly, this developed integrated thermal model has been used for various building systems and applications, such as the estimation of building load and/or energy saving, the determination of the appropriate set point and position of room thermostat, and the prediction of indoor thermal comfort levels. In these applications, two systems have been considered, the UnderFloor Air Distribution (UFAD) system and the general heating system. Distinct advantages of

this developed model over the conventional single/multi-zone thermal modeling approach have been demonstrated.

CHAPTER 1

Introduction

A building is a complex system where different heat and mass transfer phenomena take place. Energy conservation in a building cannot be fulfilled without an accurate predictive tool. Although conventional single-zone (one-zone) and multi-zone models do a good job for building load calculation and energy modeling, with the fast development of computer techniques, building designers are not satisfied with the relatively low accuracy and the limited information from the single-zone or multi-zone modeling approach. Also, these models are overwhelmed by the detailed data of Computational Fluid Dynamics (CFD) models. CFD models, as a well-developed technique, have been applied in many areas such as aerospace, industry manufacturing, and architecture. Lots of commercial CFD software packages have been developed to meet the need of these applications, such as Phoenics (2010), Star-CD (2005), COMSOL (2010), FLUENT (2001), and FLOVENT (2011). Zonal models, as another substitute for single-zone models in building load calculations and energy modeling, are not as popular and well-known as CFD models. In fact, these models not only can solve many complex problems like CFD models do, but require less computer resources. Besides, more detailed and accurate information can be obtained with zonal models than the single-zone modeling approach. Hence, more researchers are interested in using these models for several case studies in different building applications. Unfortunately, there is no available commercial software based on the zonal modeling approach, and the research on applying zonal models into building load and energy prediction is also limited. Therefore, optimization and improvement of zonal models for a wide number of application and commercialization are some of the goals of this promising model (Megri, 2007).

Typically, there are three types of models used in building environment for building load calculation, energy modeling, and indoor air quality analysis. They are single-zone (one-zone) or multi-zone models, zonal models, and CFD models. Different models have different assumptions, principals, solvers, and results. Basically, it is difficult to distinguish which model is the best among these three because of the various requirements of modeling and simulations, such as the degree of required accuracy, the speed of calculations, the definition of problems, and the results expected. However, general advantages and disadvantages of these three models are not difficult to generalize.

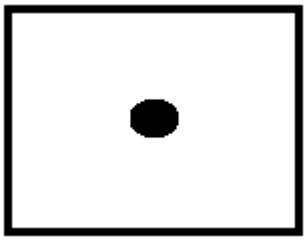

Figure 1.1 Single-zone model

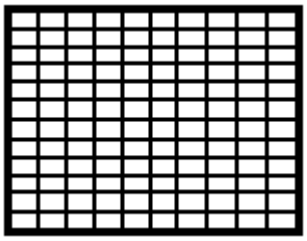

Figure 1.2 CFD model

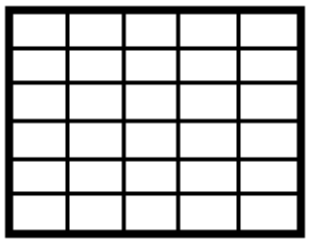

Figure 1.3 Zonal model

1.1 Single-zone or Multi-zone Modeling Approach (Figure 1.1)

This method usually regards an entire structure or system as a single zone, in which the parameters are perfectly homogenous, such as the pressure, temperature, and density. This structure or system usually is an entire house or building for single-zone models or is a room in a building for multi-zone models. Many software, systems and techniques for building load calculations and energy simulations are based on this single-zone or multi-zone modeling approach (Megri, 2007), such as Type 19 and Type 56 of TRNSYS (2000), eQUEST (2010), EnergyPlus (2011), COMIS (Feustel, 1998), CONTAMW (Dols & Walton, 2002), and ESP-r (2002). In fact, the advantages of this modeling approach are obvious, such as the fast calculations and the simple definition of problems. Therefore, up to now, this modeling approach

is still considered as an interesting research topic in the building engineering. In 1993, Diasty et al. developed a multi-zone model for air humidity behavior predictions in a multi-room building. Haghighat and Li (2004) performed a comprehensive comparison and validation of these three multi-zone models, COMIS, CONTAM, and ESP-r. An analytical computer tool was developed by Majali et al. in 2005 to simulate a transient periodic heat transfer analysis of non-air-conditioned multi-zone buildings. After the validation of this tool, a comparison of the results between a single zone model and a multi-zone model was conducted, and more accurate results were obtained when the multi-zone model was used. In 2006, Yang et al. analyzed the nonlinear dynamic behaviors of airflow and natural ventilation in multi-zone buildings. They found that the multi-zone model gave good prediction results in a steady state, while failed in unsteady state situations. Grundwald and Kikkawa, in 2011, applied a new multi-zone simulation model prototype to investigate heat, air, moisture, and pollutants transport in a library building. They demonstrated the enhanced ability of this new multi-zone model to predict and deal with mold risk issues. Generally, most of the research and publications, regarding room or building thermal behaviors and heat transfer, are about the single-zone or multi-zone modeling approach, if the other detailed models, such as zonal models or CFD models, are not specified. Although this single-zone (multi-zone) approach has its benefits, its disadvantages cannot be ignored, such as poor accuracy, limited results, and a narrow scope of applications (Megri & Haghighat, 2007). Hence, sooner or later, this simplified method will be substituted by other detailed modeling approaches such as zonal and CFD models.

1.2 CFD Modeling Approach (Figure 1.2)

Unlike single-zone or multi-zone models, this approach subdivides a structure or system into thousands of cells, and in each cell, momentum and energy equations are applied.

Therefore, adequate results and information are provided by this modeling approach. Also, the accuracy of the results is enhanced using this approach compared to single-zone or multi-zone models. Because of these reasons, this approach has been one of the most popular methods used in buildings, especially for predicting airflow and temperature distribution within buildings, and sometimes for building energy modeling. Many researchers have been dedicating themselves in this research area. In 2002, Zhai et al. proposed several efficient mathematical approaches to integrate energy simulations with CFD models in order to avoid the errors created by the separate applications of energy simulation and CFD. Later on, based on this research, Zhai and Chen (2003) found that a unique solution of this coupled energy simulation and CFD simulation exists, using theoretical analysis and numerical experimentation. Then, they published the advantages of the integration of building energy simulation and CFD programs over the separated energy simulation and CFD applications. Among the advantages, this integrated model produced more accurate results. The results of this integrated building simulation were compared with experimental data, and good agreements were achieved (Zhai & Chen, 2005). The results of the sensitivity analysis and the application guides of this integrated building energy and CFD simulation program were displayed, as well, by the same authors in 2006 (Zhai & Chen, 2006). In their works, they investigated if a coupled program is needed and which coupling approach needs to be used, according to the building and environmental characteristics and the solution accuracy requirement (Zhai & Chen, 2006). Hiyama et al. (2005) coupled computational fluid dynamics (CFD) program with flow network model, to give a more accurate prediction considering the building characteristics. Natural ventilation was used at the design stage and the performance of this natural ventilation was investigated using the integrated CFD and flow network model analysis. In the same year, Tan and Glicksman (2005) integrated a multi-zone

model with CFD simulation to enhance the prediction capability for natural ventilation cases in buildings. A new modeling approach to optimize building energy efficiency in a tropical climate was developed by Bastide et al. (2006). They proposed a term named the well-ventilated percentage of a living space, which allows a time analysis of the air motion behavior of the building in its environment with the assistance of the CFD model. This approach is useful for designers to design the rooms according to their use and environment. One year later, Zhang et al. (2007) applied the computational fluid dynamics model, FLUENT, for building energy calculations in order to improve the prediction quality and accuracy of the building energy consumption. Results of energy consumption were compared with the measured data, and good agreements were achieved. Axley and Chung (2007) integrated a multi-zone model with a CFD model. The mathematical problems regarding this integration were proposed and analyzed. In 2010, Pan et al. coupled CFD into the energy simulation method, EnergyPlus, to predict atrium building cooling load. The results of this coupled model were compared with those from the simplified method. Suggestions about the usage of appropriate simulation methods based on different types of atrium buildings were proposed. More recently, Hiyama and Kato, in 2011, developed a calculation method, in which the three-dimensional CFD results were integrated into building energy simulation program to achieve more accurate time-series analysis of building energy than conventional energy simulation programs, which are based on the assumption of well-mixed room space. In their works, they introduced a term called advection-diffusion response factor, which was calculated using a CFD approach and then integrated into the energy simulation program. However, despite the richness of the results in terms of detailed information regarding the flow and temperature fields within a building structure, the huge calculation work makes CFD techniques unlike to be used in the applications of system designs under industrial

requirements of accuracy, in which rapid computational time is a more significant issue than perfectly accurate results. Furthermore, CFD models suffer due to a need for significant problem definition by the user. Thus, in building environment, CFD models are difficult to apply to situations involving a number of rooms over long periods of time (Clarke et al., 1995).

1.3 Zonal Modeling Approach (Figure 1.3)

This method is considered as an intermediate approach between single-zone (multi-zone) and CFD models because it requires fewer zone divisions than CFD models and provides enough detailed results compared to single-zone or multi-zone models. It combines the simplicity of single zone (multi-zone) models with the comprehensiveness of CFD models, and becomes a better substitute to predict detailed thermal and flow behaviors in buildings. Besides, in each zone, simplified mass and energy balance equations are utilized, which significantly reduces the computational time. This approach allows defining the physical parameters accurately within each zone in order to provide a tool that could be applied to a detailed investigation of thermal comfort, indoor air quality, and energy analysis in building systems. The zonal modeling approach is a promising way to predict air movement in a room with respect to comfort conditions and the gradient of temperature because these models require extremely little computer time and could easily be integrated with multi-zone thermal models (Jiru & Haghighat, 2004; Megri et al., 2005; Megri & Haghighat, 2007).

In this dissertation, one of the popular zonal models, Pressurized zOnal Model with the Air diffuser (POMA) (Lin et al., 1999; Haghighat et al., 2001; Megri & Yu, 2010; Yu & Megri, 2011; Yu, 2012; Megri et al., 2011) has been introduced and utilized to develop a comprehensive numerical building thermal model by integrating POMA with a multi-zone thermal model. The application of this integrated thermal model have been also accomplished in building

environment considering distinct systems, such as the general heating system and UnderFloor Air Distribution (UFAD) system, in terms of building load/energy, thermostat set point, as well as indoor thermal comfort. The objective of this research is not only to quantify the advantages of the zonal modeling approach over single-zone or multi-zone models, but also to provide a simple but accurate simulation tool for building applications.

In particular, the objectives of this dissertation are as follows,

- Investigate the feasibility of the development of a comprehensive building thermal model by integrating a zonal model into a multi-zone thermal model;
- Evaluate and verify the developed integrated thermal model using CFD approach in terms of indoor air thermal behavior;
- Demonstrate the applications of this integrated thermal model for different air conditioning systems;
- Provide direct comparisons between the zonal and single-zone (multi-zone) predictions in terms of building energy/load, indoor thermal comfort, and so on;
- Demonstrate the improvement of the predictability of building load and energy simulations, when a zonal model is applied.

CHAPTER 2

Literature Review of Zonal Model Development

Zonal model approach has existed for more than four decades, since the first zonal model scheme was developed during the 1970s (Lebrun, 1970) from experimental observations realized in a test cell. The development of zonal model was very slow and only in 1980, Laret (1980) proposed a new scheme, slightly different from the configuration developed by Lebrun. This model followed the same general flow with assumptions that allowed the analytical determination of the air temperature within the volume. Later, Ngendakumana (1988) applied a five-zone scheme to determine the temperature distribution within the same volume. In his scheme, he suggested seven airflow paths between the five zones (total of 12 unknowns). Inard and Buty (1991) authenticated Lebrun's model using an extensive experimental study measuring the distribution of temperature within a controlled environment, a Minibat cell (Megri & Haghighat, 2007).

Later on, Bouia (1993) initiated the development of a new generation of zonal models. He solved the pressure fields to predict the airflow and thermal behaviors in large indoor spaces. Togari et al. in 1993 developed a temperature-based zonal model without the pressure drop and power law, i.e., the BLOCK model. This model uses correlations on the basis of vertical temperature gradient in combination with special laws for jets and plumes. The temperature-based zonal model has less unknowns than the pressure based one, and simpler in calculaltions. In 1995, Wurtz developed a new zonal model where mass and energy balances were applied in each subzone, while the mass flow rates at the interfaces were calculated using the power-pressure law. Musy (1999) showed that it was possible to establish zonal models automatically that have the ability to predict the air movement, temperature distribution, and indoor air quality

parameters not only in a specific zone, but in the entire building. Haghighat et al. (2001) put forth a zonal model named Pressurized zOnal Model with the Air diffuser (POMA) in the framework of Annex 35 of the International Energy Agency (IEA). They provided a comprehensive background and validation of this model, which is based on both mass and energy conservations and, as a simplified numerical model, uses pressure-driven power laws to estimate the mass flow rate between two subzones or cells instead of momentum equations in CFD models. POMA is able to predict the airflow patterns and thermal distributions within a space. Jet characteristic equations were also introduced in the model in order to generalize its application to mechanically ventilated rooms or buildings. Axley (2001) developed an alternative formulation to model airflow resistance in zonal models, known as surface-drag flow relations for zonal modeling. He pointed out that "the power-law relation is physically inconsistent and grossly overestimates viscous losses in room airflow". An alternative approach based on a surface-drag viscous loss mechanism more accurately reflected the physical mechanisms of the airflow in natural convection situations. A modified version of COMIS (Conjunction Of Multizone Infiltration Specialists) (Allard et al., 1990; Megri, 1993) was proposed in order to simulate airflow, temperature (Ren & Stewart, 2003), and concentration (Stewart & Ren, 2003) distributions inside buildings. The authors applied zonal model processes to the COMIS computer program to produce COMIS with subzones (CWSZ) (Stewart & Ren, 2006). In 2010, Gao et al. improved the performance of the temperature-based zonal model (BLOCK model) that was proposed by Togari et al., by the determination of a heat transfer factor between air layers. Norrefeldt et al. (2012) developed a new zonal model, named VEPZO, to estimate the airflow pattern and temperature distributin in a confined space. In this model, a derived equation

considering the forces acting on a flow path was used to simulate the airflow between two zones instead of using the power law model.

Many efforts have also been made in order to imporve the prediction of zonal models using CFD or other models. Mora (2003) and Mora et al. (2003a, 2003b) developed an approach, in which the zonal model uses the airflow structure from CFD simulation results in the same volume. Bellivier (2004) defined the conditions, under which a CFD model can be simplified with enlarging meshes to reach the zonal model's level. Griffith and Chen (2003) simplified the Navier-stocks equations with the assumption of inviscid flow (Euler equations), reduced the grid cell number, and then proposed a monentum-zonal model to predict zone airflow and temprature distributons.

Over the years, zonal models were coupled with many systems to simulate the vairous thermal behaviors of a room or building, such as hydronic radiator system (or baseboard heating system) (Howarth, 1985; Lebrun & Ngendakumana, 1987; Inard & Molle, 1989; Inard & Buty, 1991; Musy et al., 2001; During, 1994); electric convector system (During, 1994; Inard et al., 1997a & 1997b; Musy et al., 2001); radiant panel system (During, 1994); heating ceiling system (During, 1994); floor heating system (Inard & Buty, 1991; During, 1994); heat pump system (Gschwind et al., 1995); and displacement ventilation system (Mundt, 1996; Rees, 1998; Rees & Haves, 1999).

Up to now, zonal models have been still applied in various research areas. In 2003, Riederer and Dexter demonstrated the effects of room model and the position of the sensor on the performance of Variable Air Volume (VAV) control systems. In their works, a zonal model was applied, and they concluded that "the room model and the position of the sensor affect the performance in different ways depending on the diffuser type and the operating mode. And there

are only small differences in terms of thermal comfort but significant different in terms of overall energy consumption". Huang and Haghighat (2005) investigated contaminant distributions with the assist of zonal model. Bozonnet et al. (2005) solved some indoor and outdoor design problems using a zonal modeling approach. In 2006b, Wurtz et al. integrated a zonal model with a building material moisture transfer model to predict the transent-state indoor humidity distribution within a building. Blandin et al. (2007) displayed the application of a pressure zonal model approach in a stratified solar tank simulation. They investigated the potential and feasibility of the pressure zonal model utilized for water instead of air and mentioned that the flow coefficient in power law model is 10^{-4} ($m\ s^{-1}\ Pa^{-n}$) for water. Later, Jiru and Haghighat (2008) applied a zonal modeling approach for estimating the airflow and temperature in ventilated double skin facades (DSF) in a transient state. A 3-D zonal model was utilized by Daoud et al. (2008) to calculate the transient-state refrigeration loads in ice rinks. In 2009, Boukhris et al. used a zonal model (Zonal AERial model) to assess the winter thermal comfort in a partitioned building. Moore and Ouzts (2012) established a model to simulate thermally stratified atria by using zonal modeling approach. MacCarty (2013) applied the concept of zonal model in the household biomass cookstoves design. Other recent applications of zonal models include Gastelurrutia et al., 2011; Megri & Yu, 2011; Yu & Megri, 2011; Yu, 2012; Song et al., 2013; Steskens et al., 2013; Beiza et al., 2014; Megri & Yu, 2014.

Therefore, this dissertation not only demonstrates the continuous development of zonal models, but also provides some useful references for the sake of approaching the final goals, which are the wide application and commercialization of zonal models.

CHAPTER 3

Description of the Zonal Model POMA and its Validation

Pressurized zOnal Model with the Air diffuser (POMA) is based on the fundamental conservation equations (both mass and energy balances) and the power law model to predict temperature and airflow distributions within a room. In this work, POMA program was rewritten in Matlab (2011) and then integrated with a multi-zone thermal model. The necessary mathematical description of this integrated model will be shown in Chapter 4.

3.1 Power Law Model

Zonal models divide a room into several zones, and each zone has a homogenous temperature. The Power Law Model (PLM) (Equation 3.1) plays a key role in the zonal model POMA. PLM defines the mass flow rate from one zone to another as,

$\dot{m} = \rho k A(\Delta P)^n$ [kg/s or lbm/s]. (3.1)

In fact, this power law model could also be written as,

$u = k(\Delta P)^n$ [m/s or ft/s] because $\dot{m} = \rho A u$ [kg/s or lbm/s], (3.2)

where ρ (kg/m^3 or lbm/ft^3) is the fluid density; A (m^2 or ft^2) is the cross-sectional area between two zones; ΔP (Pa or lbf/ft^2) is the pressure difference between two zones; k ($m\,s^{-1}\,Pa^{-n}$ or $ft\,s^{-1}\,(lbf/ft^2)^{-n}$) is the flow coefficient, which is assumed to be 0.83 $m\,s^{-1}\,Pa^{-n}$ or 18.85 $ft\,s^{-1}\,(lbf/ft^2)^{-n}$ for all zones; n is called flow exponent, which is 0.5; and u (m/s or ft/s) is cross-sectional velocity between two zones.

From the equation 3.2, the power law model is a simplified version of the momentum equation, since it uses a constant flow coefficient k to correlate the velocity with the pressure term together; while, in the momentum equation, the correlation between velocity and pressure

becomes a complex differential equation. It is the main reason that makes the zonal models, in particular POMA, faster than CFD models in terms of computational time.

In POMA, pressures in each zone are assumed to be horizontally homogenous and vertically affected only by the gravity, and the pressure losses due to frictions are only considered on the cross-sectional boundary between two zones. Thus, to determine the ΔP that is in the equation 3.1, the pressure differentials between two zones have to be computed differently. The horizontal pressure difference ΔP (Figure 3.1) in the power law model can be defined as,

$$\Delta P = P_1 - P_2 = \left(P_{ref1} - \rho_1 g z\right) - \left(P_{ref2} - \rho_2 g z\right)$$

$$= \Delta P_{ref} - \Delta\rho g z = \Delta\rho g (z_n - z) \qquad \text{[Pa or lbf/ft}^2\text{]}, \qquad (3.3)$$

where P_{ref1} (Pa or lbf/ft^2) is the reference pressure at the bottom of zone 1; P_{ref2} (Pa or lbf/ft^2) is the reference pressure at the bottom of zone 2; P_1 (Pa or lbf/ft^2) is the pressure in zone 1 at a certain height level z; P_2 (Pa or lbf/ft^2) is the pressure in zone 2 at a certain height level z; z (m or ft) is the height level from the bottom of the zone; ρ_1 (kg/m^3 or lbm/ft^3) is the density of the fluid in zone 1; ρ_2 (kg/m^3 or lbm/ft^3) is the density of the fluid in zone 2; ΔP (Pa or lbf/ft^2) is the pressure difference at the same height level; ΔP_{ref} (Pa or lbf/ft^2) is the reference pressure difference, which equals to $P_{ref1} - P_{ref2}$; $\Delta\rho$ (kg/m^3 or lbm/ft^3) is the fluid density difference between the zone 1 and zone 2, which equals to $\rho_1 - \rho_2$; g (m/s² or ft/s^2) is the gravitational acceleration; and z_n (m or ft) is the height of neutral plane at which height, the pressure difference between two zones is equal to zero, which is defined as,

$$z_n = \frac{\Delta P_{ref}}{\Delta\rho g} \quad \text{[m or ft]}; \qquad (3.4)$$

H (m or ft) is the height of the zone (Figure 3.1).

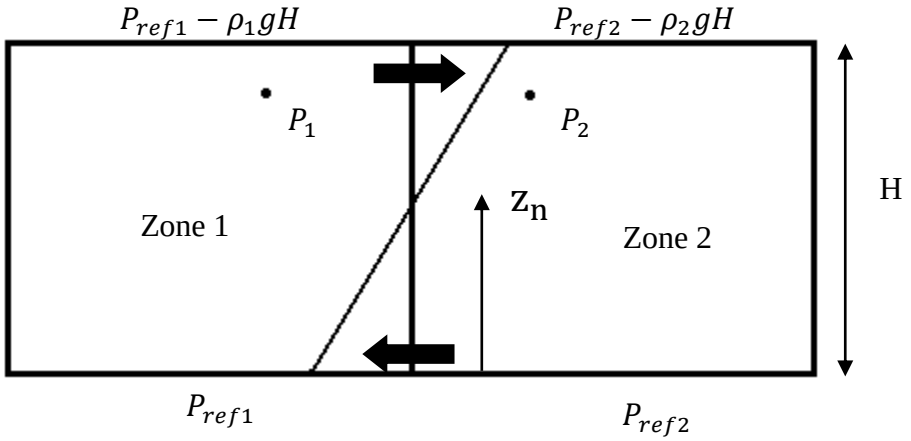

Figure 3.1 Two horizontal zones

The vertical pressure difference ΔP (Figure 3.2) used in the power law model can be defined as,

$$\Delta P = P_{ref2} - P_{ref1} - \rho_2 gH \quad \text{[Pa or lbf/ft}^2\text{]}, \tag{3.5}$$

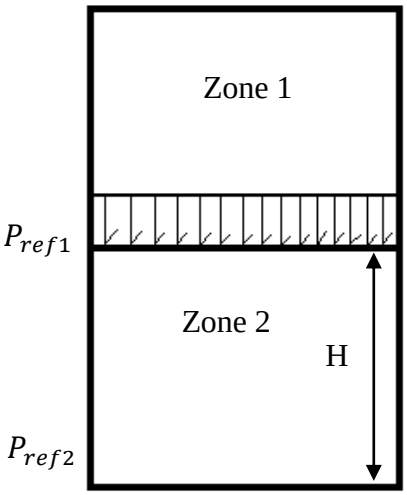

Figure 3.2 Two vertical zones

where P_{ref1} (Pa or lbf/ft^2) is the reference pressure at the bottom of zone 1; P_{ref2} (Pa or lbf/ft^2) is the reference pressure at the bottom of zone 2; ΔP (Pa or lbf/ft^2) is the pressure difference at the cross-section boundary between two zones; ρ_2 (kg/m^3 or lbm/ft^3) is the density of the fluid in zone 2; H (m or ft) is the height of the zone; and g (m/s² or ft/s^2) is the gravitational acceleration.

Then the horizontal mass flow rate $\dot{m}$ (kg/s) is defined as follows,

$$\dot{m} = \dot{m}_{0-z_n} + \dot{m}_{z_{n-H}} = \int_0^{z_n} kA\rho|\Delta P|^n dz + \int_{z_n}^{H} kA\rho|\Delta P|^n dz\,, \quad \text{[kg/s or lbm/s]} \tag{3.6}$$

where k, A and ΔP are the same as those of the equations 3.1 and 3.3; $\dot{m}_{0-z_n}$ (kg/s or lbm/s) is the mass flow rate from the height zero to z_n; $\dot{m}_{z_{n-H}}$ (kg/s or lbm/s) is the mass flow rate from

the height z_n to H; and ρ (kg/m^3 or lbm/ft^3) is the fluid density of the zone from which the flow comes and can be calculated using ideal gas law.

The vertical mass flow rate $\dot{m}$ (kg/s or lbm/s) is calculated from the equation 3.1 directly.

3.2 Mass and Energy Conservations

Conservations of mass and energy are the main equations used by POMA, which are defined below.

Mass balance equation

$$\frac{dM_{ij}}{dt} = \sum \dot{m}_{ij} + \dot{m}_{source} + \dot{m}_{sink} \text{ [kg/s or lbm/s]}, \quad (3.7)$$

where M_{ij} (kg or lbm) is the fluid mass of zone ij; $\dot{m}_{ij}$ (kg/s or lbm/s) is the rate of mass from surrounding zone to zone ij, and is calculated using the power law model; $\dot{m}_{source}$ (kg/s or lbm/s) is the rate of mass supplied as a source in the zone, i.e. the airflow from a diffuser; and $\dot{m}_{sink}$ (kg/s or lbm/s) is the rate of a mass removed from the zone.

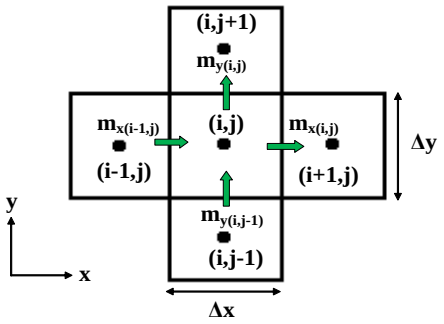

Figure 3.3 Zones for mass flow balance

Energy balance equation

$$\frac{dQ_{ij}}{dt} = \sum \dot{q}_{ij} + \dot{q}_{source} + \dot{q}_{sink} \quad \text{[W or Btu/hr]}, \quad (3.8)$$

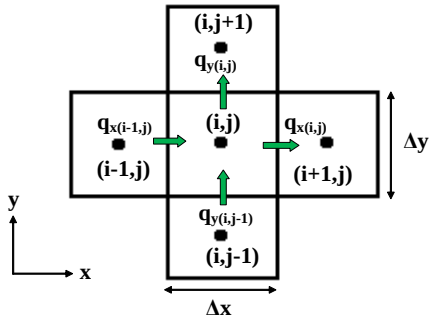

Figure 3.4 Zones for energy balance

where Q_{ij} (J or Btu) is the heat energy in zone ij; $\dot{q}_{ij}$ (W or Btu/hr) is the rate of heat energy from surrounding zones to zone ij, which is defined as $\dot{q}_{ij} = \dot{m}_{ij} cp \Delta T_{ij}$, cp (J/(kg ^{o}C) or Btu/(lbm ^{o}F)) is the specific heat; ΔT_{ij} (^{o}C or ^{o}F) is the temperature difference between two zones; $\dot{m}_{ij}$ (kg/s or lbm/s) is the rate of mass from surrounding zone to

zone *ij*; $\dot{q}_{source}$ (W or Btu/hr) is the rate of heat energy supplied by a source in the zone; and $\dot{q}_{sink}$ (W or Btu/hr) is the rate of heat energy removed from the zone.

3.3 Boundary Conditions

The boundary conditions can be represented by the convective heat transfer (Figure 3.5) that occurs between the wall surfaces and nearby fluid flow, which is defined as,

$$\dot{q}_{i,wall} = h_i \cdot A_i \cdot (T_{i,surface} - T_{ij})[\text{W or Btu/hr}], \qquad (3.9)$$

where h_i (W/m^2 °C or Btu/hr ft^2 °F) is the convective heat transfer coefficient of surface *i*; A_i (m^2 or ft^2) is the cross-sectional area between the zone and the boundary surface *i*; $T_{i,surface}$ (^{o}C or ^{o}F) is the boundary temperature of the surface *i*; T_{ij} (^{o}C or ^{o}F) is the nearby zone *(i,j)* flow temperature; and $\dot{q}_{i,wall}$ (W or Btu/hr) is the rate of heat energy between the nearby zone *(i,j)* and the boundary surface *i*.

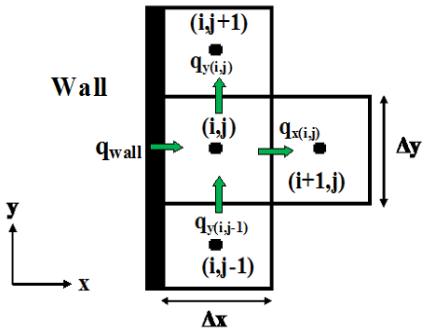

Figure 3.5 Boundary convective heat transfer

3.4 Nonlinear Equation Solver

In POMA, a room is mathematically subdivided into *n* zones. The total number of unknowns (represented using *X*) is *2n*, i.e. the temperatures and pressures of these *n* zones. There is the same number of independent equations as the unknowns based on mass and energy balance equations of all the zones. The Newton global convergence method (Press et al., 2007) was used to solve this set of nonlinear conservation equations (Equations 3.7 and 3.8). This method needs reasonable initial trial guesses (temperatures and pressures of all the zones) and then calculates the final results simultaneously using an iteration approach. In this method, these unknowns will be initialized at the beginning and then substituted into these corresponding balance equations to compute residuals. After that, a matrix *A* representing the Jacobian matrix will be formed based on these unknowns and corresponding residuals. The linear matrix system *Ax = b* then can be

solved by using the *LU* decomposition method (Watkins, 2010), and the results, *x*, represent the correction values for these unknowns. Consequently, a new set of unknowns, *X* + *x*, will be used for the next iteration. The brief description of this approach is shown below, and detailed descriptions can be found from Press et al., 2007.

If the conservation equations are represented using *F(X)* with the unknowns *X*, then

$$F(X) = 0; \tag{3.10}$$

$$X_{new} = X + x; \tag{3.11}$$

$$x = -J^{-1} \cdot F; \tag{3.12}$$

where *x* is the correction values of the unknowns for each iteration step ; X_{new} is the updated solutions for the next iteration step; and *J* represents the Jacobian matrix. The program converges when the Max residual ϵ of all the zones is less than a very small value, as defined by the user (let say 1.0×10^{-3}) i.e. $\epsilon = \text{Max}(\text{residuals}) < 1.0 \times 10^{-3}$. Figure 3.6 describes the computational process of the zonal model POMA.

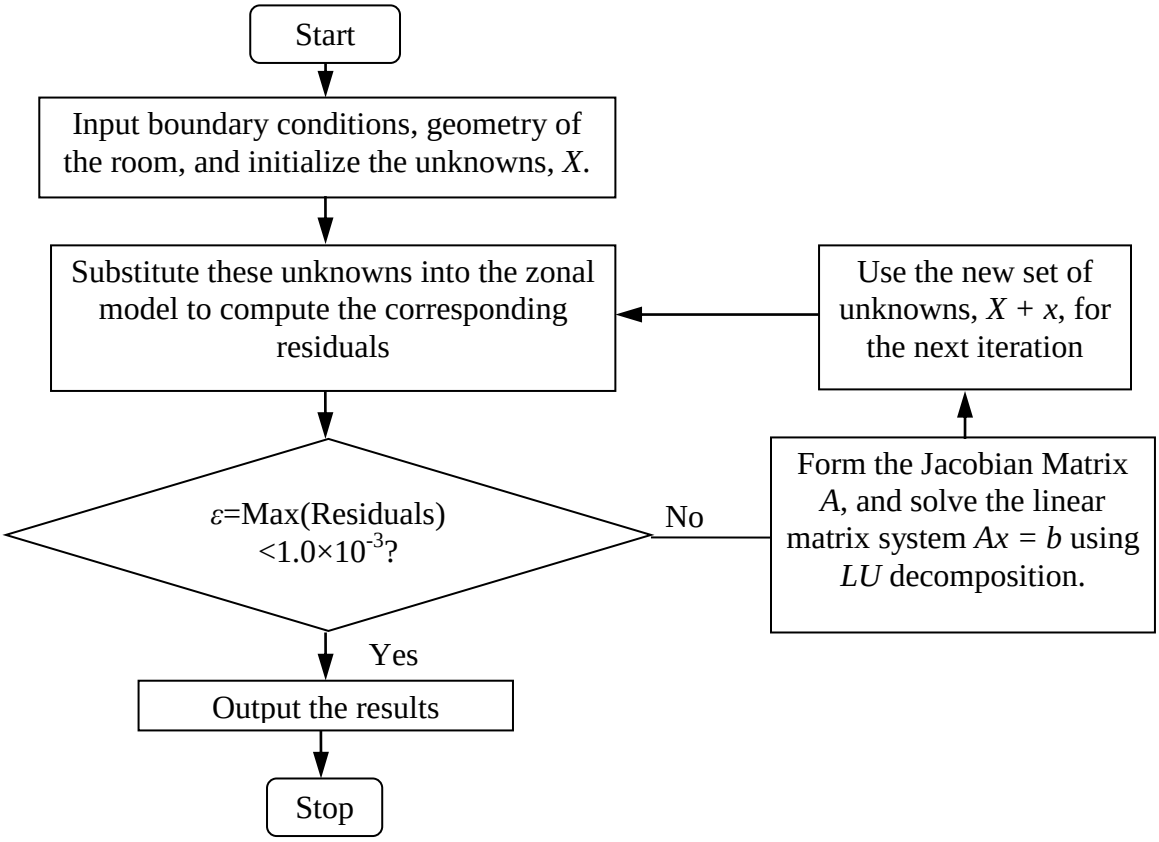

Figure 3.6 Flow chart of the zonal model POMA

3.5 Zonal Model Validation of Steady-State Natural Convection Cases (Haghighat et al., 2001)

The zonal model POMA had been validated by Haghighat et al. in 2001. Steady-state results of two natural convection cases of the zonal model POMA (6 × 1 × 10 zones) were compared with the experimental data that were collected in the MINIBAT test cell (Inard & Buty, 1991). The MINIBAT test cell (Figure 3.7), located in CETHIL (Centre de Thermique de l'INSA de Lyon) with the dimensions of L (3.1m or 10.2ft) × W (3.1m or 10.2ft) × H (2.5m or 8.2ft), was specially designed to measure temperature distributions in a controlled environment. Measured inside surface temperatures of this test cell (the necessary boundary conditions for POMA) for those two natural convection cases are listed in the table 3.1.

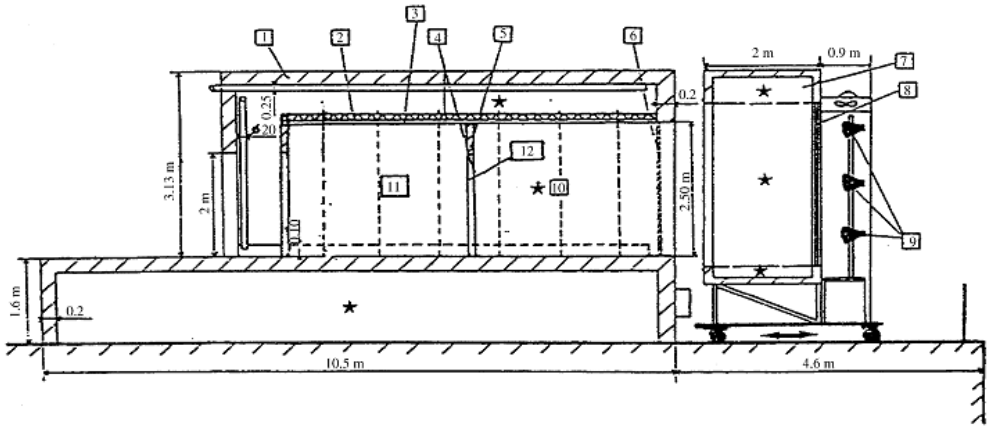

Nomenclature :

1 : external envelope (cellular concrete e = 20 cm)
2 : fibreglass (e = 5 cm)
3 : plywood (e = 2.5 cm)
4 : gypsum board (e = 1 cm)
5 : fibreboard (e = 5 cm)
6 : glazing (e = 1 cm)
7 : mobile climatic housing
8 : double glazing (10-8-10 mm)
9 : solar simulator (12 lamps CSI 1000 W)
10 : test cell 1
11 : test cell 2
12 : doorway

Figure 3.7 MINIBAT test cell (Haghighat et al., 2001)

Table 3.1 *Measured surface temperatures [$^oC(^oF)$] of two natural convection cases*

	South	North	East	West	Ceiling	Floor
Case 1	6.0 (42.8)	13.9 (57.0)	14.1 (57.4)	14.1 (57.4)	13.5 (56.3)	11.8 (53.2)
Case 2	11.2 (52.2)	23.8 (74.8)	23.5 (74.3)	23.7 (74.7)	42.1(107.8)	21.1 (70.0)

In these two cases, temperature stratifications were created by using a relatively low temperature on the south surface for the case 1 and high temperature on the ceiling surface for the case 2 in order to investigate the prediction ability of POMA in both cooling and heating applications.

Since the temperature boundary conditions of the east and west surfaces are close (Table 3.1), just one zone was applied in the east-west direction in POMA validations. 10 zones in the floor-ceiling direction were utilized because of the relatively large temperature difference and the effects of buoyancy and gravity.

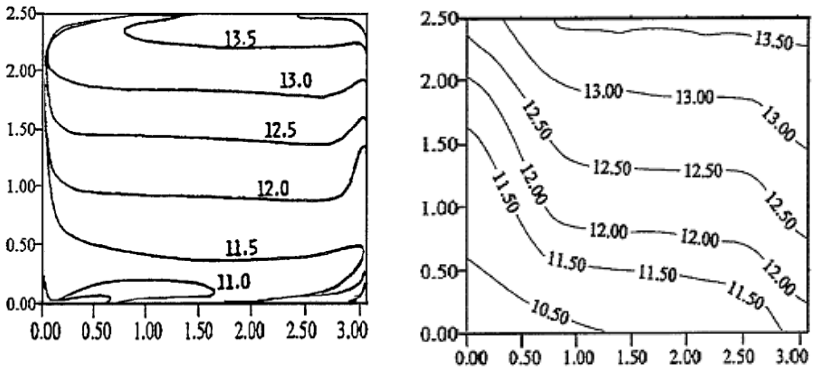

Figure 3.8 Temperature distributions of Case 1
(Haghighat et al., 2001)

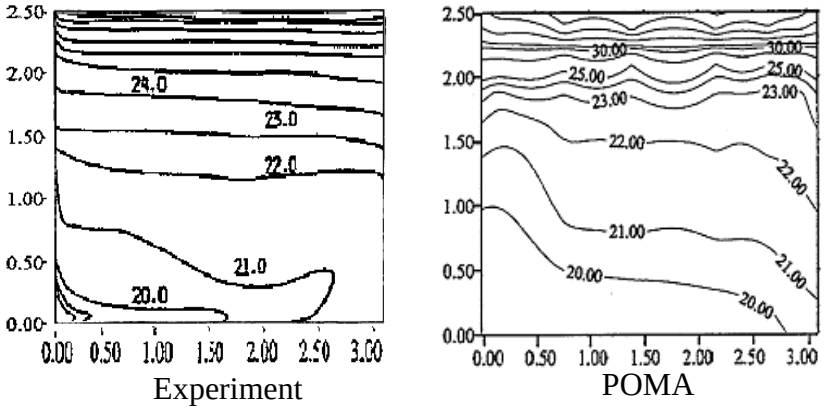

Figure 3.9 Temperature distributions of Case 2
(Haghighat et al., 2001)

Figure 3.8 and 3.9 show the comparisons of temperature distributions between the experimental data and the POMA result, respectively, for both the cases 1 and 2. From above comparisons (Case 1 and 2), good agreements are observed between the results of POMA and the experimentation due to the quite similar patterns of these two temperature distributions, which demonstrates the ability and potential of POMA to predict thermal behaviors of a room.

CHAPTER 4

Development of an Integrated Zonal / Multi-zone Thermal Model in a Building Environment

Heating, Ventilating, and Air Conditioning (HVAC) systems are different in terms of cost, comfort, and performance, depending on the weather conditions, the envelope performance, and the fuel used. Each system is unique given that it interacts differently in each single room or building and depends on many factors, such as the system itself, the locations of diffusers and thermostats, the indoor design conditions, the outdoor weather conditions, and the control schemes associated with the HVAC system. Similarly, a building energy prediction approach is unique and associated with HVAC systems used, building envelop characteristics, and weather conditions. Although a single-zone (multi-zone) model has its own advantages, like simple and fast computations for design purposes, the accuracy of this model is questionable. The assumption of a uniform temperature in a room or building, obviously, reduces the accuracy of the final results; moreover, a single-zone (multi-zone) model, as a general thermal calculation method, could not differentiate various building thermal behaviors according to different HVAC systems, locations of diffusers and thermostats, inside design temperatures, and control schemes. Therefore, in this chapter, a comprehensive integrated thermal model has been developed by the integration of the zonal model POMA into a building multi-zone thermal model. This integrated thermal model is not only able to accurately predict detailed indoor thermal behaviors like the zonal model does, but also to provide a new simulation tool in the estimations and analysis of building load and energy consumption. In this chapter, the mathematical description of the multi-zone thermal model has been demonstrated. In addition, the integration approach of this thermal model with the zonal model POMA has been introduced.

4.1 Description of the Multi-zone Thermal Model

To describe the multi-zone thermal model, a one-room residential house is considered (Figure 4.1). In these descriptions, three important energy balance equations are demonstrated. These balance equations include the room air heat balance equation, the room interior surface heat balance equation, and the room exterior surface heat balance equation.

4.1.1 Heat energy balance of the room air (ASHRAE Fundamentals, 2005). In this room (Figure 4.1), the air temperature is affected by several factors, such as the heat transfer from the room surfaces ($\dot{q}_{surf.}$), the ventilation heat energy ($\dot{q}_{vent.}$), the infiltration ($\dot{q}_{inf.}$), and the internal heat source/sink ($\dot{q}_{inter.}$). Therefore, the heat balance equation of the room air is defined as,

$$C\frac{dT_{air}}{dt} = \dot{q}_{surf.} + \dot{q}_{inf.} + \dot{q}_{vent.} + \dot{q}_{inter.} \text{ [W or Btu/hr].} \quad (4.1)$$

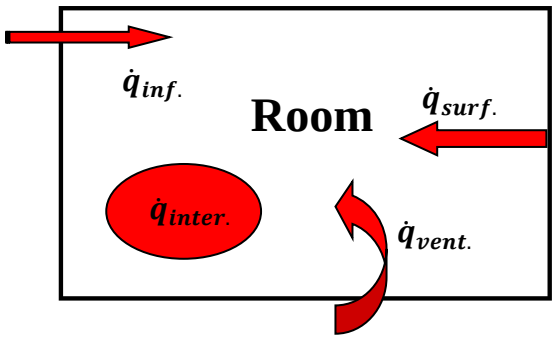

Figure 4.1 Room air heat balance

In the equation 4.1, $C\frac{dT_{air}}{dt}$ is the room air thermal storage effect, which is equal to zero for a steady-state situation, where T_{air} (^{o}C or ^{o}F) is the room air temperature; C (J/^{o}C or Btu/°F) is the room air thermal capacitance; and t (second) is time. $\dot{q}_{surf.}$ (W or Btu/hr) is the convective and radiative heat transfer energy between the room surfaces and the room air, which can be solved using $\dot{q}_{surf.} = \frac{1}{R_{star}}(T_{star} - T_{air})$, called the star network approach (Seem, 1987). In this

star network approach, an artificial temperature T_{star} (^{o}C or ^{o}F) and the corresponding star resistance R_{star} ((m^2 °C)/W or (hr ft^2 °F)/Btu) are used, which combine the convection heat between the surfaces and the room air with the long wave radiation heat between the one surface and all of the other surfaces together and can be determined based on the room interior surface temperatures, $T_{surface}$ (^{o}C or ^{o}F). Detailed descriptions of this approach can be found in Seem, 1987. $\dot{q}_{inf.}$ (W or Btu/hr) is the convective heat transfer energy accounted for by infiltration, which is defined as, $\dot{q}_{inf.} = \dot{m}_{inf.} \cdot c_p \cdot (T_{outdoor} - T_{air})$, where $\dot{m}_{inf.}$ (kg/s or lbm/s) is the mass flow rate of infiltration; c_p (J/(kg ^{o}C) or Btu/(lbm °F)) is the specific heat of air; $T_{outdoor}$ (^{o}C or ^{o}F) is the outdoor temperature or the temperature of the infiltration; and T_{air} (^{o}C or ^{o}F) is the room air temperature. $\dot{q}_{vent.}$ (W or Btu/hr) is the convective heat transfer energy accounted for by ventilation, which is defined as, $\dot{q}_{vent.} = \dot{m}_{vent.} \cdot c_p \cdot (T_{supply} - T_{air})$, where $\dot{m}_{vent.}$ (kg/s or lbm/s) is the mass flow rate of ventilation; c_p (J/(kg ^{o}C) or Btu/(lbm °F)) is the specific heat of air; T_{supply} (^{o}C or ^{o}F) is the supply air temperature of ventilation; and T_{air} (^{o}C or ^{o}F) is the room air temperature. $\dot{q}_{inter.}$ (W or Btu/hr) is the convective heat transfer energy accounted for by internal gains, such as people, equipment, etc.

In the equation 4.1, in order to compute the room air temperature T_{air}, the only unknowns are the room surface temperatures $T_{surface}$, which can be solved using the room interior surface heat balance equation.

4.1.2 Heat energy balance of the room interior surface (ASHRAE Fundamentals, 2005). The room interior surface temperatures are determined by four heat transfer approaches. They are short wave radiation (solar radiation), long wave radiation, convection between surfaces and room air, and conduction (Figure 4.2).

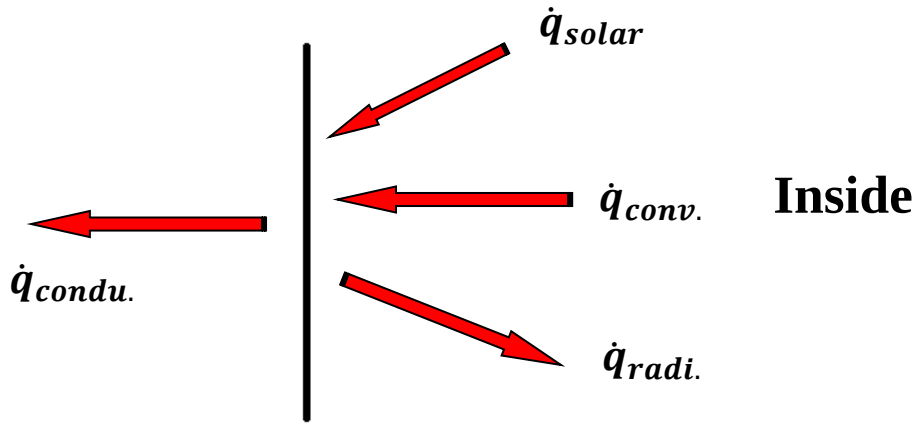

Figure 4.2 Room interior surface heat balance

Therefore, the heat energy balance of the room interior surface is represented by,

$$\dot{q}_{condu.} = \dot{q}_{conv.} + \dot{q}_{solar} - \dot{q}_{radi.} \text{ [W or Btu/hr],} \quad (4.2)$$

where, $\dot{q}_{condu.}$ (W or Btu/hr) is the conduction heat flux in the house construction; $\dot{q}_{radi.}$ (W or Btu/hr) is the net long-wave radiation of this surface; $\dot{q}_{solar}$ (W or Btu/hr) is the solar radiation incident on this surface; and $\dot{q}_{conv.}$ (W or Btu/hr) is the convective heat transfer energy between this room surface and the room air.

In the equation 4.2, $\dot{q}_{radi.}$ stands for the net long wave radiation, which is the result of radiation heat exchange between this surface and the other surfaces. As mentioned, in order to estimate $\dot{q}_{radi.}$, the star network approach is applied (Seem, 1987), in which the room convection heat $\dot{q}_{conv.}$ and the room long wave radiation heat $\dot{q}_{radi.}$ are coupled and solved together. $\dot{q}_{solar}$ is the solar radiation incident on this surface through glazing materials. The detailed descriptions about how to determine $\dot{q}_{solar}$ can be found in ASHRAE Fundamentals, 2005.

The room surface temperature, $T_{surface}$, can be calculated in the equation 4.2 as long as $\dot{q}_{condu.}$ is known.

To estimate the conduction heat flux $\dot{q}_{condu.}$, a transient heat transfer model has to be established because of the thermal mass storage effects of constructions. In this work, the Transfer Function Method (TFM) is utilized to determine the transient thermal conduction heat transfer through the house constructions (ASHRAE Fundamentals, 2005). This model is able to describe the transient thermal behaviors of walls, roofs, and floor constructions. In this model, TFM coefficients have to be determined before the estimations of the conduction heat. These coefficients vary depending on different construction materials and can be determined using some commercial software, such as TRNSYS (2000).

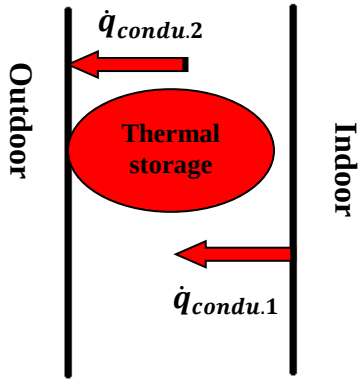

Figure 4.3 Heat balance in constructions

In the figure 4.3, $\dot{q}_{condu.1}$ represents the conduction heat flux at the interior surface, and $\dot{q}_{condu.2}$ represents the conduction heat flux at the exterior surface. In fact, $\dot{q}_{condu.1}$ and $\dot{q}_{condu.2}$ are different because of the thermal storage effects of construction materials.

4.1.3 Heat energy balance of the room exterior surface (ASHRAE Fundamentals, 2005). At the exterior surfaces of the house, solar radiation, convection, and long wave radiation take place, which estableish a heat energy balance along with the conduction in the house construction (Figure 4.4).

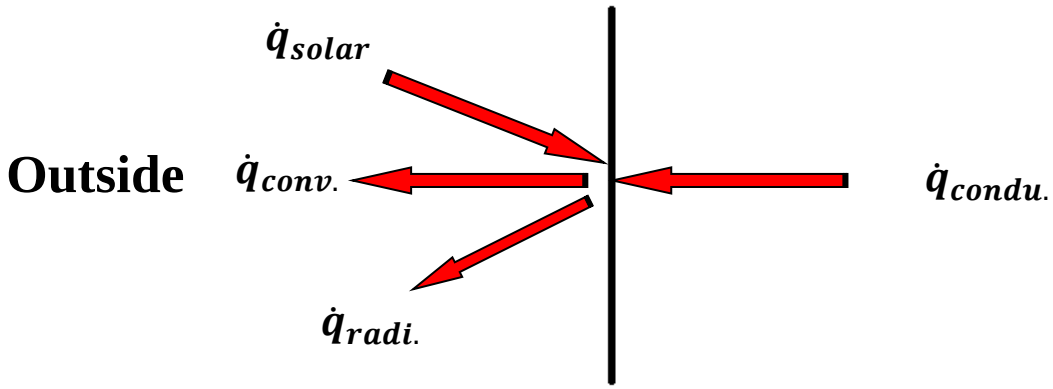

Figure 4.4 House exterior surface heat balance

The heat energy balance of the room exterior surface is represented by,

$$\dot{q}_{condu.} = \dot{q}_{conv.} + \dot{q}_{radi.} - \dot{q}_{solar} \text{ [W or Btu/hr]}, \quad (4.3)$$

where, $\dot{q}_{condu.}$ (W or Btu/hr) is the conduction heat flux in the house construction; $\dot{q}_{radi.}$ (W or Btu/hr) is the net long-wave radiation between this exterior surface and surrounding radiation sources, such as other buildings and the sky; $\dot{q}_{solar}$ (W or Btu/hr) is the solar radiation incident on this surface; and $\dot{q}_{conv.}$ (W or Btu/hr) is the convective heat transfer energy between this exterior surface and the outdoor air.

Based on pre-defined boundary conditions, such as outdoor air temperatures, solar radiation, and the sky temperatures, this equation system including the equations 4.1, 4.2, and 4.3 can be solved. Then, the indoor thermal behaviors, such as the room air temperature, room interior surface temperatures, as well as the room heat loads can be obtained.

4.2 Description of the Model Integration

Once the multi-zone thermal model has been numerically established, the integration between POMA and the thermal model can be accomplished based on the fact that in the multi-zone thermal model, there are the parameters that can be regarded as the inputs or boundary conditions of the zonal model POMA. These parameters include interior surface temperature,

supply air temperature and volume of supply diffuser, etc. Although these parameters vary depending on the associated mechanical system used in buildings, there are some parameters that are commonly used in each system, such as interior surface temperature (as shown in the figure 4.5). Therefore, in the model integration, these two models (POMA and the multi-zone thermal model) are able to be coupled together by using these inter-parameters. This integration allows the zonal model to estimate the indoor room temperature distribution based on the calculated results of the multi-zone thermal model. Once the inter-parameters are determined in the multi-zone thermal model, they can be used by the zonal model as the inputs or boundary condition to predict the current room airflow and thermal behaviors, including temperature distribution and airflow pattern. Therefore, this integrated thermal model is able to provide corresponding indoor thermal responds with various outdoor weather conditions. Additionally, unlike the original multi-zone thermal model, a detailed description regarding the indoor thermal behavior and airflow pattern can be obtained using this integrated model. Consequently, an accurate energy simulation can be established based on this detailed room thermal description, in which more factors that is able to impact the building energy consumption can be considered, such as the different thermostat set points and locations which are difficult to simulate in the original multi-zone thermal model. Although the integration procedures are different depending on mechanical systems, a general integration approach is displayed in the figure 4.6. As shown in this figure, an energy-effect parameter is adjusted numerically in order to meet the room requirement, such as the requirement of local room air temperature or specified thermal comfort level. This energy-effect parameter represents the sensitive factor that can directly or indirectly affect the change of the room requirement. Therefore, this energy-effect parameter can be the supply air temperature or supply air volume for a forced air distribution system, or the electrical energy input for an

electric floor radiation system. Once the room requirement is met, the energy consumption of the Air Conditioning (AC) system can be determined based on the current value of the energy-effect parameter.

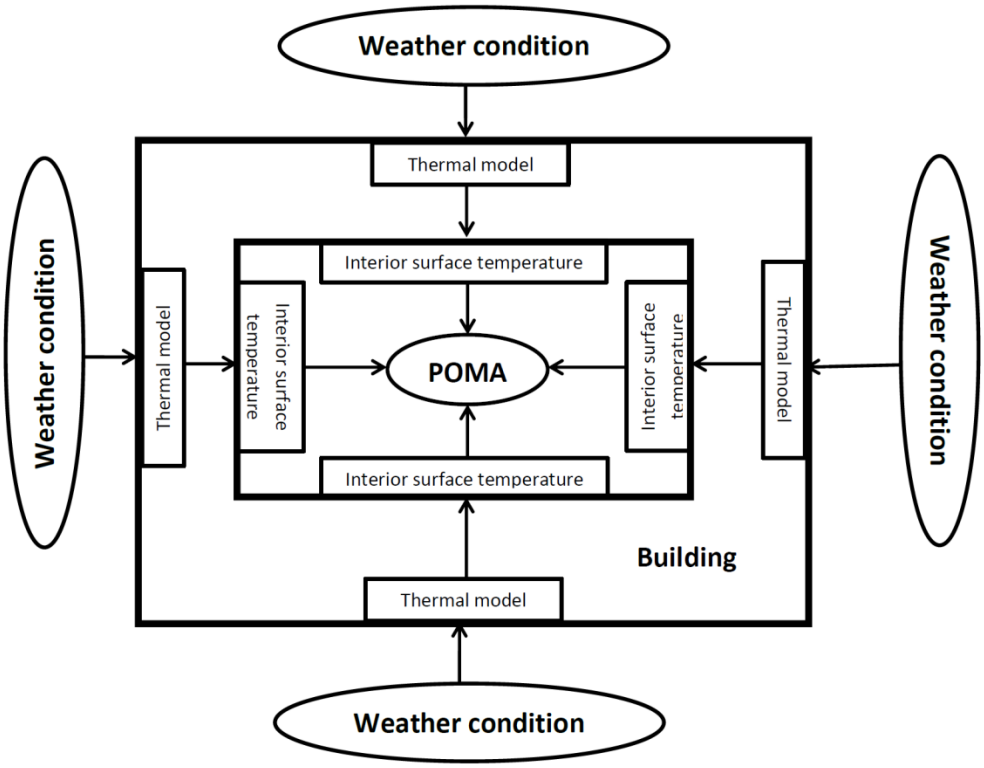

Figure 4.5 Integration of POMA and the thermal model

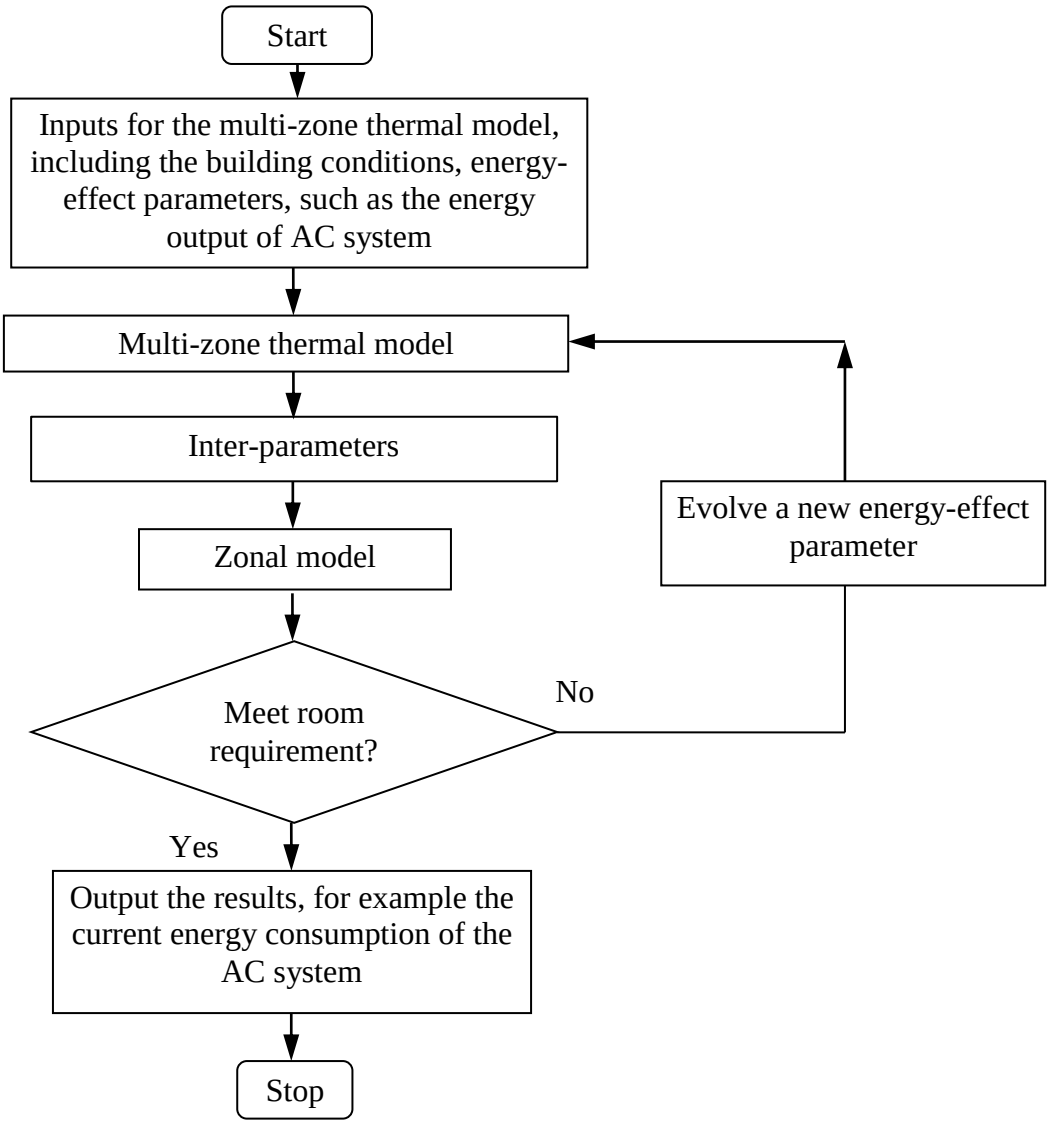

Figure 4.6 Flow chart of a general integration procedure

4.3 Description of the Application of the Integrated Thermal Model

In order to apply the integrated thermal model into building environment, several considerations need to be taken into account, such as the determination of the number of zone divisions, the applicability analysis of the integrated model used in the situations for different air conditioning systems and for the rooms characterized with complicated geometry, and the

investigation of the potential for year-around energy simulation using the integrated thermal model.

4.3.1 Determination of the number of zone divisions. Theoretically, to determine the number of zone divisions in the integrated thermal model, an independent analysis is commonly used, in which the number of zone divisions will keep increased (usually doubled) from simulation to simulation, until the difference of the results between the current simulation and the previous one is not significant. Consequently, the number of zone divisions is determined. Actually, the number of zone divisions is dependent on the complexity of the problem that needs to be solved. The number of zone divisions for a room filled with furnishings is much greater than that for an empty room. In addition, the more number of zone divisions is involved, the more time is needed for computations. In the integrated thermal model, the Newton global convergence method with *LU* decomposition technique is used, and thus theoretically when the number of zone divisions increased, for example from *n* to *2n*, the computational time would be approximately raised by $2^3 = 8$ times, since the time complexity of *LU* decomposition is $O(2/3\ n^3)$ (Watkins, 2010). As a matter of fact, a small number of zone divisions would cause unreliable results and sometimes the failure to converge for the Newton method; whereas a large number of zone divisions would result in an unnecessary long computational time. Therefore, the reasonable selection of the number of zone divisions plays a significant role in the application of the integrated thermal model applied in building environment.

4.3.2 Situations for different air conditioning systems. The zonal model POMA described in Chapter 3 is especially suitable for natural convection problems, in which the indoor airflow and thermal behaviors are dominated by the impacts of buoyancy and gravity. Nevertheless, for the forced air distribution problems, corresponding sub-models have to be

accordingly included and numerically interconnected in the zonal model (Haghighat et al., 2001), in order to describe the different physical phenomena. Generally, these sub-models include jet flow models, thermal plume models, and so on. Jet flow models are used to distribute cool or warm air into an indoor room space for both cooling or heating applications and are various depending on the different jet characteristics (thermal/isothermal jet, free/wall jet, circular/plane/radial jet, and horizontal/vertical jet). Thermal plume models are caused by indoor heat sources, such as people, convection heater, equipment, etc. (Heiselberg et al., 1998), and are various depending on the different plume characteristics (circular/plane plume, wall/corner/multiple plume). In these sub-models, important parameters, including centerline flow velocity and temperature and trajectory/penetration length/throw, are represented by using empirical equations that were usually obtained from both conservation equations and experiments. The centerline flow velocity and temperature represent the central velocity and temperature of the jet flow or thermal plume; and the trajectory/penetration length/throw represent the effective length of the jet flow or thermal plume. Table 4.1 shows several jet and thermal plume models.

Table 4.1 *Selected sub-models*

Isothermal Free linear jet model (Haghighat et al., 2001)	Centerline velocity: $v_x = v_0\sqrt{\frac{KH_0}{X}}$
Isothermal Free compact and radial jet model (Haghighat et al., 2001)	Centerline velocity: $v_x = v_0 K\frac{\sqrt{A_0}}{X}$
Thermal Free circular jet model (Heiselberg et al., 1998)	Trajectory: $y = \frac{0.02}{K_a}\frac{\Delta T_0 A_0}{u_0^2}\left(\frac{x}{\sqrt{A_0}}\right)^3$
Thermal plume (convector with horizontal air outlet) (Riederer et al., 2002)	Plume flow rate: $\dot{m(z)} = 0.012\emptyset(z)^{0.33}(z-0.3)$
Thermal plume (convector with vertical air outlet) (Riederer et al., 2002)	Plume flow rate: $\dot{m(z)} = 0.0083\emptyset(z)^{0.33}(z-0.3)$
Thermal plume (Radiator) (Riederer et al., 2002)	Plume flow rate: $\dot{m(z)} = 0.0095\emptyset(z)^{0.33}(z-0.1)$
Free thermal plume (Heat Gain) (Riederer et al., 2002)	Plume flow rate: $\dot{m(z)} = 0.0061\emptyset(z)^{0.33}(z-0.3)^{1.67}$

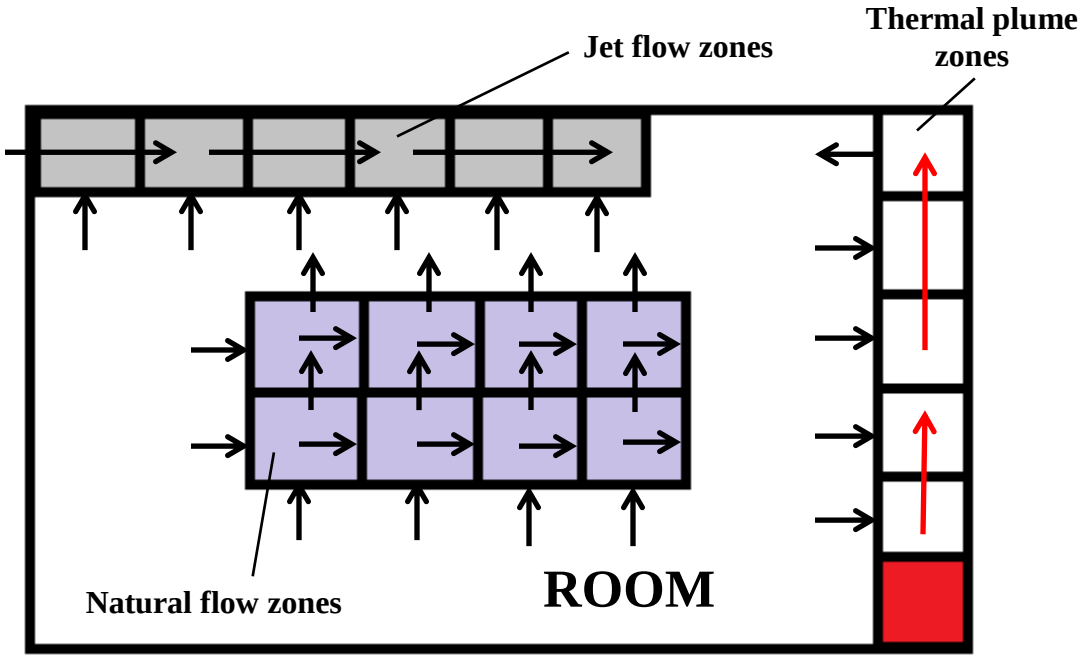

Figure 4.7 Demonstration of different sub-model zones

Figure 4.7 shows the usages of the different sub-models in a room. The corresponding jet flow models and thermal plume models may be used in the specified zones. In the natural flow zones, the original zonal model POMA is applied. Table 4.2 provides a reference for the different sub-models.

Table 4.2 *References for different sub-models*

Jet models:	Grimithin, 1970; Jackman, 1970; Holmes & Sachariewicz, 1973; Beltaos, 1976; Skåret, 1976; Rajaratnam, 1976; Hestad, 1976; Nielsen, 1976, 1980, 1983; Nielsen et al., 1987; Nielsen & Moller, 1985, 1987, 1988; Murakami et al., 1991; Guthrie et al., 1992; Guthrie, 1996; Mundt, 1996; Vialle & Blay, 1996; Inard et al., 1996a, 1996b; Rees, 1998; Rees & Haves, 1999; Wurtz et al., 1999b; Haghighat et al., 2001; Gagneau & Allard, 2001; Musy et al., 2002; Riederer et al., 2002; Huang et al., 2002; Mora et al. 2003b; Huang, 2003; Stewart & Ren, 2003; Gharbi et al., 2004; Ren & Stewart, 2005.
Thermal plume models:	Howarth, 1985; Skåret, 1986; Lebrun & Ngendakumana, 1987; Nielsen et al., 1988; Inard & Molle, 1989; Kofoed & Nielsen, 1990; Inard & Buty, 1991; Mundt, 1992; During, 1994; Milke & Mowrer, 1995; Popiolek, 1996; Inard et al., 1996a, 1996b; Inard et al., 1997a, 1997b; Wurtz et al., 1999b; Musy et al., 2001; Gagneau and Allard, 2001; Musy et al., 2002; Riederer et al., 2002; Stewart & Ren, 2003; Ren & Stewart, 2003;

4.3.3 Situations for rooms characterized with complicated geometry. The integrated thermal model has the characteristics of both the zonal model POMA and the multi-zone thermal model. For the situations involving complex room shape, the sizes of the zone divisions can be defined differently in the integrated thermal model. For example, using fine grid meshes near boundary-surface regions where the air is characterized with turbulent flow and coarse grid

meshes in the others would allow the zonal model to effectively capture the physical characteristic of the airflow of the entire room. Additionally, different coordinate systems may be used in the zonal model depending on the different problems to be solved. Megri and Yu (2011) predicted the water thermal behavior of a cylindrical mantle tank using a zonal model. In this study, the traditional rectangular coordinate cannot be used because of the cylindrical shape of the mantle tank. Instead, a cylindrical coordinate (Figure 4.8) was used in the zonal model whose results were compared with the experimental data, and a good agreement was achieved.

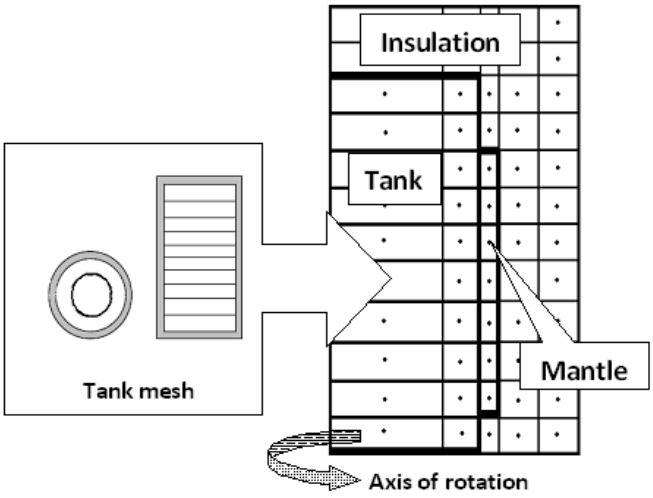

Figure 4.8 Computational grid mesh of cylindrical mantle tank

4.3.4 Potential for year-around energy simulation. As a matter of fact, the simplified mathematical model and the reduced computational time make this integrated thermal model possible to perform the year-around building energy simulation, in which the indoor thermal behavior of each room would be predicted hour by hour, minute by minute, or even second by second over a year, as long as the corresponding weather conditions are available. In addition, the impacts of building control system can be included in the simulation, such as the controls of the thermostat, supply air temperature or volume, etc. Megri and Yu (2014) investigated the

possibility of improving the heating energy calculation of a building equipped with an electric floor radiation system. In this study, three thermostat setpoint strategies (room air, mean radiant and operative temperatures) along with night/daytime setback control were considered in the simulation where the integrated thermal model was used.

Although the theoretical practicability of the integrated thermal model in various situations has been described above, a comprehensive evaluation of this model is needed, in which numerical and experimental validation should be conducted in the future.

CHAPTER 5

Applications of the Integrated Zonal / Multi-zone Thermal Model

In the U.S., buildings consume approximately 41% of primary energy and are responsible for approximately 40% of U.S. carbon dioxide emissions, and HVAC energy consumption is one of the major parts (U.S. DOE, 2012). In order to reduce primary energy consumption and greenhouse gas emissions, building energy conservation has to bear the brunt. In order to accomplish energy savings within buildings, various advanced techniques, such as active/passive usage of solar energy, geothermal heat pump, wind power, integrated designs, intelligent Building Management System (BMS), and so on, have been developed and applied. Additionally, the simulation of building energy consumption has been carried out by using computers with various commercial software packages, such as TRNSYS (2000), EnergyPlus (2011), Trace 700 (2010), eQUEST (2010), CODYBA (1992) and so on. In these building energy simulation tools, several air conditioning systems can be modeled and used in a comparative study in order to select the most appropriate and energy-efficient system, based on cost effectiveness. Therefore, with the assistance of these tools and techniques, designers are capable of having various design solutions, based on several criteria, system characteristics, building locations, and other requirements imposed by the owner. In fact, at the design stage, besides an appropriate mechanical system selection, there are other crucial parameters that have to be considered carefully, such as indoor room design temperature. This parameter determines not only the capacities of cooling/heating units, but also the sizes of air/water distribution systems (Lam, 2000). Fortunately, plenty of researches have been performed with respect to the correct selection of indoor room design temperatures (ASHRAE Standard 55, 2004). Nicol and Roaf (1996) replaced the existing inappropriate indoor temperature requirements of thermal

comfort standards by using field surveys involving summer and winter seasons of five climatic regions of Pakistan. Lam (2000) investigated 146 commercial buildings in order to find the prevailing architectural design and construction practices in Hong Kong, including indoor design conditions and other parameters. Wan et al. (2009) proposed a new method to determine the indoor temperature and relative humidity based on a parameter variation study, in which the parameter sensitivities of the indoor temperature and relative humidity were investigated based on human thermal sensation. Huang et al. (2012) developed a physical-rules-based adaptive neuro-fuzzy inferential sensor (ANFIS) model which was used into space heating systems and demonstrated the obvious improvement of accuracy in the perdition of indoor temperatures compared to unphysical-rules-based ANFIS model. Although the concepts between indoor design temperature and thermostat set point are different, the indoor design temperature should be selected properly to be able to reflect the actual room set temperature when the building is in operation. In other words, the temperature set point of a room thermostat should be close to the value of the indoor room design temperature. Otherwise, the air conditioning system will not operate efficiently and under stable condition.

Like the indoor design temperature, the magnitude of the thermostat set point affects not only the thermal comfort levels of the indoor occupants but also the energy consumption of a HVAC system (Moon & Han, 2011). Unfortunately, the thermostat feedback temperature value cannot reflect the actual air temperature of the occupied space in a room, since the thermostat is always attached to a wall rather than to the center of the room. Consequently, although the thermostat feedback temperature value receives a certain level, at which the requirement of indoor thermal comfort can be met, the temperature of the occupied space may be higher or lower than this value. It follows that the people in the occupied space do not feel as comfortable

as reflected by the thermostat feedback temperature. A temperature difference exists between the occupied space and the position where a thermostat is located. Therefore, how to determine this temperature difference and how it affects the energy consumption become essential in the processes of the HVAC system design and operation.

Additionally, besides indoor design temperature, there is another parameter that also plays a significant role in building load calculation, energy prediction, as well as system's selection and sizing. This parameter is the design location of the thermostat, which is usually ignored by designers and needs to have more attention at the building design stage. Like the indoor design temperature, the thermostat location is not only able to affect the capacities of mechanical systems at the design stage, but also to determine the indoor air quality and people's thermal comfort levels (Madsen et al., 1990). For instance, locating a thermostat near a heat source such as a computer in summer and near a cold wall in winter will not only increase the unnecessary energy consumption significantly, but also lower people's thermal comfort levels because of the overcooling and overheating in summer and winter respectively. Therefore, at the design stage, thermostat locations should be optimized and selected properly in consideration of reducing building energy consumption and/or improving human thermal comfort.

The current commercial software packages used for building load calculation and energy prediction are based on single/multi-zone models and thus need to be integrated with more advanced numerical models such as zonal models. The single/multi-zone models, also known as well-mixed models, are not able to predict the temperature difference between two locations within a space, since they usually regard an entire volume or room as a single zone, in which the physical properties of the indoor air parameters are perfectly uniform and homogenous, such as pressure, temperature, and density (Yu, 2012). Based on this assumption, the concept of

thermostat becomes meaningless, since wherever the thermostat is located, the results in terms of load and energy will be the same because of the assumed uniform temperature distribution. Hence, in order to solve this problem, advanced numerical models, like zonal models, which have the ability to predict the actual air temperature gradient, should be applied.

In this chapter, several applications of this integrated thermal model involving forced air distribution system and general heating system have been included. In the application of the forced air distribution system, the integrated thermal model has been used not only to predict the appropriate thermostat set point, corresponding to less energy consumption of an UnderFloor Air Distribution (UFAD) system and/or to a comfortable environment, but also to improve the computational quality and accuracy of the required energy of the UFAD system. Similarly, in the application of the general heating system, the integrated thermal model has been used to predict the appropriate thermoset set point as well as the heating load corresponding to different thermostat locations. Instead of using an UFAD system, in this application, a general heating system is considered, which stands for the non-specified air-conditioning system in load calculations. Like the general method and principle regarding building load prediction in most HVAC handbooks (ASHRAE fundamentals, 2005), with this system, the building loads are determined through using the heat loss equations from building structures and thus the room thermal behavior associated with this system are dominated by natural convection, i.e. the impacts of buoyancy and gravity.

These applications are intended to demonstrate the practicability of this integrated thermal model for different air conditioning systems and the improvement of the prediction of building load and energy consumption using this integrated model. Additionally, direct

comparisons are performed between the integrated thermal model and the conventional single/multi-zone thermal model in terms of building energy/load and indoor thermal comfort.

5.1 Predictions of Thermostat Set Point and Design Heating Load for Energy Saving and/or Better Indoor Thermal Comfort of an UFAD System – Forced Air Distribution Cases

5.1.1 Introduction. Although the single/multi-zone models have been proved to be acceptable for traditional overhead air distribution systems, they are not appropriate to be used in a non-uniform environment created by other HVAC systems, i.e. UFAD systems (Schiavon et al., 2011). In the UFAD systems, a room is separated by a raised floor into two spaces, the occupied room space and the floor plenum space. Conditioned airflow from a terminal Air Conditioning (AC) unit is delivered to the floor plenum and then supplied to the occupied space above through floor diffusers (Figure 5.1). Consequently, new energy prediction approaches based on the characteristics of these air distribution systems should be developed, in consideration of the limited applications of the existing single/multi-zone models in the building energy prediction for these systems.

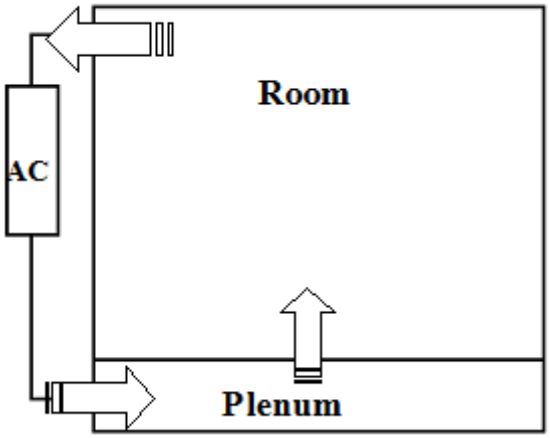

Figure 5.1 Demonstration of UFAD system used in a room

Griffith and Chen (Griffith & Chen, 2004) stated that "the assumption that room air is well mixed may lead to significant errors in HVAC system sizing" and developed a coupled momentum-zonal model with building energy and load calculations to accurately predict hourly building loads of a single thermal zone. Zhai et al. (2002) demonstrated several efficient methods to integrate energy simulations into CFD models in order to improve the accuracy and quality of building energy prediction. Additionally, several approaches (Bauman et al., 2006; Schiavon et al., 2011) regarding UFAD systems have been developed in order to improve the prediction capacity of energy simulation programs. Bauman et al. (2006) investigated the primary pathways of UFAD systems for heat to be removed from a room in a cooling application. They found that, under cooling operation, a stratification produced by UFAD systems changes the dynamic characteristics of heat transfer and mentioned that "Up to 40% of the total room cooling load is transferred into the supply plenum and only about 60% is accounted for by the return air extraction rate". Skchiavon et al. (2011) proposed a simplified method to design building room cooling loads for UFAD systems, based on numerous EnergyPlus simulations and regression models. They demonstrated the differences in design cooling load calculations between UFAD and conventional well-mixed overhead systems and found that a peak cooling load of UFAD systems is 19% higher than an overhead cooling load.

UFAD systems have been widely used for years, especially in the cooling of commercial buildings. The UFAD system supplies cold air from the raised-floor plenum through the floor diffuser. The cold air pushes the warm air up near the ceiling which maintains the cool air in the lower level of the room because of the density variation between the cold and warm airs. Researches regarding UFAD systems can be easily found, but most of them are focusing on the application of this system in commercial buildings and under cooling operation (Schiavon et al.,

2010 & 2011; Alajmi & El-Amer, 2010). The researches regarding the applications of UFAD systems in residential houses and/or under heating operation are very limited. As a matter of fact, in commercial buildings, heating systems are usually separated from cooling systems, which makes the UFAD system exclusive for cooling purposes. However, in residential houses, two separated systems for both heating and cooling are not economically feasible, because of the high first cost. Therefore, in order to take advantage of the UFAD system in residential houses, especially considering the benefit of this system under cooling operation, the UFAD system has to operate under both cooling and heating cycles. Thus, the importance of how well the UFAD system will perform in a residential house under heating operation becomes significant.

In this application, the zonal model POMA coupled with a vertical thermal jet model (Vialle & Blay, 1996) has been used to predict room air temperature distributions when an UFAD system is applied for heating purposes in a residential house. Additionally, the coupled zonal model has been integrated with a multi-zone thermal model, in order to quantify the temperature difference between the occupied space and the thermostat position, to determine the appropriate thermostat set point corresponding to less energy consumption of the UFAD system and/or to a comfortable environment for occupants, and to improve the heating energy predictions of the UFAD system. This integrated thermal model is not only able to investigate the factors that influence the magnitude of this temperature difference, but also to perform predictions related to building load and energy consumption according to different thermostat locations. Then, the optimization of thermostat location can be carried out at the design stage for the sake of the achievement of building energy savings and/or the improvement of people's thermal comfort levels.

5.1.2 Model description and validation.

5.1.2.1 Numerical model for an UFAD system. In this application, the zonal model POMA coupled with a vertical thermal jet model has been used to simulate the indoor air behaviors of an UFAD system.

The jet flow can be divided into three regions, shown in the figure 5.2, determined by the dimensionless distance *Y* (Vialle & Blay, 1996):

$$Y = \frac{y}{\sqrt{A_0}}, \qquad (5.1)$$

where A_0 (m^2 or ft^2) is the supply diffuser area; *y* (m or ft) is a certain distance in the jet flow direction.

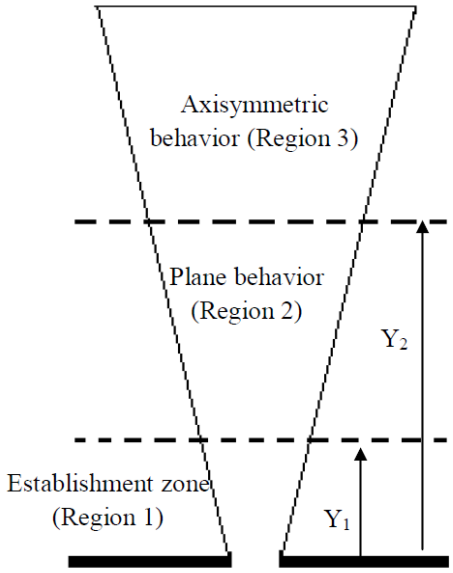

Figure 5.2 Three regions of a positive buoyancy jet
(Vialle & Blay, 1996)

As shown in the figure 5.2, in Region 1, $Y<Y_1=2$, the flow is established; in Region 2, $Y_1=2<Y<Y_2=7$, the jet flow has a behavior similar to a plane jet; and in Region 3, $Y>Y_2=7$, the

flow behaves as an axisymmetrical jet. The decay laws of centerline velocity and temperature are given in the table 5.1, which are determined by the Archimedes number (Vialle & Blay, 1996):

$$Ar = \frac{g\beta(T_0 - T_s)\sqrt{A_0}}{v_0^2}, \qquad (5.2)$$

where v_0 (m/s or ft/s) is the initial supply air velocity from a diffuser; T_0 (^{o}C or ^{o}F) is the initial supply air temperature; T_s (^{o}C or ^{o}F) is the surrounding temperature; A_0 (m^2 or ft^2) is the supply diffuser area; g (m/s^2 or ft/s^2) is the acceleration of gravity; and β (1/K or 1/R) is the expansion coefficient.

In this coupled model (the vertical thermal jet model with POMA), at the zones where the jet flows occur, the air mass flow rates are calculated based on the vertical thermal jet model using the jet flow rates which are defined as $\dot{m} = \rho A v$, where v (m/s or ft/s) is the jet velocity defined in the table 5.1; ρ (kg/m^3 or lbm/ft^3) is the air density; A (m^2 or ft^2) is the cross-sectional area between two zones; whereas at the other zones, POMA is utilized, as shown in the figure 5.3. Similarly, the centerline zone temperatures of the jet are computed by using the centerline temperature T defined in the table 5.1; and the temperatures of the other zones are still calculated using POMA. For the interactive zones that are affected by both the jet and zonal models as shown in the figure 5.3, the combined effect of these two models is considered in the calculation (Haghighat et al., 2001).

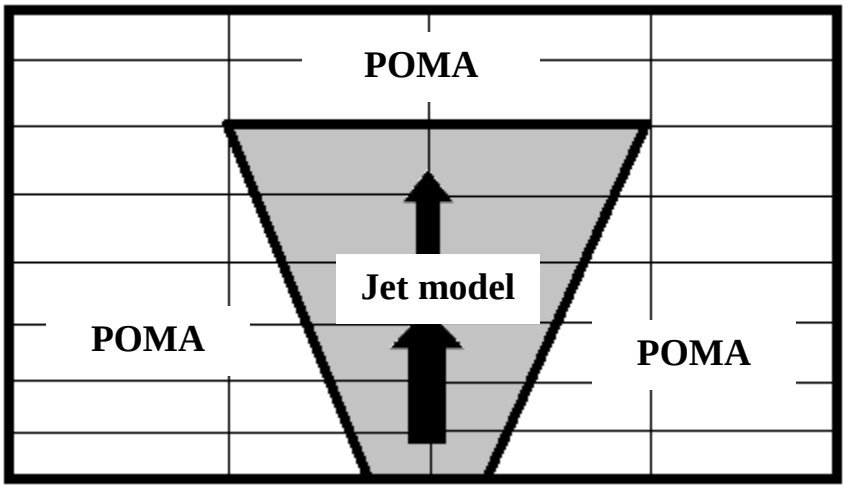

Figure 5.3 Demonstration of the model coupling

Table 5.1 *Decay laws of centerline velocity and temperature (Vialle & Blay, 1996)*

Region		Velocity	Temperature
Region 1		$v = v_0$	$T = T_0$
0<Y<Y1	*Y1=2*		
Region 2		$\frac{v}{v_0} = \left(\frac{Y_1}{Y}\right)^{b_2}$ $b_2 = 0.28\frac{0.22Ar + 0.07}{Ar + 0.07}$	$\frac{T - T_s}{T_0 - T_s} = \left(\frac{Y_1}{Y}\right)^{b_2}$ $b_2 = 0.28\frac{5.4Ar + 1.26}{Ar + 1.26}$
Y1<Y<Y2	*Y2=7*		
Region 3		$\frac{v}{v_0} = \left(\frac{Y_1}{Y_2}\right)^{b_2}\left(\frac{Y_2}{Y}\right)^{b_3}$ $b_3 = 0.73\frac{0.203Ar+0.028}{Ar+0.028}$	$\frac{T - T_s}{T_0 - T_s} = \left(\frac{Y_1}{Y_2}\right)^{b_2}\left(\frac{Y_2}{Y}\right)^{b_3}$ $b_2 = 0.73\frac{1.63Ar+0.06}{Ar+0.06}$
Y>Y2	*Y1=2;Y2=7*		

5.1.2.2 Model validation and grid independence analysis. Before using the coupled model in case studies, a model validation needs to be accomplished. The size of the room used for the validation is 3.1 m × 3.1 m × 2.5 m (10.2 ft × 10.2 ft × 8.2 ft). Since the height of the floor plenum for the UFAD system is 0.254 m (10 inches), the actual height of the simulation

room is 2.246 m (7.37 ft). This room has a 3.1 m^2 (3.1 m × 1.0 m) or 33.46 ft^2 (10.2 ft × 3.28 ft) window on the west wall. A floor air diffuser with the size of 0.5334 m × 0.2286 m (1.75 ft × 0.75 ft) is placed at the center of the room. One return grille (0.62 m × 0.23 m or 2.03 ft × 0.75 ft) is located on the south wall (Figure 5.4). Boundary conditions including the surface temperatures of the room, as well as the supply air temperature and velocity of the diffuser, are given in the table 5.2.

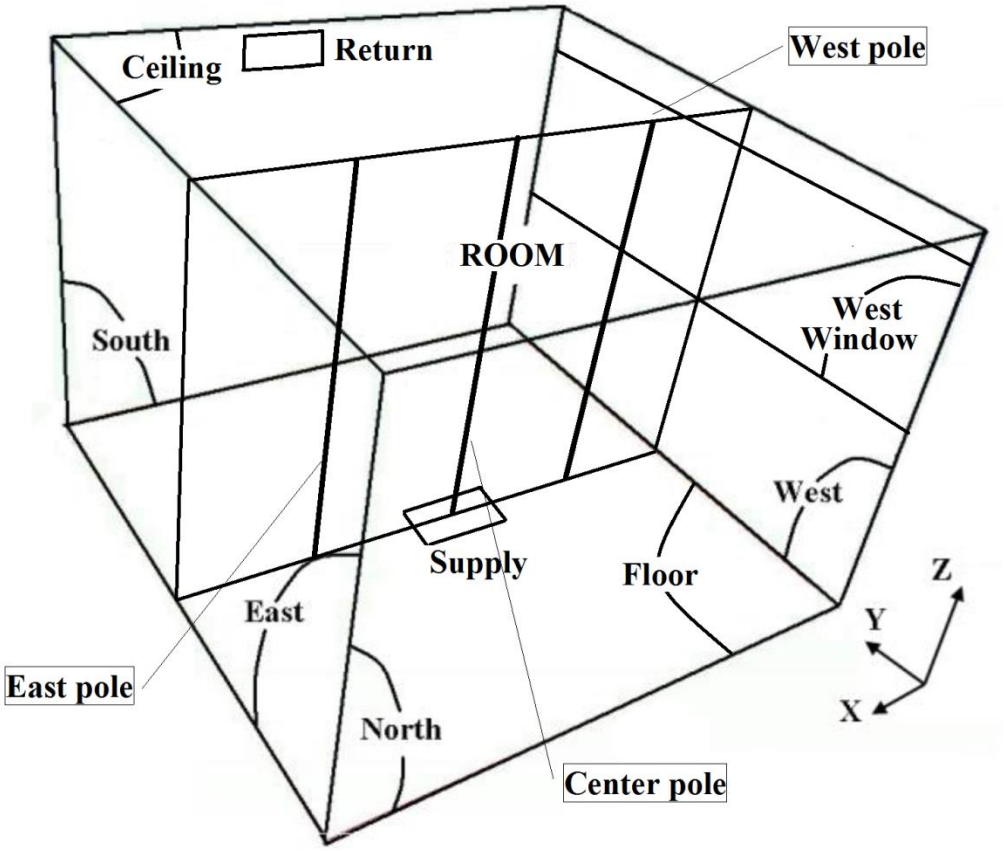

Figure 5.4 Shape and diffuser location of the simulation room

Table 5.2 *Boundary conditions for this validation*

	North [^{o}C] ([^{o}F])	South [^{o}C] ([^{o}F])	East [^{o}C] ([^{o}F])	West [^{o}C] ([^{o}F])	Ceiling [^{o}C] ([^{o}F])	Floor [^{o}C] ([^{o}F])	West Window [^{o}C]([^{o}F])	Supply Air [^{o}C]([^{o}F])
Temperature	20.7 (69.3)	21.1 (70.0)	21.1 (70.0)	20.6 (69.1)	21.1 (70.0)	21.2 (70.2)	17.4 (63.3)	32.2 (90.0)
Diffuser airflow velocity: 1.0 m/s (3.28 ft/s)								

Firstly, for the coupled zonal model, the grid independence is checked by using different grid resolutions, including 100 meshes (5×5×4), 200 meshes (5×5×8), 490 meshes (7×7×10), and 810 meshes (9×9×10). The results in terms of temperature corresponding to these grid resolutions are compared with the results of the CFD model, FLOVENT (2011). Since the temperature boundary conditions of the north and south surfaces are close compared to the east and west surfaces (Table 5.2), the temperature gradient in the east-to-west direction is significant compared to that in the north-to-south direction. Therefore, the vertical temperature distributions of the three verticals (the three poles shown in the figure 5.4) are used in the comparison. The three verticals (poles) are located on the medium plane of the *y* direction. The center pole is located at the center point of the supply diffuser, and the east and west poles are located near the east and west wall surfaces respectively. The horizontal distances from the east and west poles to their nearby wall surfaces are 0.775 m (2.54 ft). The comparison results are displayed in the figure 5.5, where R100, R200, R490, and R810 correspond to the different gird resolutions; CFD and CFD200 represent the results of the CFD model with the grid resolutions, 18,009 (29×27×23) and 200 (5×5×4) meshes; T (^{o}C or ^{o}F) is the simulated air temperature; T_{in} (^{o}C or ^{o}F) is the supply air temperature which is 32.2 ^{o}C (90 ^{o}F); z (m or ft) is the elevation from the room bottom; and H (m or ft) is the height of the room space, which is 2.246 m (7.37 ft).

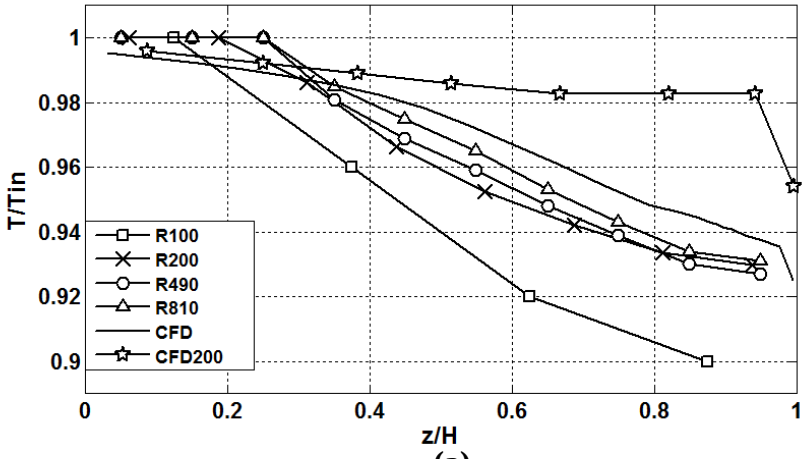

(a)

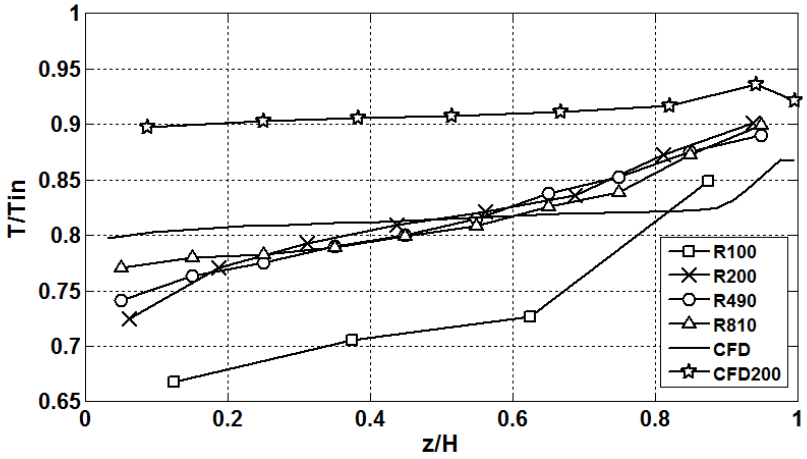

(b)

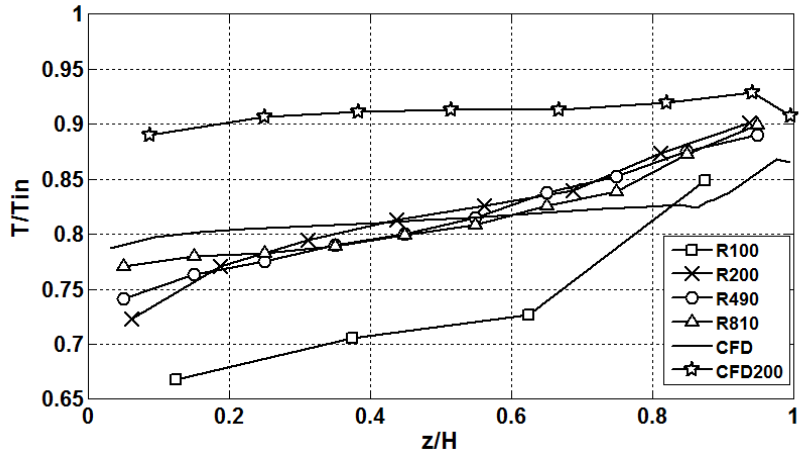

(c)

Figure 5.5 Comparison of the different grid resolutions of POMA and CFD (FLOVENT) model with a gird of 29 × 27 × 23 (a) Center pole; (b) East pole; (c) West pole

Figure 5.6 shows the typical thermostat location which is on the south wall, below the return grill, approximately 1.5 m (4.9 ft) above the raised floor, and 2.2 m (7.2 ft) away from the west wall.

As shown in the figure 5.5, the results of the east (b) and west (c) poles are very close, because the room is dominated by forced air distribution considering the size of the room and the supply airflow rate and temperature. Additionally, when the grid resolution is equal to or greater than 200, the coupled zonal model produces a reasonably good result compared with that of the CFD model with the 18,009 grid resolutions. Also, the corresponding results of the grid resolution 200, 490, and 810 are very close, due to the fact that the impact of the thermal jet model is significant compared to the zonal model POMA. In fact, when 200 grid resolutions are used in the CFD model, its result (the curve of CFD200 shown in the figure 5.5) is not as good as the result of the coupled zonal model with the grid resolution 200 (shown as R200 in the figure 5.5). On the one hand, the thermal jet model derived from experimentation is coupled with the zonal model, and thus this coupled zonal model is able to provide a reasonable and acceptable prediction result of indoor thermal behavior, even though the grid resolution used is low. On the other hand, the low grid resolution cannot allow the CFD model to capture the detailed description of the physical phenomena of this room because of the characteristics of CFD, and thus errors would be introduced by using this low-grid-resolution CFD model. Figure 5.7 displays the air temperatures of the typical thermostat location (Figure 5.6) of the coupled zonal model (considering different grid resolutions) against the CFD model with the grid resolution, 18,009 meshes (29×27×23). In

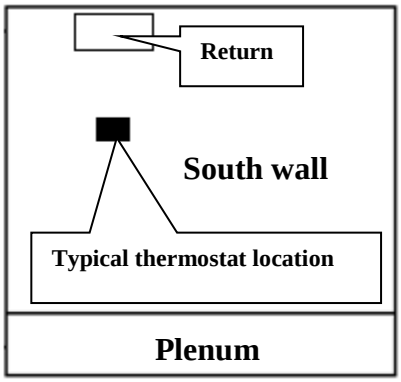

Figure 5.6 Thermostat location

this figure, CFD200 represents the result of the CFD model with the grid resolution, 200 (5×5×4). Similarly, the low-grid-resolution CFD model overestimates the air temperature of the typical thermostat location, and thus cannot be used in the application compared to the results of the coupled zonal model. In addition, when the grid resolution of the coupled zonal model is equal to or greater than 200, the air temperatures of the thermostat location are much closer to the CFD results. Therefore, the coupled zonal model with the grid resolution 200 (5×5×8) is decided to be used in the following case studies.

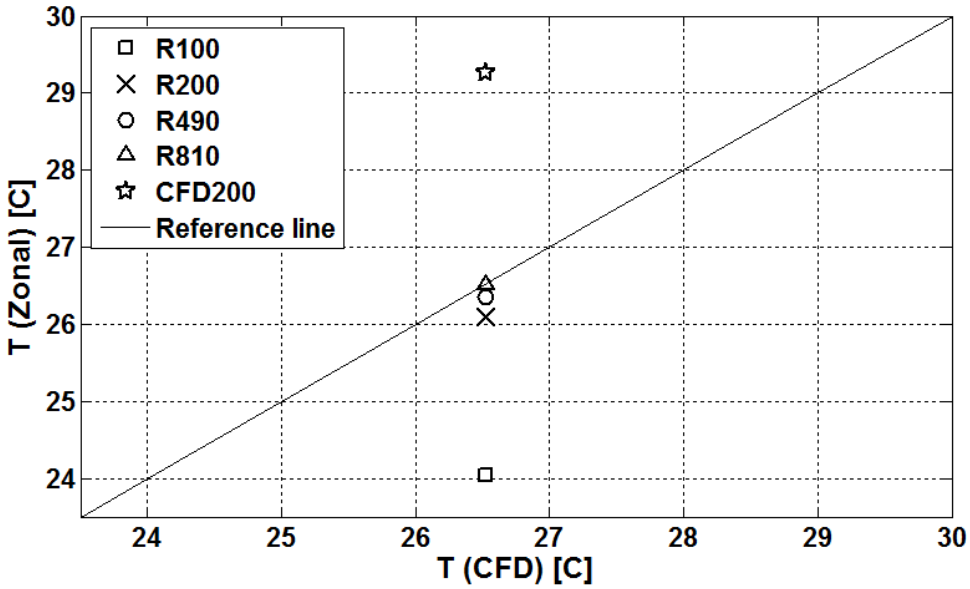

Figure 5.7 Temperatures of the typical thermostat location considering different grid resolutions

The time complexities of the coupled zonal model and CFD model are shown in the figure 5.8. These models were executed on a computer with the characteristics of CPU-1.83GHZ and RAM-3GB. As shown in this figure, the model execution time increases as the growth of the grid resolution. Theoretically, in the coupled zonal model, the time complexity can be represented using $O(\frac{2}{3}n^3)$ because of the usage of LU decomposition method (Watkins, 2010) in

the computation, where *n* is the problem size, i.e. the grid resolution. Thus, the execution time would be increased by approximately n^3, as the growth of the grid resolutions from R100 to R810. However, in reality, the execution time is also affected by other factors, such as the memory access, the dynamic resource allocation of the CPU, etc. Therefore, as shown in the figure 5.8, the results are not exactly following the theoretical increasing rate. Also, although the execution times of R200 and CFD200 are very close to each other due to the same grid resolution used, the model CFD200 failed to produce a reasonable good result compared to the other models, as shown in the figure 5.5 and 5.7. Therefore, the CFD model at a low level of grid resolution for the sake of reducing the computational time cannot be regarded as the alternative to the low-grid-resolution zonal model, which demonstrates the superiority of the coupled zonal model.

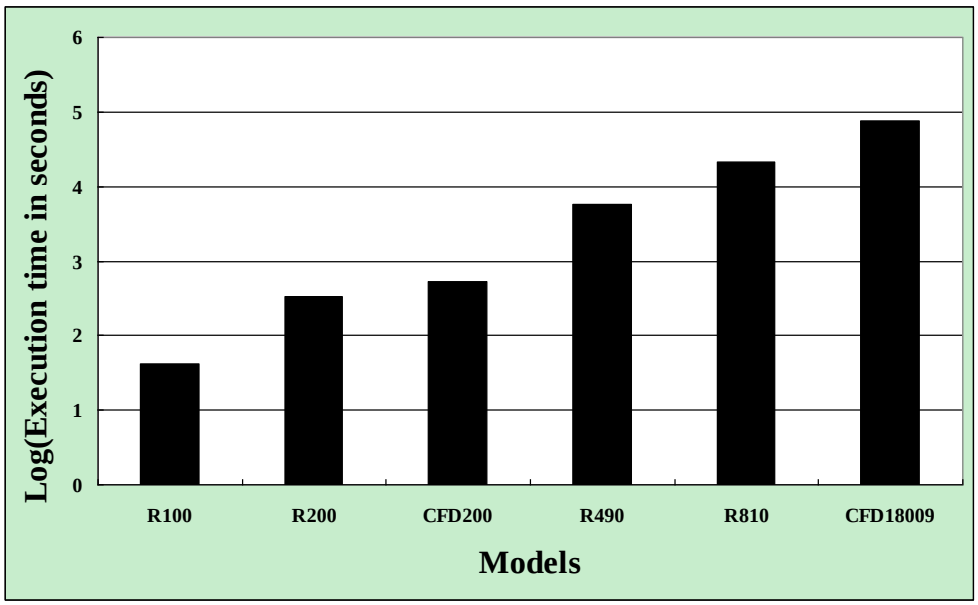

Figure 5.8 Time complexities of these coupled and CFD models

Figure 5.9 shows the comparison of the temperature distributions between the coupled zonal model and the CFD (FLOVENT) model, when the medium plane is specified in the *y* direction (Figure 5.4). Total 200 zones are applied in the zonal model and 18,009 cells for the

CFD model. As shown in the figure 5.9, an acceptable agreement is achieved, which demonstrates that with the relatively low grid resolution, the zonal model POMA coupled with the thermal jet model is able to predict the characteristics of the air temperature distribution of an UFAD system in a room.

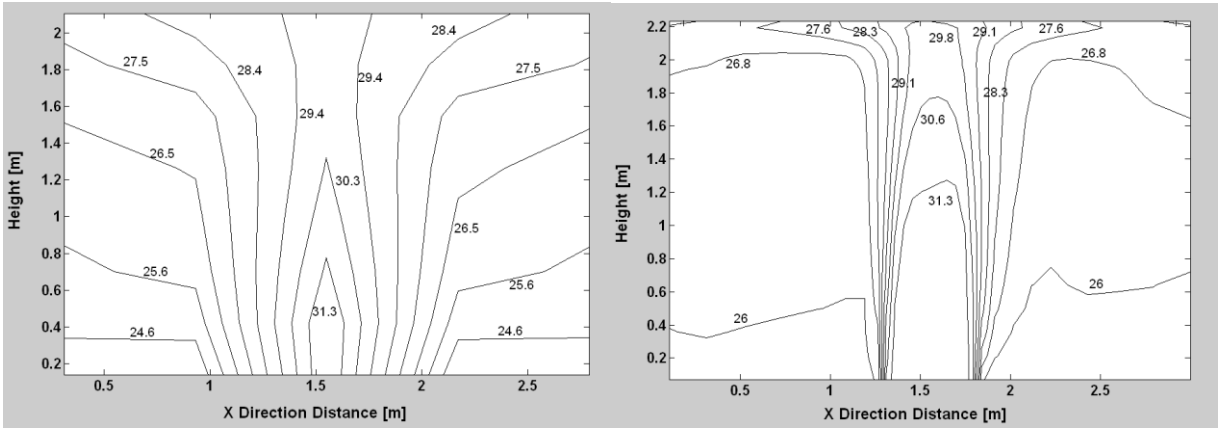

(a) (b)

Figure 5.9 Air temperature distributions (^{o}C) of the UFAD system under heating operation (a) POMA model with a grid of 5 × 5 × 8; (b) CFD (FLOVENT) model with a gird of 29 × 27 × 23.

5.1.3 Comparison of steady-state heating energy calculation between conventional air distribution and UFAD systems. The existing single/multi-zone models are mostly used in energy and load simulations, especially for the conventional air distribution systems, such as the overhead air distribution system. These models consider a room or a structure as a whole and assume that the indoor air is well mixed. Therefore, the heat energy $\dot{q}_{system}$ is defined as (Figure 5.10),

$\dot{q}_{in} = \dot{q}_{system} + \dot{q}_{out}$ [W or Btu/hr], (5.3)

and $\dot{q}_{in} = \dot{q}_{loss} + \dot{q}_{out}$ [W or Btu/hr], (5.4)

So $\dot{q}_{system} = \dot{q}_{loss}$ [W or Btu/hr], (5.5)

where $\dot{q}_{in}$ (W or Btu/hr) is the rate of the heat energy going into the room; $\dot{q}_{out}$ (W or Btu/hr) is the rate of the heat energy going out of the room; $\dot{q}_{loss}$ (W or Btu/hr) is the rate of the heat loss from the room; $\dot{q}_{system}$ (W or Btu/hr) is the rate of the heat energy generated by an Air Conditioning (AC) unit.

For the case of UFAD system, the entire room needs to be physically and structurally divided into two separated enclosures, a room space and a floor plenum space (Figure 5.11). In fact, the approach (described in the figure 5.10) which is for the conventional air distribution system is not able to accurately estimate the energy consumption of the UFAD system, since this approach treats the entire room as a whole and ignores the structural division of these two separated spaces.

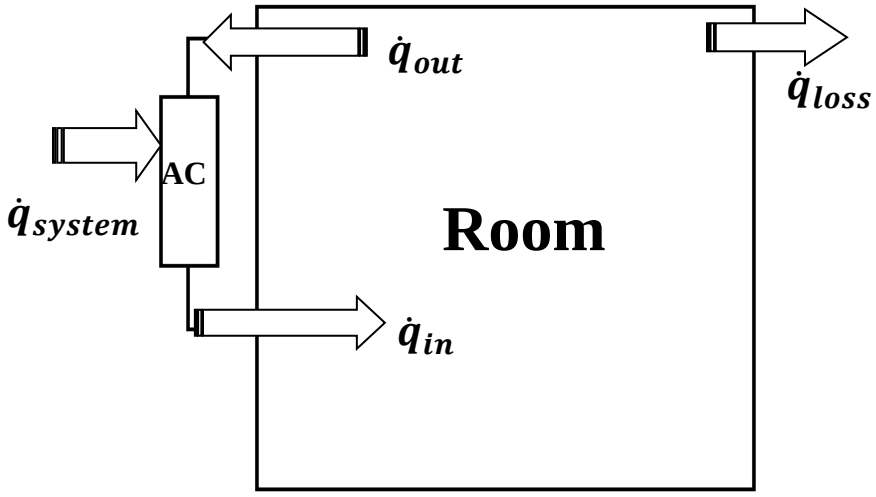

Figure 5.10 Energy balance demonstration of the conventional air distribution system

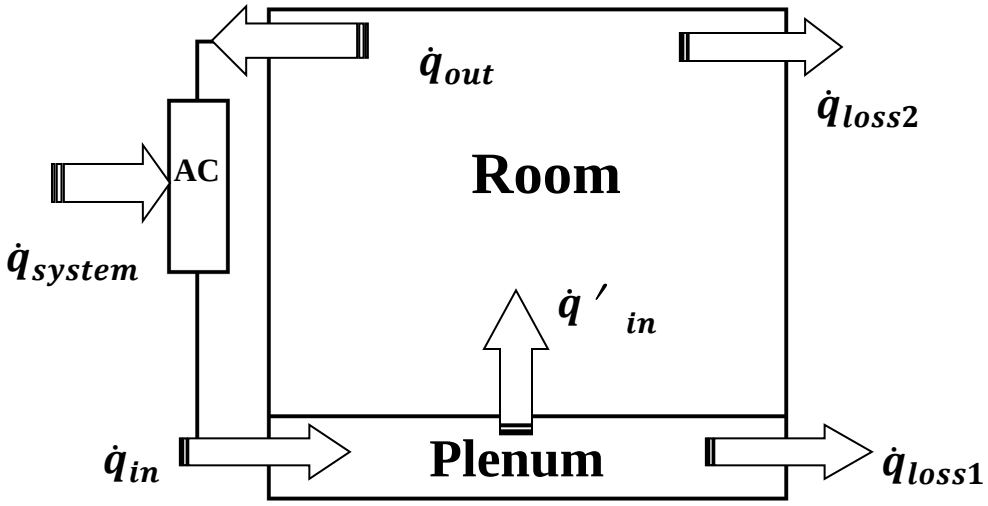

Figure 5.11 Energy balance demonstration of the UFAD system

Therefore, for energy and load predictions of the UFAD system, these two spaces need to be treated separately, because of the presence of thermal stratification using UFAD system and the different thermal characteristics of these two spaces. Then the $\dot{q}_{system}$ is defined as,

$$\dot{q}_{in} = \dot{q}_{system} + \dot{q}_{out} \quad \text{[W or Btu/hr],} \quad (5.6)$$

$$\dot{q}_{in} = \dot{q}_{loss1} + \dot{q}'_{in} \text{ and } \dot{q}'_{in} = \dot{q}_{loss2} + \dot{q}_{out} \quad \text{[W or Btu/hr],} \quad (5.7)$$

$$\text{so } \dot{q}_{system} = \dot{q}_{loss1} + \dot{q}_{loss2} \quad \text{[W or Btu/hr],} \quad (5.8)$$

where $\dot{q}_{in}$ (W or Btu/hr) is the rate of the heat energy going into the room; $\dot{q}_{out}$ (W or Btu/hr) is the rate of the heat energy going out of the room; $\dot{q}_{loss1}$ (W or Btu/hr) is the rate of the heat loss from the plenum space; $\dot{q}_{loss2}$ (W or Btu/hr) is the rate of the heat loss from the room space; $\dot{q}'_{in}$ (W or Btu/hr) is the rate of the heat energy from the plenum to the room space through floor diffusers and the raised floor construction; $\dot{q}_{system}$ (W or Btu/hr) is the rate of the heat energy generated by the Air Conditioning (AC) unit.

Theoretically, $\dot{q}_{loss}$ in the equation 5.5 is not equal to $\dot{q}_{loss1} + \dot{q}_{loss2}$ in the equation 5.8 because of the different thermal characteristics between the conventional air distribution and UFAD systems.

5.1.4 Basic simulation conditions for the applications. To demonstrate the capability of our developed computer program, the 26th of December at Cheyenne, Wyoming, is selected for the winter season simulation. Figure 5.12 and 5.13 display the local outdoor temperatures and the horizontal solar radiation respectively on the simulation day. A single-room residential house is considered for the simulation. The size of this room is 3.1 m × 3.1 m × 2.5 m (10.2 ft × 10.2 ft × 8.2 ft). Since a 0.254 m (10 inches) height floor plenum is used, the actual height of the room space is 2.246 m (7.37 ft) (Figure 5.4). The house has a 3.1 m^2 (33.46 ft^2) window (U-value 5.68 W/m^{2}K (1.0 Btu/hr ft^2 °F); Solar heat gain coefficient (SHGC) 0.855; Internal shading device: Transmission: 30%, Absorption: 43.4% and Reflection: 26.6%) on the west wall. The thermal characteristics of the four external walls, the floor, and the roof are presented in the table 5.3 and 5.4. An UFAD system is used in this house as the heating system in the winter season. Lighting and internal gains are not considered in this simulation. A seated man wearing trousers and a long-sleeved shirt is considered for the comfort Predicted Mean Vote (PMV) and Predicted Percent Dissatisfied (PPD) calculations. PMV (PPD) is the human thermal comfort index (percentage), usually used to predict people's steady-state comfort responses within a space (ASHRAE Fundamentals, 2005). The simulation is carried out without air leakage and air heat storage effects. Also, the thermal influences of the air jet flow on the room surfaces are ignored in the simulation.

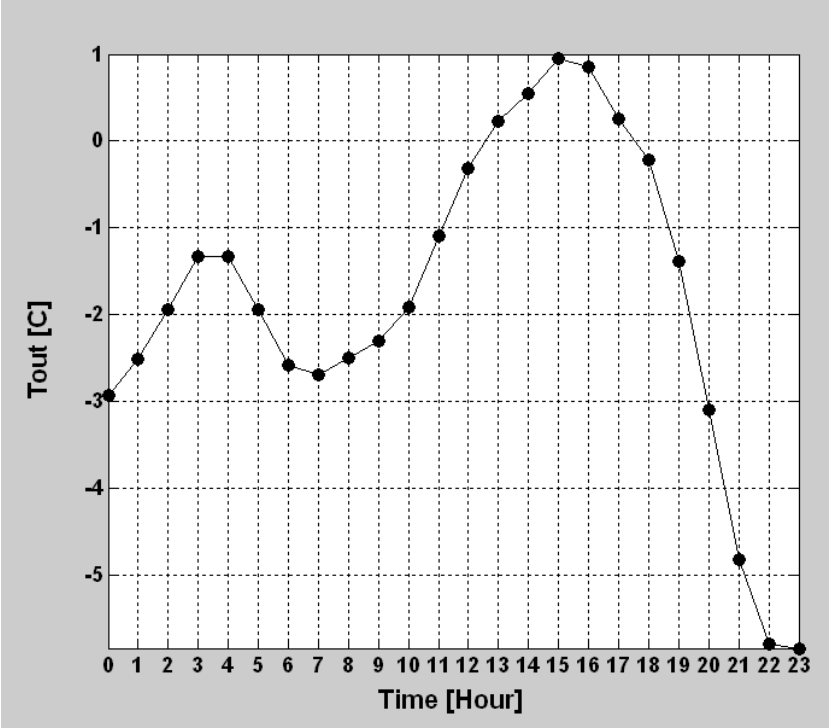

Figure 5.12 Outdoor temperatures

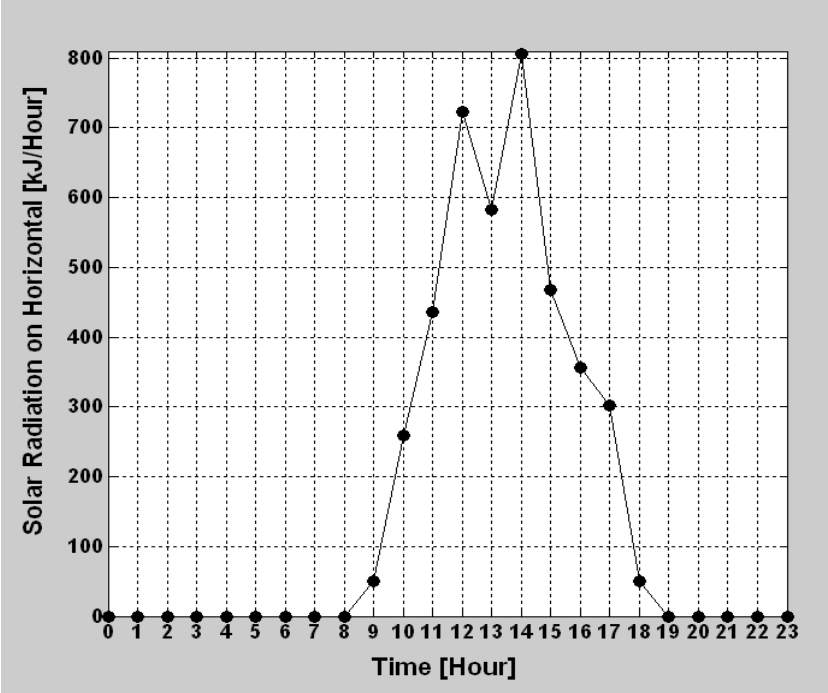

Figure 5.13 Solar radiation on horizontal

Table 5.3 *Characteristics of the external walls*

External Walls	Area m^2 (ft^2)	U-Value W/m^2 K (Btu/hr ft^2 °F)	Solar Absorptance		Convective Heat Transfer Coefficient W/m^2 K (Btu/hr ft^2 °F)	
			Inside	Outside	Inside	Outside
North	7.75 (83.4)	0.339 (0.06)	0.75	0.3	4.2 (0.74)	17.8 (3.13)
South	7.75 (83.4)	0.339 (0.06)	0.75	0.3	4.2 (0.74)	17.8 (3.13)
East	7.75 (83.4)	0.588 (0.1)	0.75	0.3	4.2 (0.74)	17.8 (3.13)
West	7.75 (83.4)	0.588 (0.1)	0.75	0.3	4.2 (0.74)	17.8 (3.13)

Table 5.4 *Characteristics of the floor and roof*

	Area m^2 (ft^2)	U-Value W/m^2 K (Btu/hr ft^2 °F)	Solar Absorptance		Convective Heat Transfer Coefficient W/m^2 K (Btu/hr ft^2 °F)	
			Inside	Outside	Inside	Outside
Raised Floor	9.61 (103)	1.671 (0.29)	0.8	0.4	4.04 (0.71)	5.0 (0.88) (Plenum)
Floor	9.61 (103)	0.313 (0.055)	0.8	-	5.0 (0.88) (Plenum)	-
Roof	9.61 (103)	0.233 (0.041)	0.35	0.75	4.04 (0.71)	17.8 (3.13)

5.1.5 The applications of the integrated thermal model in building environment. In this section, the integrated thermal model (the coupled zonal model and the multi-zone thermal model) has been used into two applications associated with the UFAD system. In the first application, the appropriate thermostat set points have been predicated corresponding to less energy consumption of the UFAD system and/or to a comfortable environment for occupants, when the thermostat is maintained at one location. In the second application, the integrated thermal model has been used to perform predictions related to building load and energy consumption according to different thermostat locations. Then, the optimization of thermostat

location has been accomplished for the achievement of building energy savings and/or the improvement of indoor thermal comfort.

5.1.5.1 The first application – the prediction of appropriate thermostat set point. In this application, several cases have been studied in order to quantify the temperature difference between the occupied space and the thermostat position and to determine the appropriate thermostat set point. In addition, the factors that influence the magnitude of this temperature difference have been investigated. This application is also intended to demonstrate the importance of this integrated thermal model not only at the building design stage but also during the operation of the building when this model is coupled with the BMS.

5.1.5.1.1 Description of the simulation conditions. In the integrated thermal model, a room is mathematically subdivided into several zones. In this room, the occupied space is defined as the space where people's activities take place. More precisely, the occupied space is defined as the space beyond 1 foot of the walls and within about 6 feet from the floor. Therefore, in order to determine the temperature difference between the occupied space and the thermostat position, the temperature of the occupied space has to be represented using a single value which is defined as the Occupied Space Temperature (OST). In this work, three different definitions have been used to represent the OST including the "Occupied-zones" scheme, the "Uniform-zones" scheme, and the "Core-zones" scheme.

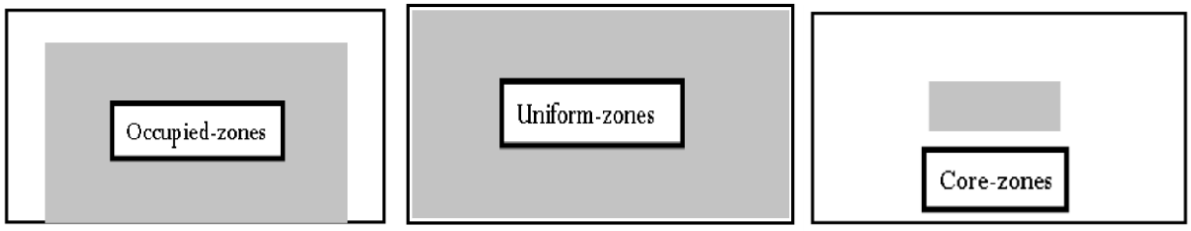

(a) (b) (c)

Figure 5.14 Three schemes (a) "Occupied-zones"; (b) "Uniform-zones"; (c) "Core-zones"

In the "Occupied-zones" scheme, the OST can be represented by the average temperature of the occupied space (the average of the *M* zones constituting the occupied space, as shown in the figure 5.14 (a)), which is defined as,

$$OST_{Occupied-zones} = \sum T_{(i,j,k)} / M, \ [^{o}C \text{ or } ^{o}F] \quad (5.9)$$

where, $T_{(i,j,k)}$ (^{o}C or ^{o}F) is the temperature of the zone (*i,j,k)* constituting the entire occupied space; and $OST_{Occupied-zones}$ (^{o}C or ^{o}F) is the average OST.

In the "Uniform-zones" scheme, the OST is calculated from the single or one-zone model (Equation 5.10), in which the homogenous and uniform temperature distribution of the entire room space is assumed, as shown in the figure 5.14 (b).

$$\sum h_{c,i} A_i (OST_{Uniform-zones} - T_{s,i}) = 0, \text{ [W or Btu/hr]} \quad (5.10)$$

where, $h_{c,i}$ (W/m^2 K or Btu/hr ft^2 °F) is the convective heat transfer coefficient of surface *i*, A_i (m^2 or ft^2) is the area of surface *i*; $T_{s,i}$ (^{o}C or ^{o}F) is the temperature of surface *i*; and $OST_{Uniform-zones}$ (^{o}C or ^{o}F) is the OST of the "Uniform-zones" scheme.

In the "Core-zones" scheme (Figure 5.14 (c)), the average temperature of the room core (central) zones is regarded as the OST which is defined as:

$$OST_{Core-zones} = \sum T_{(i,j,k)} / N, \quad [^{o}C \text{ or } ^{o}F] \quad (5.11)$$

where, $T_{(i,j,k)}$ (^{o}C or ^{o}F) is the temperature of the zone (*i,j,k)* located at the core (center) of the room; and $OST_{Core-zones}$ (^{o}C or ^{o}F) is the OST of the "Core-zones" scheme. *N* is the number of the zones constituting the core (center) of the room.

In order to estimate the appropriate thermostat set point as well as the corresponding energy consumption, the OST should be predefined, similarly as the predefined indoor design temperature in the single/multi-zone thermal models. This predefined OST represents the

intended temperature of the occupied space in consideration of the occupants' comfort and should be determined based on standards, such as ASHRAE Standard 55 (2004). Therefore, from this point of view, the predefined OST can be also called Objective Temperature (OT).

This integrated thermal model is able to estimate the appropriate thermostat set point that makes the specified point or region (according to different schemes) meet the predefined OST, whereas, the thermal behaviors of the other points or regions in the room are not concerned.

5.1.5.1.2 Description of the simulation procedures. The procedure to estimate the thermostat set points and the corresponding required heating energy for the room space, $\dot{q}_{heating}$, i.e. $\dot{q}_{loss2}$ (assuming that the heat loss of the floor plenum $\dot{q}_{loss1}$ is ignored in this application), are described as follows:

- Step 1: Selections of the OT value and the thermostat position

The values of OT considered in our cases are selected. The selection is based on criteria, such as economic, comfortable or other considerations. Usually, the OT value, for economic reasons, is 20^{o}C (68 ^{o}F) (ASHRAE Standard 55, 2004). In this work, three values of OT are investigated, 18^{o}C (64.4 ^{o}F), 20^{o}C (68 ^{o}F), and 22^{o}C (71.6 ^{o}F).

Actually, any subdivision of the room in the coupled zonal model is a potential thermostat location. An accurate thermostat location that reflects the actual situation contributes to improving the reliability of prediction results. The thermostat location considered in this application is displayed in the figure 5.6.

- Step 2: Determination of the thermostat set point

The predefined values of the OST, which are the OT values in Step 1, will be approached by gradually adjusting the supply airflow rate (energy-effect parameter) of an UFAD system (the supply air temperature maintains a constant value shown in Step 3), when the integrated thermal

model is utilized to predict the temperature distributions corresponding to the different schemes, “Uniform-zones”, “Core-zones”, and “Occupied-zones”. When the predefined OST value is reached, the current temperature value of the zone where the thermostat is located is regarded as the thermostat set point, and the temperature difference between the occupied space and the thermostat position may be determined as well.

- Step 3: Computation of the required heating energy

Once the thermostat set point was determined in Step 2, the required heating energy $\dot{q}_{heating}$ for the room space (Figure 5.11) will be calculated using the relation as follows:

$$\dot{q}_{heating} = \dot{m}_s cp(T_{in} - T_{out}), \text{ [W or Btu/hr]} \quad (5.12)$$

where $\dot{m}_s$ (kg/s or lbm/s) is the current supply airflow rate from the diffuser; cp (J/kg K or Btu/lbm ^{o}F) is the specific heat; T_{in} (^{o}C or ^{o}F) is the supply air temperature that is a constant (32.2^{o}C or 90 ^{o}F); and T_{out} (^{o}C or ^{o}F) is the return temperature which is the air temperature of the zone that is close to the return opening. T_{out} is sensitive to many factors, such as thermostat locations, diffuser locations, house envelop and constructions, outdoor weather conditions, and so on.

In a simulation, these three steps will be repeated at every time step to compute the hourly thermostat set point and required heating energy.

5.1.5.1.3 Case studies. In this application, three cases have been studied, using the aforementioned integrated thermal model and simulation procedures, in order to estimate the appropriate thermostat set points and the corresponding heating energy, and also to investigate how the room thermostat set points affect the required heating energy and indoor thermal comfort.

In this simulation, the room is evenly subdivided into 200 zones (5×5×8) by using the integrated thermal model. Therefore, $T_{(i,j,k)}$ represents the air temperature of the zone (*i,j,k),* where *i* =1~5, *j* = 1~5, and *k* = 1~8.

For the "Core-zones" scheme, the average temperature of the room core zones, (2,3,4), (2,3,5), (3,3,4), (3,3,5), (4,3,4), and (4,3,5), is regarded as the OST which is defined as:

$$OST_{Core-zones} = (T_{(2,3,4)} + T_{(2,3,5)} + T_{(3,3,4)} + T_{(3,3,5)} + T_{(4,3,4)} + T_{(4,3,5)})/6. \ [^{o}C \text{ or } ^{o}F] \quad (5.13)$$

For the "Occupied-zones" scheme, the average temperature of the occupied space (the average temperature of the *M* = 63 zones constituting the occupied space) is the OST which is defined as:

$$OST_{Occupied-zones} = (\sum T_{(i,j,k)})/M, \ [^{o}C \text{ or } ^{o}F] \quad (5.14)$$

where *i* and *j* varies from 2 to 4, and *k* varies from 1 to 7.

The three cases are studied considering a constant supply air temperature (32.2^{o}C or 90 ^{o}F) of the UFAD system and three different OT values (18^{o}C (64.4 ^{o}F) – Case 1, 20^{o}C (68 ^{o}F) – Case 2, and 22^{o}C (71.6 ^{o}F) – Case 3) corresponding to these three case studies.

5.1.5.1.4 Simulation results. Figure 5.15, 5.21, and 5.27 display the thermostat set points of the different schemes ("Uniform-zones", "Core-zones", and "Occupied-zones") for the cases 1, 2, and 3, respectively. Figure 5.16, 5.22, and 5.28 display the temperature differences between the OTs (various OST schemes) and the thermostat set points (the temperature at the thermostat location) of the cases 1, 2, and 3, respectively. Figure 5.17 (Case 1), 5.23 (Case 2), and 5.29 (Case 3) show the corresponding required heating energy of these different schemes and the one-zone model. Figure 5.18, 5.19, and 5.20 display the zonal and one-zone PMV profiles of these three schemes, "Uniform-zones", "Core-zones", and "Occupied-zones", respectively, of the case 1; Figure 5.24, 5.25, and 5.26 display the zonal and one-zone PMV profiles of these different

schemes of the case 2; and Figure 5.30, 5.31, and 5.32 display the zonal and one-zone PMV profiles of these different schemes of the case 3. In these figures of the cases 1, 2 and 3, the "One-zone" represents the results of the conventional single/multi-zone thermal model.

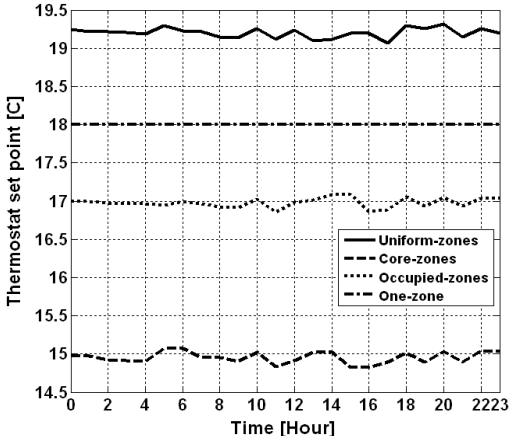

Figure 5.15 Thermostat set points of Case 1

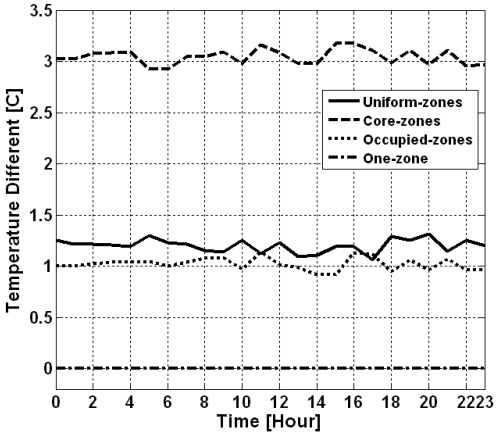

Figure 5.16 Temperature differences between the thermostat set points and the OTs of Case 1

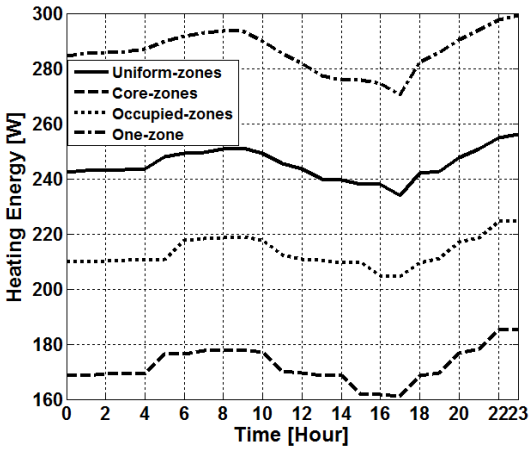

Figure 5.17 Required heating energy of Case 1

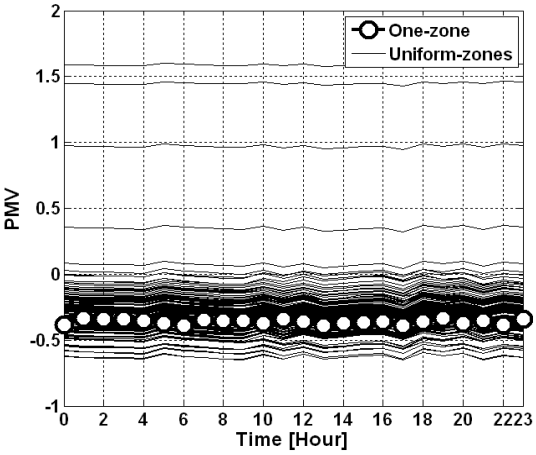

Figure 5.18 PMVs for the "Uniform-zones" scheme of Case 1

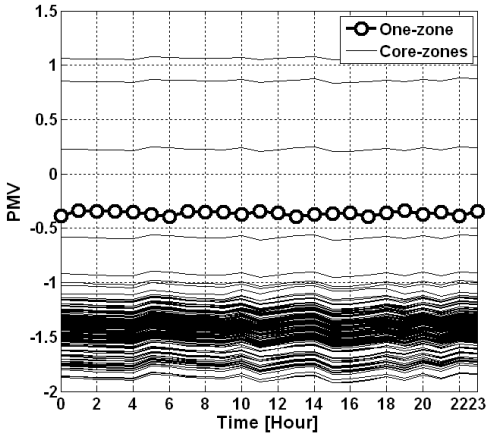

Figure 5.19 PMVs for the "Core-zones" scheme of Case 1

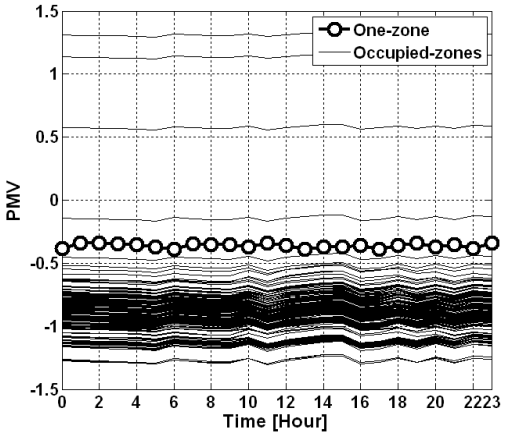

Figure 5.20 PMVs for the "Occupied-zones" scheme of Case 1

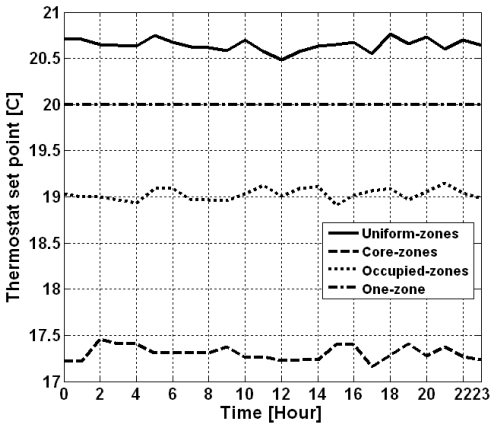

Figure 5.21 Thermostat set points of Case 2

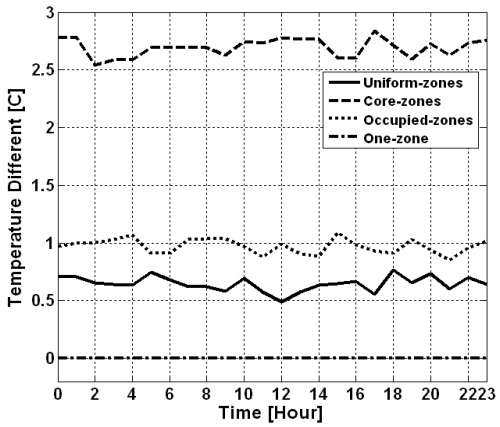

Figure 5.22 Temperature differences between the thermostat set points and the OTs of Case 2

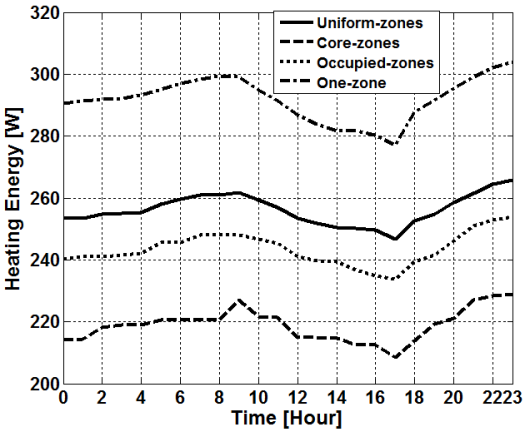

Figure 5.23 Required heating energy of Case 2

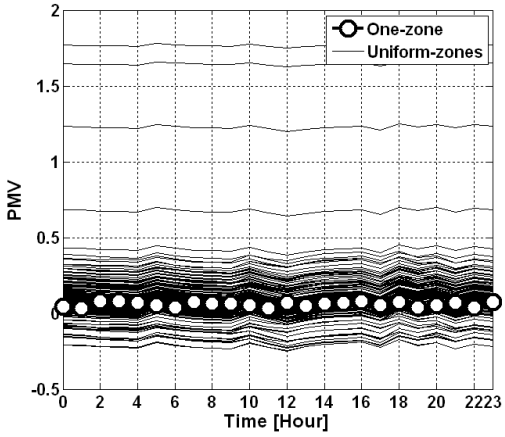

Figure 5.24 PMVs for the "Uniform-zones" scheme of Case 2

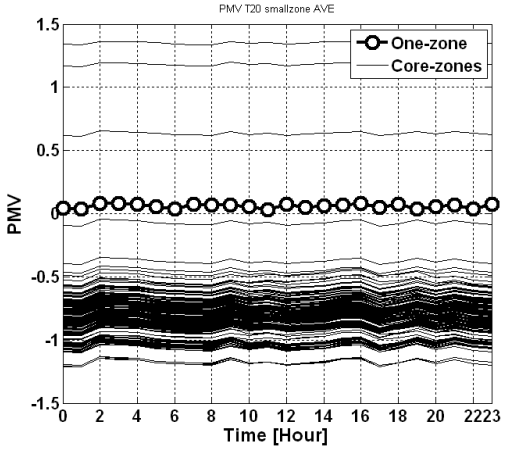

Figure 5.25 PMVs for the "Core-zones" scheme of Case 2

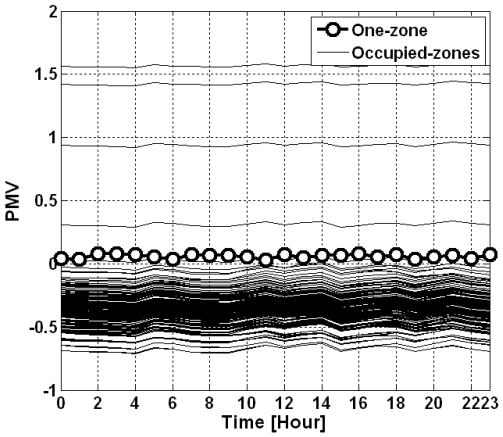

Figure 5.26 PMVs for the "Occupied-zones" scheme of Case 2

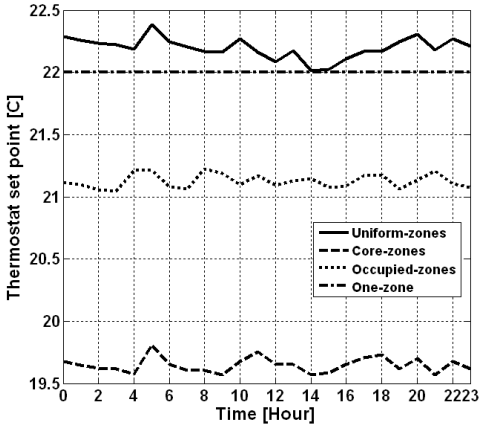

Figure 5.27 Thermostat set points of Case 3

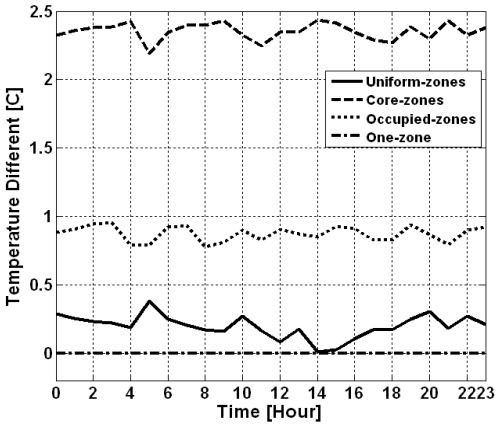

Figure 5.28 Temperature differences between the thermostat set points and the OTs of Case 3

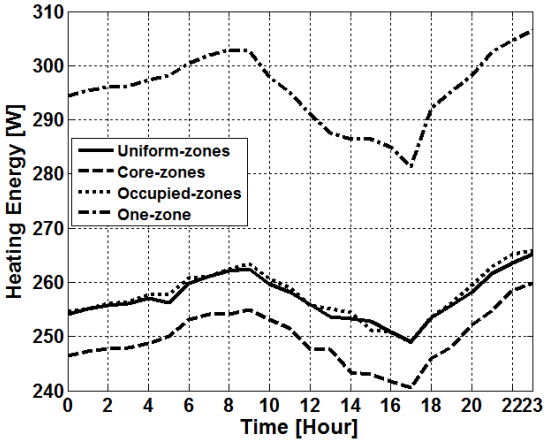

Figure 5.29 Required heating energy of Case 3

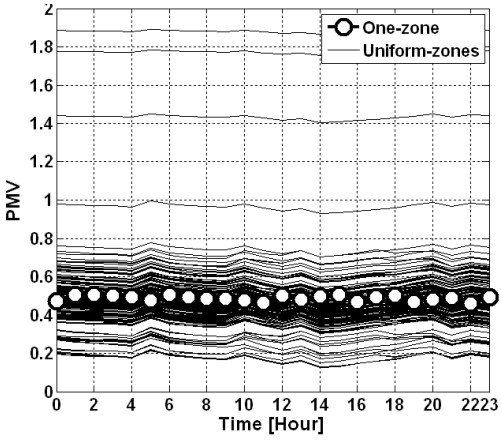

Figure 5.30 PMVs for the "Uniform-zones" scheme of Case 3

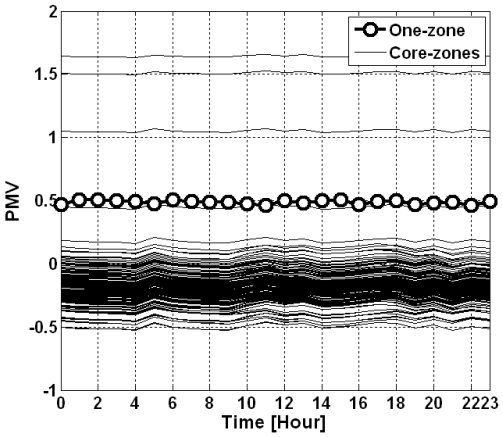

Figure 5.31 PMVs for the "Core-zones" scheme of Case 3

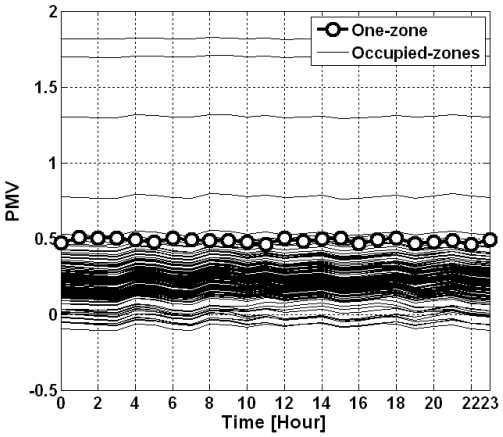

Figure 5.32 PMVs for the "Occupied-zones" scheme of Case 3

As shown in the figures 5.15, 5.21, and 5.27, the different OST schemes and OT values account for the different thermostat set point profiles. These thermostat set points are higher or lower than the corresponding OT values, depending on the different OST schemes ("Uniform-zones", "Core-zones", and "Occupied-zones"). When the "Core-zones" scheme is used, the thermostat set points have the lowest values, since this scheme considers only the central zones in the calculation of OST, thus a significant temperature difference between the center (OT) and the perimeter space (thermostat set point) of the room exists (Figure 5.16, 5.22, and 5.28). When the involved zone number for OST scheme calculations is increased, such as the "Uniform-zones" and "Occupied-zones" schemes, the thermostat set points are approaching the result of the conventional single/multi-zone thermal models, especially for the "Uniform-zones" scheme. In the conventional single/multi-zone thermal models, constant set point temperatures are utilized, and thus there is no difference between the thermostat set point and the OT, as shown in the figures 5.16, 5.22, and 5.28. In these figures, significant temperature differences are observed especially when the "Core-zones" scheme is used. These figures also reflect the different levels of the uniformity of the room temperature distribution when diverse OST schemes applied. From

the figures 5.16, 5.22, and 5.28, as the OT values increase from 18^{o}C (64.4 ^{o}F) to 22^{o}C (71.6 ^{o}F), the magnitudes of the temperature differences of these three schemes decrease. This implies that, in these cases, higher OT values may lead to more uniform room temperature distributions.

As shown in the figures 5.17, 5.23, and 5.29, the conventional single/multi-zone thermal models always give the highest heating energy, even though its thermostat set point is not at its highest value. These significant differences of required heating energy between the conventional single/multi-zone models and the integrated model are caused by the simplified method used by the single/multi-zone models at the level of thermal and airflow modeling. In the conventional single/multi-zone thermal models, a uniform environment is assumed, in which air is perfectly mixed. The difference between these two models is even more important when significant temperature gradients exist in a space. Additionally, although, in these three cases, the "Core-zones" scheme always gives the lowest heating energy (Figure 5.17, 5.23, and 5.29), it causes an uncomfortable indoor environment, especially when the OT value is low (18^{o}C or 64.4 ^{o}F). When a high OT value is used (22^{o}C or 71.6 ^{o}F), an acceptable indoor environment is created by the "Core-zones" scheme, and the corresponding heating energy are also lower than the other two schemes.

The PMV index profiles of these three cases show that, in consideration of thermal comfort, the "Uniform-zones" scheme is preferred for use (especially for a room characterized by a significantly non-uniform temperature distribution) when the OT value is low, like 18^{o}C (64.4 ^{o}F). Higher OT values, i.e. 22^{o}C (71.6 ^{o}F), are needed, when the "Core-zones" scheme is used. The results of the "Occupied-zones" scheme have intermediate values between the results of the other two schemes. The PMV results of the conventional single/multi-zone thermal models seem to be in between the PMV values of the "Uniform-zones" scheme in these three cases. It is

difficult to conclude about the best scheme that needs to be used. In various circumstances, adjusting the design OT values and using different schemes is a suggested method to optimize the thermostat set points and then to achieve less HVAC system energy consumption or a comfortable environment, or both, as required by the designer. Therefore, for these three cases, the OT = 20^{o}C (68^{o}F) with the "Uniform-zones" scheme is suggested if the indoor thermal comfort levels are critical; otherwise, the OT = 18^{o}C (64.4^{o}F) with the "Uniform-zones" scheme, the OT = 20^{o}C (68^{o}F) with the "Occupied-zones" scheme, or the OT = 22^{o}C (71.6 ^{o}F) with the "Core-zones" scheme is suggested for energy saving consideration.

The results and discussions mentioned above demonstrate the heating performance and feasibility of an UFAD system used in a residential house. Further investigations of the performance of an UFAD system under heating operation will be carried out in the following application where the comparison of this system with an overhead air distribution system in terms of required heating energy and thermal comfort will be performed.

5.1.5.1.5 Summary. In this application, a temperature control strategy, along with three different schemes, "Uniform-zones", "Core-zones", and "Occupied-zones", has been investigated through three case studies, in which different OTs have been considered, in order to determine the appropriate thermostat set points, room required heating energy, and thermal comfort indices (PMV) of an UFAD system applied in a one-room residential house.

After the comparisons and analysis of the results, we conclude that at the building design stage:

- If a room is characterized by a significantly non-uniform temperature distribution, the "Uniform-zones" scheme is preferred for use, especially when the design OT value is low, like 18^{o}C (64.4^{o}F), for winter seasons. If the "Core-zones" scheme is

applied in this situation, analysis and simulations are needed to determine the appropriate OT, instead of the common value 20^{o}C (68^{o}F). Otherwise, an uncomfortable environment would be created.

- The existence of the difference between the OT and the thermostat-position temperature has been proved. This difference increases, when the temperature distribution becomes non-uniform.
- The conventional well-mixed single/multi-zone model in building energy prediction is not appropriate to use for UFAD systems. Instead, a detailed air model, such as the zonal model POMA, should be applied.

Besides, this integrated thermal model may be used when the building is under operation. For example, the information, such as the thermostat set points determined by using the approach mentioned in this section, can be obtained at the design stage through pre-simulations considering different factors that can affect the indoor air thermal behaviors, such as outdoor weather conditions, thermostat locations, the characteristics of HVAC system diffusers, or even people's activities. The results from these pre-simulations may be stored as a data base in the BMS of a building. When the building is under operation, the BMS may compute the appropriate set point for every room space, based on the current room thermostat feedback and the information included in the data base. This set point is not only able to maintain a desirable comfort level in the occupied space, but also to optimize the energy consumption, as designed at the design stage. The more factors considered in the pre-simulations, the more accurate results from the BMS are achieved.

Moreover, this integration approach may be utilized in existing buildings to correct the unreasonably high energy bills and/or to deal with occupants' complaints regarding discomfort by resetting the thermostat set points without making significant changes and retrofits.

5.1.5.2 The second application – the prediction of required heating energy corresponding to different thermostat locations. In this application, two cases considering different slab-on-grade floor constructions have been studied. The thermal characteristics of the four external walls, the floor, as well as the roof used in the first case study are presented in the tables 5.3 and 5.4. In the second case study, the same thermal characteristics of the four external walls (Table 5.3), the raised floor, and the roof (Table 5.4) are utilized; while the U-value of the slab-on-grade floor construction is changed from 0.313 to 0.834 (W/m^2 K) (0.055 to 0.15 Btu/hr ft^2 ^oF) as a consequence of the absence of insulation materials. In these two cases, the thermostat set point is assumed as a constant, i.e. 20^{o}C (68 ^{o}F), and 200 subdivisions are used in the integrated thermal model.

5.1.5.2.1 Description of the simulation procedures. In this simulation, the developed integrated thermal model is used to estimate the hourly required heating energy of the residential building and to quantify the impact of the different thermostat locations on the building heating energy. The simulation procedure is described below:

- Step 1: Selection of the supply air temperature for the room space (Figure 5.11)

A supply air temperature for the residential house under heating operation needs to be selected. In consideration of the characteristics of UFAD systems and the thermal comfort of the occupants, a constant supply air temperature 29.4^{o}C (85^{o}F) from the floor diffuser is selected for this application. Although a higher temperature is acceptable, it may cause draft and discomfort of the occupants (ASHRAE Standard 55, 2004).

- Step 2: Selection of the location of thermostat

Typically, the thermostat location in a space is defined using the mesh grid of the simulation model. Any zone or subdivision within the space may be used for the thermostat location. A typical thermostat location (shown in the figure 5.6) is considered in this application. Several zones vertically above the floor diffuser are not considered as the thermostat locations, since the heating energy results would be close to zero.

- Step 3: Determination of the Design Temperature Distribution (DTD)

In order to be able to use the integrated thermal model to predict the heating energy, a new concept needs to be introduced, which is equivalent to the concept of the Indoor Design Temperature (IDT) of the conventional single/multi-zone thermal model. Unlike the IDT of the single/multi-zone thermal model, this new concept uses an intended temperature distribution, instead of a single value, to represent the indoor design temperatures. This intended temperature distribution is called Design Temperature Distribution (DTD) that can be used to determine the hourly required heating energy of the house. In fact, DTD has the same meaning with the IDT of the single/multi-zone thermal model. The only difference between them is that, IDT is a single temperature value representing the average air temperature of the room, while DTD is a temperature distribution calculated by using the integrated thermal model.

For the IDT of the single/multi-zone thermal model, it is easy to be determined, for example 20^{o}C (68^{o}F) (ASHRAE Fundamentals, 2005; ASHRAE Standard 55, 2004). However, the pre-determination of DTD is not as simple as the determination of IDT. DTD is sensitive to many factors, such as the location of thermostat, the type of HVAC system, etc. Different HVAC systems or various thermostat locations would have distinct DTDs. The approach to determine the DTD of an UFAD system is shown below.

The supply airflow rate (energy-effect parameter) of the UFAD system (the supply air temperature maintains a constant value shown in Step 1) is adjusted (increased or decreased) gradually. When the supply airflow rate changed, the room thermal behaviors, i.e. the room air temperature distributions, would be changed as well. Therefore, for each airflow rate, there is a corresponding room air temperature distribution profile predicted using the integrated thermal model. In particular, the air temperature of the zone where the thermostat is located is observed. As soon as this zone air temperature is equal to the thermostat set temperature, for example 20^{o}C (68^{o}F), the current air temperature distribution profile is used as the DTD for this time step, and the corresponding supply airflow rate is regarded as the room supply airflow requirement.

- Step 4: Calculation of the hourly required heating energy of the room space (i.e. $\dot{q}_{loss2}$ shown in Figure 5.11)

Once the DTD was obtained in Step 3, the required heating energy $\dot{q}_{heating}$ can be calculated using the equation,

$$\dot{q}_{heating} = \dot{m}_s cp(T_{in} - T_{out}) \qquad \text{[W or Btu/hr]} \ , \qquad (5.15)$$

where $\dot{m}_s$ (kg/s or lbm/s) is the supply airflow rate from the diffuser, which was determined in Step 3; *cp* (J/kg K or Btu/lbm ^{o}F) is the specific heat; T_{in} (^{o}C or ^{o}F) is the supply air temperature that is a constant and equal to 29.4^{o}C (85^{o}F) determined in Step 1; and T_{out} (^{o}C or ^{o}F) is the return air temperature based on the current DTD, which is the air temperature of the zone that is close to the return opening and is obtained from the integrated thermal model.

- Step 5: Calculation of the total required heating energy $\dot{q}_{system}$ of the house (i.e. the room space $\dot{q}_{loss2}$ + floor plenum space $\dot{q}_{loss1}$ (Figure 5.11))

To determine the required heating energy of the floor plenum space, a similar procedure as mentioned in Step 3 and 4 can be applied. In this procedure, instead of the supply airflow rate, the supply air temperature (energy-effect parameter) of the floor plenum from the outlet of the

air conditioning unit is adjusted gradually and needs to be determined. The supply airflow rate, which was determined in Step 3 and the leaving air temperature of the floor plenum, which was determined in Step 1 and regarded as the supply air temperature of the room space, i.e. 29.4^{o}C (85^{o}F), are known. Therefore, for each supply air temperature of the floor plenum space, a corresponding leaving air temperature of this space can be predicted by using the multi-zone thermal model. As soon as the predicted leaving air temperature is equal to 29.4^{o}C (85^{o}F), the current supply air temperature will be determined for this floor plenum space. Then, using the equation 5.15, the required heating energy of the floor plenum space can be calculated. Finally, the total heating energy $\dot{q}_{system}$of the entire house can be computed by the summation of the required heating energy for both the room space and the floor plenum.

These steps for various thermostat locations and different time steps can be repeated, if needed. The flowchart in the figure 5.33 demonstrates this procedure.

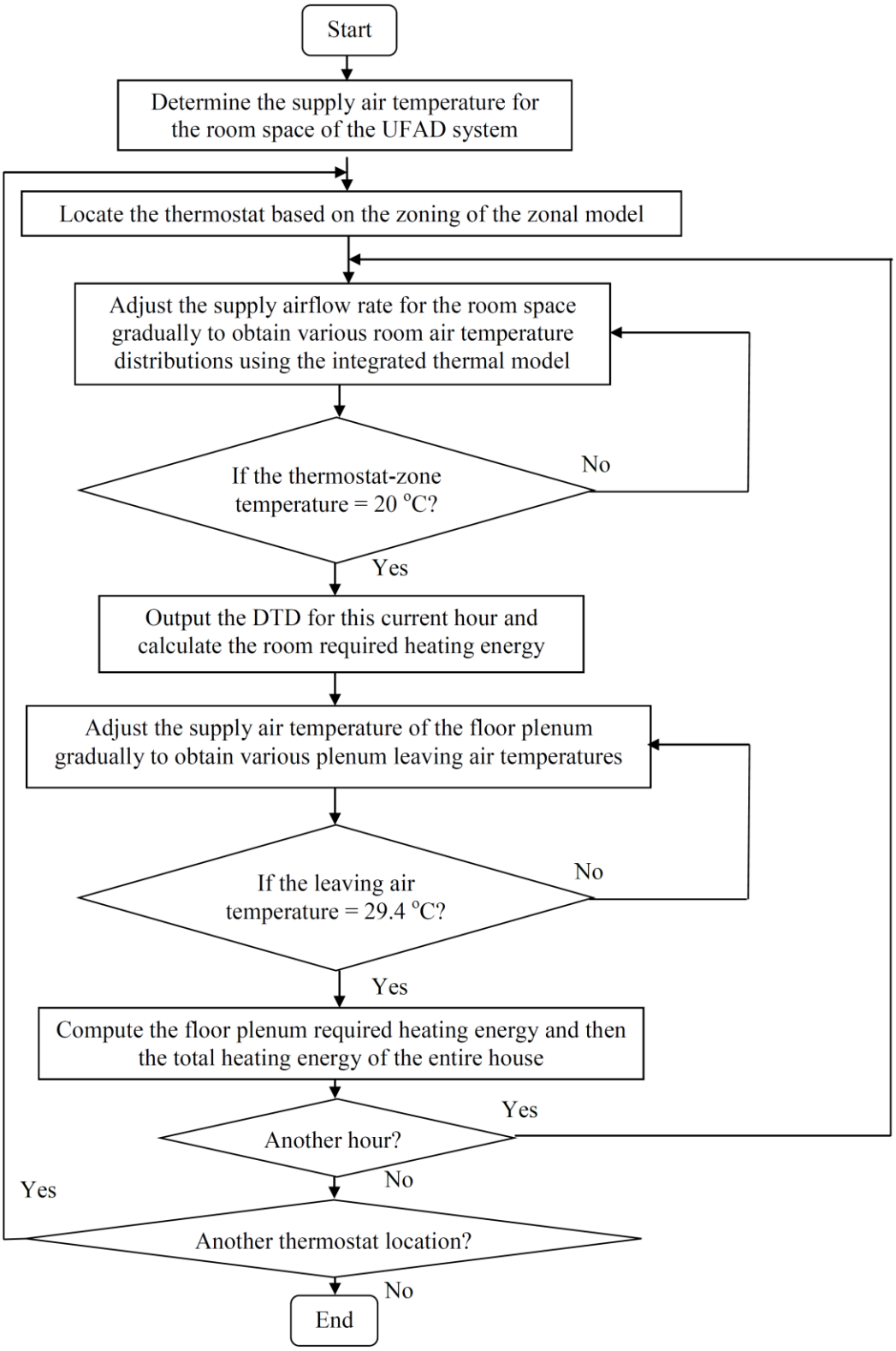

Figure 5.33 Flow chart of the simulation procedure

5.1.5.2.2 Results and discussions. The results of the cases 1 and 2 are shown below. In the figures 5.34 and 5.35, "Single Zone" represents the required heating energy result of the conventional single/multi-zone thermal model, which is equivalent to $\dot{q}_{loss}$ in the figure 5.10; "Single Zone Rm+Plnm" represents the result of the total required heating energy of the room and plenum, which is equivalent to $\dot{q}_{loss1} + \dot{q}_{loss2}$ in the figure 5.11 and is calculated by applying the conventional single/multi-zone thermal model to the room space and the floor plenum respectively; "Typical thermostat location Rm+Plnm" represents the required heating energy summation of the room and plenum when the thermostat is located at the typical position (Figure 5.6) and applying the integrated thermal model to the room space and the single/multi-zone thermal model to the plenum; and "Different thermostat locations Rm+Plnm" represents the different required heating energy summations of the room and plenum according to different thermostat positions, applying the integrated thermal model to the room space and the single/multi-zone thermal model to the plenum. In the figures from 5.34 to 5.41, if they are not specified, these above-mentioned terminologies keep the similar meanings in terms of the use of the corresponding simulation model, i.e. "Single Zone" represents the use of the single/multi-zone thermal model to the entire house; "Single Zone Rm+Plnm" represents the use of the single/multi-zone thermal model to the room space and the floor plenum respectively; "Typical thermostat location Rm+Plnm" represents the use of the integrated thermal model to the room space and the single/multi-zone thermal model to the plenum, when the thermostat is located at the typical position (Figure 5.6); and "Different thermostat locations Rm+Plnm" represents the use of the integrated thermal model to the room space and the single/multi-zone thermal model to the plenum considering different thermostat positions.

The required heating energy of the cases 1 and 2 are displayed in the figures 5.34 and 5.35, respectively. Different thermostat locations account for various heating energy behaviors. Additionally, the results of "Single zone" ($\dot{q}_{loss}$) and "Single zone Rm+Plnm" ($\dot{q}_{loss1} + \dot{q}_{loss2}$) are different, demonstrating that the conventional single/multi-zone thermal model is not able to accurately predict the required heating energy of the UFAD system if considering the entire room as a whole (Figure 5.10). In these two figures, the results of "Single zone" show that the conventional method that is suitable for overhead air distribution systems can significantly overestimate the heating energy for the UFAD system, which can lead to a wrong HVAC system sizing. Although the "Single zone Rm+Plnm" model that treats the entire room into two separated spaces (the room space and the plenum) gives relatively reasonable results, it still overestimates the required heating energy in comparison with the results of "Typical thermostat location Rm+Plnm". Compared to the results of the case 1 (Figure 5.34), higher heating energy are observed for the case 2 (Figure 5.35) because of the poor slab-on-grade floor construction and the absence of insulation materials in the case 2. Moreover, in comparison of the figure 5.34 with 5.35, the results of either "Single Zone Rm+Plnm" or "Typical thermostat location Rm+Plnm" between these two figures demonstrate an 15% difference in terms of heating energy, and an 8% difference for the "Single Zone" results. Therefore, it is concluded that about 15% heating energy is able to be saved in the UFAD system under heating operation if the slab-on-grade floor construction of the residential house is well thermally protected. This implies that, for UFAD systems used in residential houses, the slab-on-grade floor construction plays a significant role in energy saving, and designers should pay more attention to the thermal protection of the floor construction, especially considering the possibility of condensation issues.

Figure 5.36 and 5.37 demonstrate the calculated supply airflow requirements for the cases 1 and 2, respectively. In these two figures, compared to the “Single Zone” airflow rates, only about a half of the supply airflow rates are needed for the UFAD system when the room space and the plenum are treated separately in the calculations. This implies that about a half of supply airflow requirements could be reduced, if UFAD systems are applied compared to the conventional overhead air distribution method. The airflow rate differences of the “Single zone” results between the figures 5.36 and 5.37 are caused by the different slab-on-grade floor constructions. The similarity of the airflow rate results of “Single zone Rm+Plnm”, “Typical thermostat location Rm+Plnm”, and “Different thermostat locations Rm+Plnm” between these two figures are due to the fact that, when the entire room is separated into two spaces (the room space and the plenum), only the plenum is significantly thermally influenced by the slab-on-grade floor construction, while the thermal behaviors of the above room space are not evidently disturbed. Therefore, even though the slab-on-grade floor construction is changed in the case 2, the supply airflow requirement for the above room space is not affected significantly between these two cases.

The “Single zone Rm+Plnm” in the figures 5.38 (Case 1) and 5.39 (Case 2) represents the required heating energy ratio of the “Single zone” to the “Single zone Rm+Plnm” results shown in the figures 5.34 and 5.35; and “Typical thermostat location Rm+Plnm” represents the required heating energy ratio of the “Single zone” to the “Typical thermostat location Rm+Plnm” results shown in the figures 5.34 and 5.35. The figures 5.38 and 5.39 indicate that the required heating energy for the UFAD system can be approximately 25% less than that for the conventional overhead air distribution system in the well-insulated house (Case 1), and 17% less if the house is poorly insulated (Case 2), when the “Typical thermostat location Rm+Plnm” results are

considered. These values become 20% less for the well-insulated house (Case 1) and 13% less for the poorly insulated house (Case 2), when the "Single Zone Rm+Plnm" results are considered. The less heating energy demonstrates the potential energy savings using UFAD systems instead of overhead air distribution systems in residential houses.

The figures 5.40 and 5.41 show the zonal PMV and PPD profiles of the room space respectively, when the thermostat is located at the typical location (Figure 5.6). These two figures are for either the case 1 or 2, because, as mentioned above, the thermal behaviors of the room space are not significantly thermally influenced by the slab-on-grade floor construction, and thus the room-space PMV/PPD profiles for both the cases 1 and 2 are very close. In these two figures, these PMV and PPD profiles display that, for several zones, the PMV values are high and reach up to 1.2 (PPD: 35%), due to the fact that these zones are close to the floor diffuser. In addition, the majority of the PMV index values of the other zones are near the neutral point (around zero), demonstrating a comfortable environment within the room space when the UFAD system is applied. However, the "Single zone" PMV/PPD results in both the figures 5.40 and 5.41 indicate a slightly uncomfortable environment (-0.4 for PMV) within the entire room space when the conventional overhead system is used.

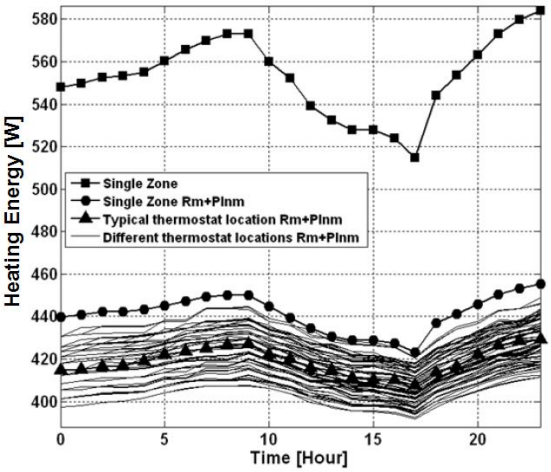

Figure 5.34 Required heating energy of the case 1

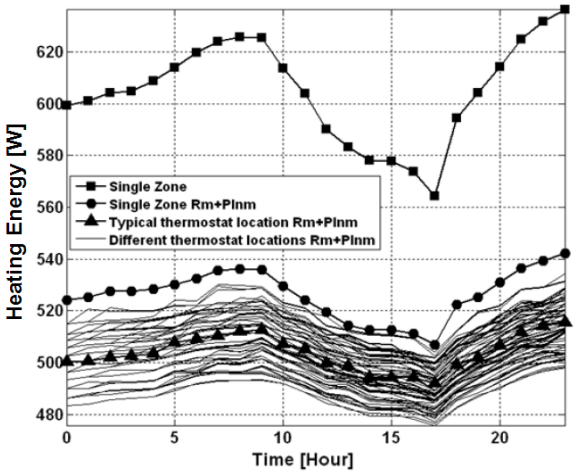

Figure 5.35 Required heating energy of the case 2

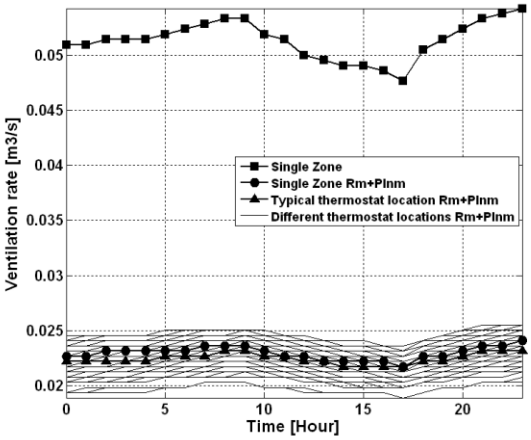

Figure 5.36 Supply airflow rate requirements of the case 1

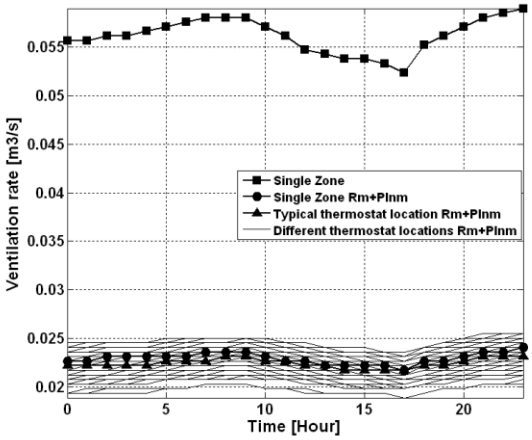

Figure 5.37 Supply airflow rate requirements of the case 2

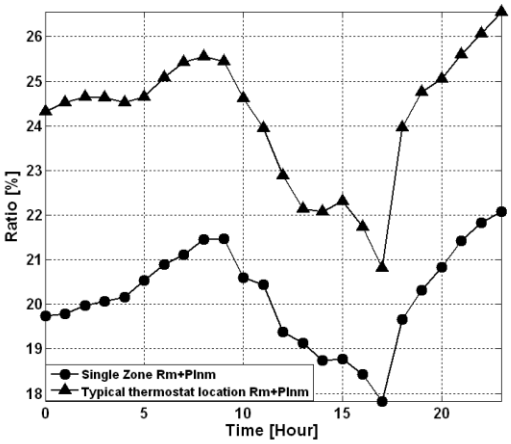

Figure 5.38 Required heating energy ratio of the case 1

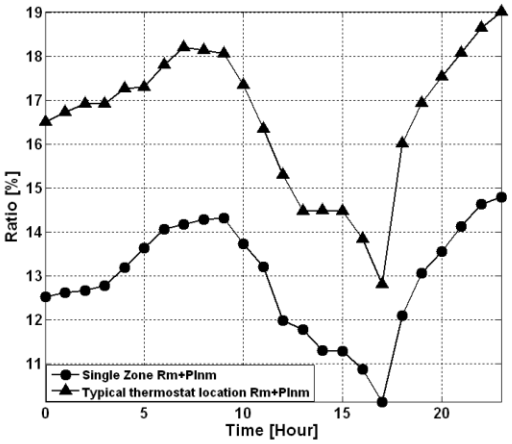

Figure 5.39 Required heating energy ratio of the case 2

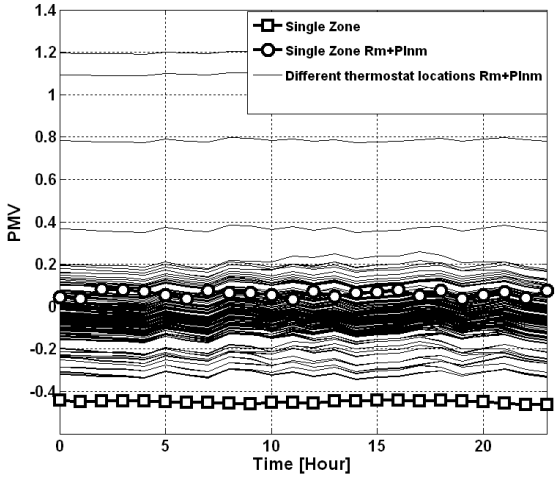

Figure 5.40 Room-space PMV profiles of the typical thermostat location

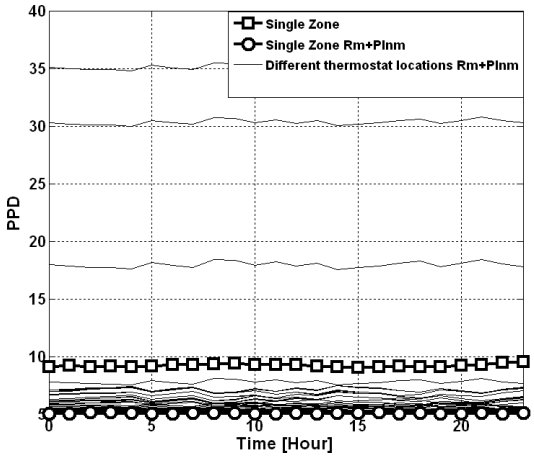

Figure 5.41 Room-space PPD profiles of the typical thermostat location

5.1.5.2.3 Summary. The case studies using the integrated thermal model have revealed the importance of detailed room air models for predicting building heating energy and have demonstrated the needs of substituting the use of conventional single/multi-zone models. The heating energy calculations for UFAD systems have been optimized by geometrically subdividing a room into several zones in the integrated thermal model and then by investigating the appropriate thermostat locations for either energy savings or better people's comfort levels.

The analysis performed show that,

- The conventional well-mixed single/multi-zone thermal method is not appropriate to use for UFAD systems in building heating energy predictions. Otherwise, as shown in the case study of this application, the overestimations in terms of heating energy (about 25% for the case 1 and 17% for the case 2) may occur. Therefore, advanced airflow models, such as zonal models, need to be used.

- When an UFAD system is applied in a residential house for heating purposes in winter, the house slab-on-grade floor construction needs to be well insulated in order to avoid excessive

heat losses. Otherwise, as shown in the case study, approximately 15% higher heating energy is required for the poorly insulated floor construction case.

- Compared to a conventional overhead air distribution system, an UFAD system has the potential to reduce the room supply airflow requirements, when it is applied under heating operation in a residential house, regardless of the ventilation requirements of codes and standards. The reduction of the room airflow requirement for the UFAD system may be around 50%, as shown in the figures 5.36 and 5.37. Furthermore, these potential savings in terms of room supply airflow requirement account for the significant savings in terms of heating energy, i.e. about 25% for the well thermally protected house and about 17% for the poorly insulated house, as shown in the figures 5.38 and 5.39, respectively.

- The predictions of PMV and PPD have shown that a more comfortable environment (around 0 for PMV) may be created using an UFAD system than a conventional overhead air distribution system (-0.4 for PMV) under heating operation in the residential house.

- The different thermostat locations indeed affect the building energy consumption/load, as shown in the figures 5.34 and 5.35. As a matter of fact, thermostat location is an important factor, which influences building energy/load, room ventilation requirements, human thermal comfort, and even the effectiveness of HVAC systems. Therefore, designers or researchers should pay more attention to the impacts of thermostat location in building energy design/simulation.

5.2 Predictions of Thermostat Set Point and Design Heating Load for Energy Saving and/or Better Indoor Thermal Comfort of a General Heating System – Natural Convection Cases

In this section, the integrated thermal model that has the ability to simulate a general heating system has been developed, described, validated, and then used to quantify the temperature difference between the occupied space and the thermostat position, under several building construction situations. The factors that influence the magnitude of this temperature difference have been also investigated. Additionally, the characteristics of this integrated thermal model to perform calculations related to building load and energy consumption according to different thermostat locations have been demonstrated, which make the optimization of thermostat location, i.e. the determination of the thermostat locations associated with the highest or lowest energy consumption, possible at the design stage for the sake of the achievement of building energy savings and/or the improvement of people's thermal comfort levels. Several case studies considering different types of building constructions of a residential house have been included.

5.2.1 Model description and validation. Unlike the forced air distribution system, a general heating system stands for a natural convection air conditioning system. Therefore, in the integrated thermal model, the thermal jet flow model is not needed, since the original zonal model POMA is able to predict the thermal behavior of a room with the general heating system. Before the usage of this integrated thermal model, the reliability of the original zonal model POMA has to be verified.

The validation of the zonal model POMA is performed in terms of temperature behavior, considering three different cases. A one-room residential house with the size 3.1 m × 3.1 m × 2.5

m (10.2 ft × 10.2 ft × 8.2 ft), is considered in the validation. Table 5.5 displays the boundary conditions (surface temperatures) for these validation cases, in which the one-room residential house is subdivided into 60 zones (6×1×10) as shown in the figure 5.42, in consideration of the fact that the inside surface temperatures of the north and south walls of this house are very close, as shown in the table 5.5, and thus only one zone is used in the north-to-south direction. In the validation, no window is considered except for the case 3, in which a window with the area of 3.1 m^2 (3.1 m × 1.0 m) or 33.46 ft^2 (10.2 ft × 3.28 ft) is installed on the west wall.

Table 5.5 *Conditions used in the validations*

	North [^oC] ([^oF])	South [^oC] ([^oF])	East [^oC] ([^oF])	West [^oC] ([^oF])	Ceiling [^oC] ([^oF])	Floor [^oC] ([^oF])	West Window [^oC] ([^oF])
Case 1	20.60 (69.1)	20.58 (69.0)	20.01 (68.0)	15.97 (60.8)	20.88 (69.6)	20.90 (69.6)	No window
Case 2	20.23 (68.4)	20.20 (68.4)	19.65 (67.4)	19.65 (67.4)	20.51 (68.9)	20.54 (69.0)	No window
Case 3	21.02 (69.8)	21.00 (69.8)	20.41 (68.7)	16.20 (61.2)	21.29 (70.3)	21.31 (70.4)	8.01 (46.4)

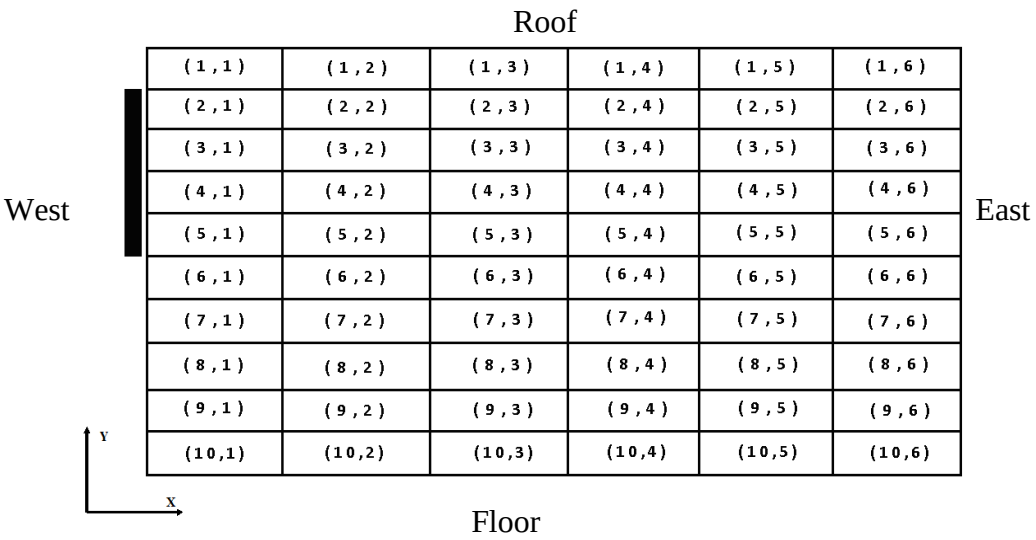

Figure 5.42 Zone divisions

These validation results corresponding to different cases are shown below, demonstrating the comparisons of temperature distribution between the zonal model and the CFD model PHOENICS (2010). The figures 5.43 and 5.44 display the temperature comparison for the case 1. The figures 5.45 and 5.46 are for the case 2; and the figures 5.47 and 5.48 are for the case 3. As shown in these figures, good agreements can be observed due to the similar patterns of the temperatures between the zonal and CFD models. This similarity verifies the ability of the zonal model to predict indoor thermal behavior of a building.

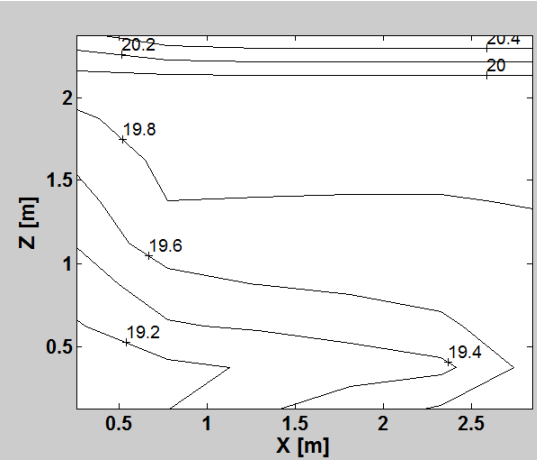

Figure 5.43 Temperature distribution [˚C] of Case 1 using zonal model (6×1×10)

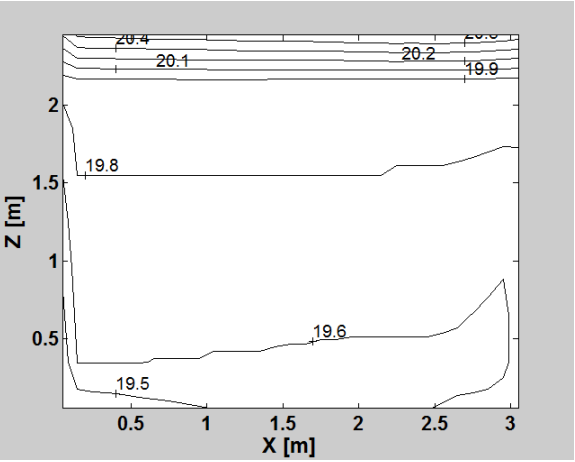

Figure 5.44 Temperature distribution [˚C] of Case 1 using CFD model PHOENICS (31×20×25)

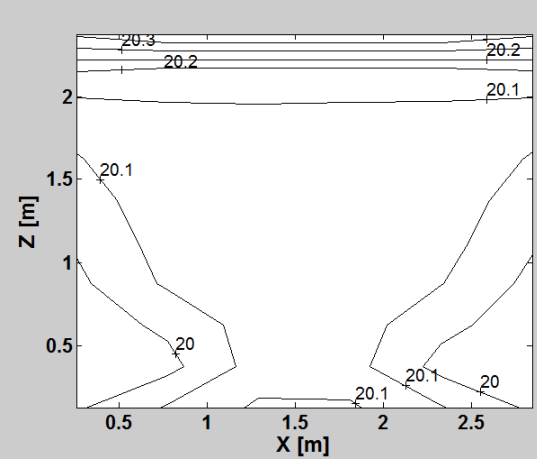

Figure 5.45 Temperature distribution [˚C] of Case 2 using zonal model (6×1×10)

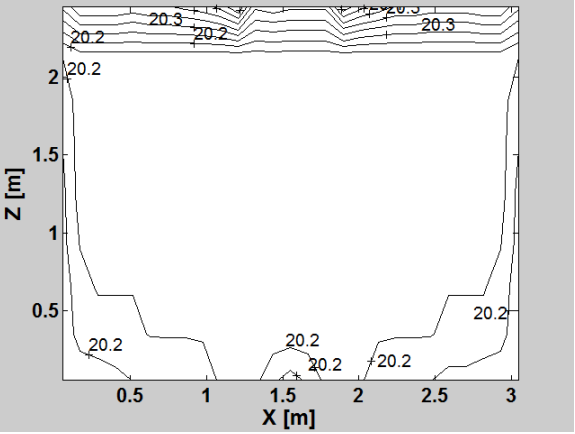

Figure 5.46 Temperature distribution [˚C] of Case 2 using CFD model PHOENICS (27×27×25)

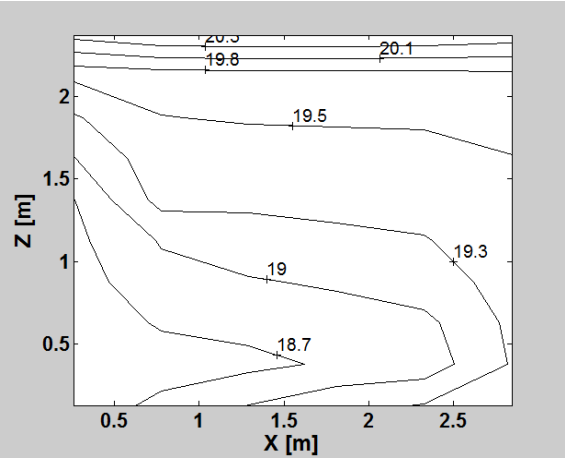

Figure 5.47 Temperature distribution [°C] of Case 3 using zonal model (6×1×10)

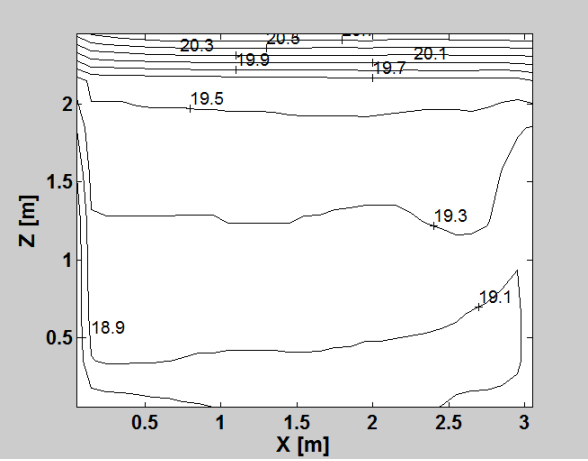

Figure 5.48 Temperature distribution [°C] of Case 3 using CFD model PHOENICS (31×20×30)

5.2.2 Basic simulation conditions for the applications. The January 1st at Geneva, Switzerland, is selected in the simulation. The figure 5.49 shows the local outdoor temperatures as well as the horizontal solar radiation on the simulation day during a typical winter season. The one-room residential house shown in the figure 5.42 is considered in the simulation with the size 3.1 m × 3.1 m × 2.5 m (10.2 ft × 10.2 ft × 8.2 ft). The preliminary simulations show that the inside surface temperatures of the north and south walls of the building are very close, and thus only one zone is applied in the north-south direction. Then, in the zonal model, this room is subdivided into 60 zones (6×1×10). Theoretically, each zone in the subdivisions can be a potential thermostat location. Thus, the location of thermostat can be any of the 60 zones shown in the figure 5.42. Also, in the figure 5.42, the location (5,6) is regarded as the typical thermostat position that is about 1.5 m (4.9 ft) above the floor and is a conventional thermostat position generally considered by HVAC designers. The infiltration and the internal gains are not considered in this simulation. A seated man with trousers and a long-sleeved shirt is assumed in the thermal comfort PMV and PPD predictions.

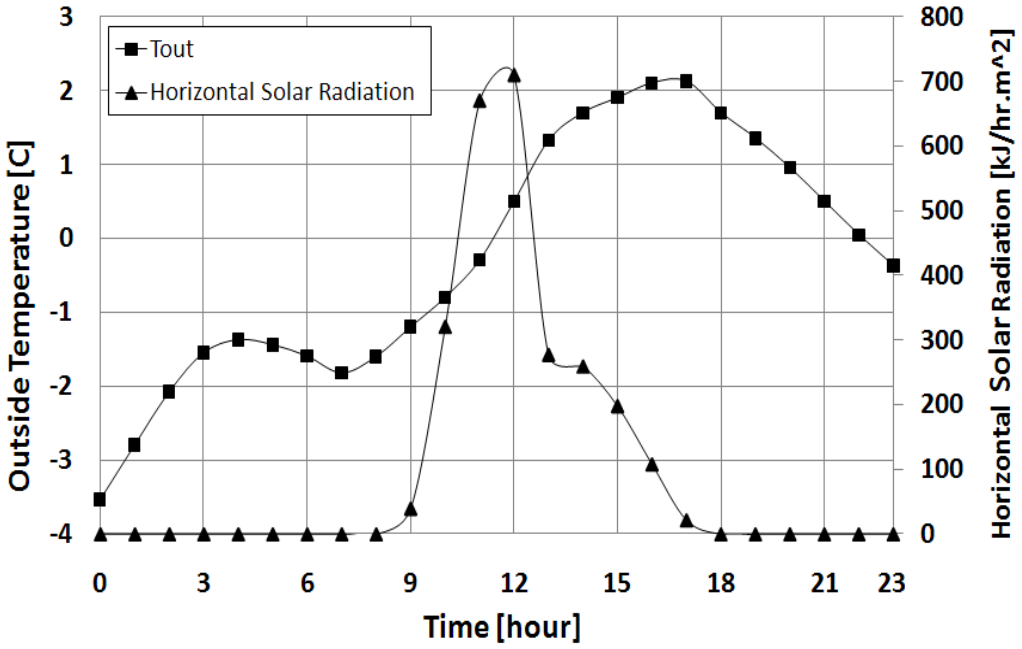

Figure 5.49 Outdoor temperatures and solar radiation

In the applications, four cases are studied, considering different house structures and constructions, in order to demonstrate the prediction ability of this integrated thermal model in terms of hourly heating load.

In the cases 1 and 2, two different thermal mass constructions (light-Case 1 and heavy-Case 2) are simulated. The thermal mass characteristics of these two building constructions are shown in the table 5.6. For these two situations (light and heavy), the overall heat transfer coefficients (U-value) of the house structures, i.e. the walls, roof, and floor, are assumed to remain constant. The thermal characteristics of the house structures are presented in the tables 5.7 and 5.8.

In the case 3, the same walls, floor, and roof of the light thermal mass construction situation (case 1) are used, except the overall heat transfer coefficient of the west wall construction which is reduced from 2.218 W/m^2 K (0.39 Btu/hr ft^2 ^oF) to 0.588 W/m^2 K (0.1 Btu/hr ft^2 ^oF), as a consequence of the addition of insulation materials on the west wall.

In the case 4, the same walls, floor, and roof of the light thermal mass construction situation (case 1) are used. Besides, a window, with the area of 3.1 m^2 (3.1 m × 1.0 m) or 33.46 ft^2 (10.2 ft × 3.28 ft), the heat transfer coefficient (U-value) of 5.68 W/m^2K (1.0 Btu/hr ft^2 ^oF), and the solar heat gain coefficient (SHGC) of 0.855, is assumed to be installed on the west wall (Figure 5.42). An ideal internal shading device is assumed to be used as well, which is capable of blocking 100% solar radiation. In other words, no solar radiation can go into the room through this window. In these four cases, no window is considered except for the case 4.

Table 5.6 *Thermal mass characteristics of building materials* (*ASHRAE Fundamentals, 2005*)

		Heavy		Light	
	Conductivity kJ/h m K (Btu/hr ft ^oF)	Specific Heat kJ/kg K (Btu/lbm ^oF)	Density kg/m^3 (lbm/ft^3)	Specific Heat kJ/kg K (Btu/lbm ^oF)	Density kg/m^3 (lbm/ft^3)
Brick	3.2 (0.51)	1 (239)	2000 (125)	0.8 (191)	1600 (100)
Insulation	0.144 (0.023)	0.8 (191)	240 (15)	0.8 (191)	40 (2.5)
Concrete	7.56 (1.21)	0.92 (220)	3000 (187)	0.8 (191)	1360 (85)

Table 5.7 *Characteristics of the external walls*

External Walls	Area m^2 (ft^2)	U-Value W/m^2 K (Btu/hr ft^2 °F)	Solar Absorptance		Convective Heat Transfer Coefficient W/m^2 K (Btu/hr ft^2 °F)	
			Inside	Outside	Inside	Outside
North	7.75 (83.4)	0.339 (0.06)	0.75	0.3	4.2 (0.74)	17.8 (3.13)
South	7.75 (83.4)	0.339 (0.06)	0.75	0.3	4.2 (0.74)	17.8 (3.13)
East	7.75 (83.4)	0.588 (0.1)	0.75	0.3	4.2 (0.74)	17.8 (3.13)
West	7.75 (83.4)	2.218 (0.39)	0.75	0.3	4.2 (0.74)	17.8 (3.13)

Table 5.8 *Characteristics of the floor and roof*

	Area m^2 (ft^2)	U-Value W/m^2 K (Btu/hr ft^2 °F)	Solar Absorptance		Convective Heat Transfer Coefficient W/m^2 K (Btu/hr ft^2 °F)	
			Inside	Outside	Inside	Outside
Floor	9.61 (103)	0.313 (0.055)	0.8	-	2.1 (0.37)	-
Roof	9.61 (103)	0.233 (0.041)	0.35	0.75	5.2 (0.92)	17.8 (3.13)

5.2.3 The applications of the integrated thermal model in building environment. In this section, this integrated thermal model has been used into two applications associated with a general heating system, with which the heating loads are determined using the heat loss equations from building structures, and thus the room thermal behavior associated with this system are dominated by natural convection. In the first application, the appropriate thermostat set points have been predicated corresponding to less heating load of the general heating system and/or to a comfortable environment for occupants, when the thermostat is maintained at one location. In the second application, the integrated thermal model has been used to perform predictions related to building load and energy consumption according to different thermostat locations.

5.2.3.1 The first application – the prediction of appropriate thermostat set point. In this application, the integrated thermal model has been applied to predict thermostat set point for energy savings and/or better indoor thermal comfort. A temperature control strategy along with three different schemes has been investigated through the four case studies, in which several construction types of a one-room residential house have been considered as described in the section 5.2.2, in order to determine the thermostat set points, room heating loads, and thermal comfort indices (PMV).

The three schemes used in the application, including “Occupied-zones” “Uniform-zones”, and “Core-zones”, have been defined in the equation 5.9, 5.10, and 5.11 respectively in the section 5.1.5.1.1.

5.2.3.1.1 Description of the simulation procedures. The procedure to estimate the thermostat set points (temperature values of the zone where the thermostat is located) and their corresponding room heating loads are described below:

- Step 1: Selection of the OT value, and the thermostat position

The value of OT in this application is selected, which is 20^{o}C (68^{o}F), for economic consideration. The position (5,6), shown in the figure 5.42, is specified as the typical thermostat position used in this application.

- Step 2: Determination of the thermostat set point

The predefined values of the OST, which are the OT values in Step 1, will be approached by gradually adjusting the IDT (energy-effect parameter) of the integrated thermal model which is utilized to predict the temperature distributions corresponding to the different schemes, “Uniform-zones”, “Core-zones”, and “Occupied-zones” (the discussion about the relationship between IDT and the integrated thermal model can be found in the section 5.2.3.2.1.). When the predefined value of the OT is reached, the current temperature value of the zone, i.e. Location (5,6) (Figure 5.42), is regarded as the thermostat set point, and the temperature difference between the occupied space and the thermostat position may be determined as well.

- Step 3: Computation of the heating loads of the house

Once the thermostat set point was determined, its corresponding room surface temperatures that were used by the integrated thermal model to compute the indoor thermal

behaviors and to approach the OT in Step 2 are also known. Using these surface temperatures and the energy balance equation

$$\sum h_{c,i} A_i (T_{New\ design\ Temperature} - T_{s,i}) = 0, \qquad \text{[W or Btu/hr]} \qquad (5.16)$$

the new indoor design temperature, $T_{New\ Design\ Temperature}$, can be calculated, where, $h_{c,i}$ (W/m^2 K or Btu/hr ft^2 ^{o}F) is the convective heat transfer coefficient of surface *i*, A_i (m^2 or ft^2) is the area of surface *i*; $T_{s,i}$ (^{o}C or ^{o}F) is the temperature of surface *i*; and $T_{New\ Design\ Temperature}$ (^{o}C or ^{o}F) is the corrected indoor design temperature for the integrated thermal model to predict the heating loads. The detailed description regarding $T_{New\ design\ Temperature}$ can be found in the section 5.2.3.2.1.

In a simulation, these three steps may be repeated at every time step to compute the hourly thermostat set point and heating load.

5.2.3.1.2 Case studies. Since the room is mathematically subdivided into 60 zones represented by *(i,j)* as shown in the figure 5.50, where *i* varies from 1 to 10 and *j* varies from 1 to 6. For the "Core-zones" scheme, the average temperature of the room core zones, (5,3), (5,4), (6,3), and (6,4), as shown in the figure 5.50, is regarded as the OST which is defined as:

$$OST_{Core-zones} = (T_{(5,3)} + T_{(5,4)} + T_{(6,3)} + T_{(6,4)})/4, \qquad [^oC \text{ or } ^oF] \qquad (5.17)$$

For the "Occupied-zones" scheme, the average temperature of the occupied space (the average temperature of the 32 zones constituting the occupied space (Figure 5.50)) is the OST which is defined as:

$$OST_{Occupied-zones} = \frac{\sum T_{(i,j)}}{32}, \qquad [^oC \text{ or } ^oF] \qquad (5.18)$$

where *i* varies from 3 to 10, and *j* varies from 2 to 5.

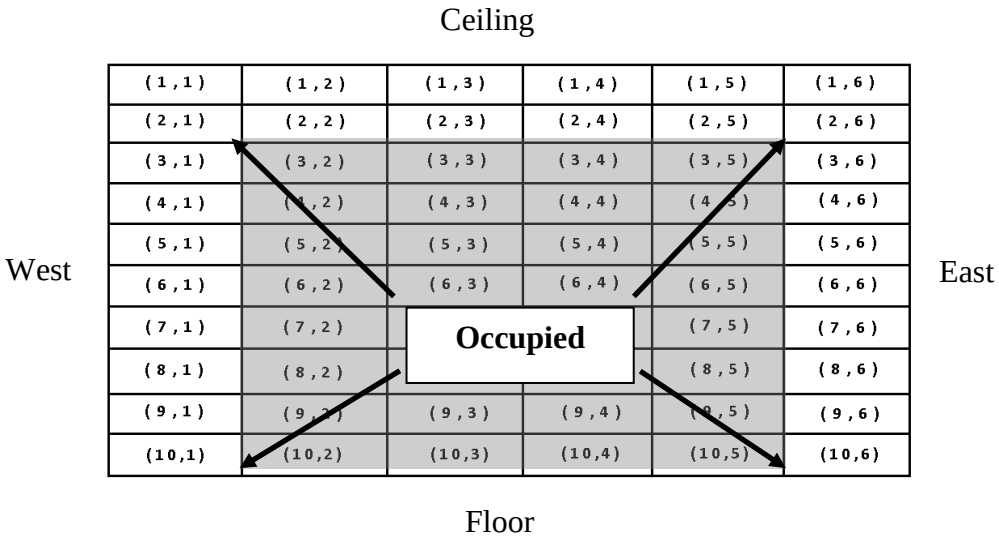

Figure 5.50 Zone divisions of a room
(The occupied zone: the regions marked in grey)

5.2.3.1.3 Simulation results. The thermostat set points of different schemes ("Uniform-zones", "Core-zones", and "Occupied-zones") for the cases 1, 2, 3, and 4 are displayed in the figures 5.51, 5.57, 5.63, 5.69, respectively. The room heating loads of these different schemes for the cases 1, 2, 3, and 4 are displayed in the figures 5.52, 5.58, 5.64, 5.70, respectively. The corresponding corrected indoor design temperatures that are used to predict the heating loads for the cases 1, 2, 3, and 4 are displayed in the figure 5.53, 5.59, 5.65, 5.71, respectively. Figure 5.54, 5.60, 5.66, 5.72 show the zonal PMV profiles of the "Uniform-zones" scheme for the cases 1, 2, 3, and 4, respectively. Figure 5.55, 5.61, 5.67, 5.73 show the zonal PMV profiles of the "Core-zones" scheme for the cases 1, 2, 3, and 4, respectively. Figure 5.56, 5.62, 5.68, 5.74 show the zonal PMV profiles of the "Occupied-zones" scheme for the cases 1, 2, 3, and 4, respectively. Table 5.9 provides a guide of figures corresponding to the different cases. In these figures, the "One-zone" represents the results of the conventional single/multi-zone thermal model.

Table 5.9 *Result figures for the different cases*

	Thermostat set points	Heating loads	Corresponding corrected indoor design temperatures	Zonal PMV profiles of "Uniform-zones" scheme	Zonal PMV profiles of "Core-zones" scheme	Zonal PMV profiles of "Occupied-zones" scheme
Case 1	Figure5.51	Figure5.52	Figure5.53	Figure5.54	Figure5.55	Figure5.56
Case 2	Figure5.57	Figure5.58	Figure5.59	Figure5.60	Figure5.61	Figure5.62
Case 3	Figure5.63	Figure5.64	Figure5.65	Figure5.66	Figure5.67	Figure5.68
Case 4	Figure5.69	Figure5.70	Figure5.71	Figure5.72	Figure5.73	Figure5.74

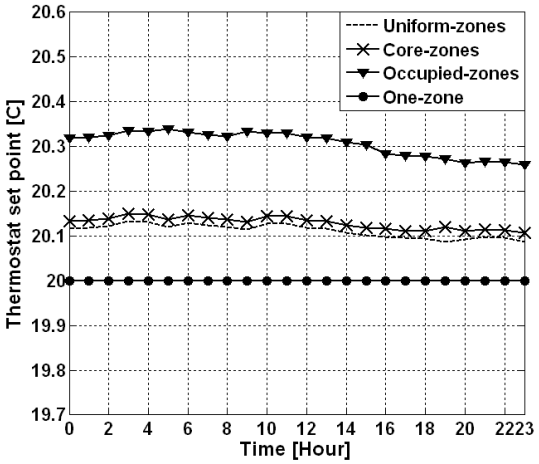

Figure 5.51 Thermostat set points of Case 1

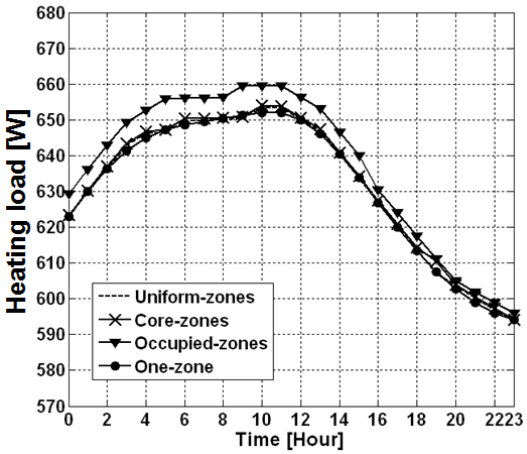

Figure 5.52 Heating loads of Case 1

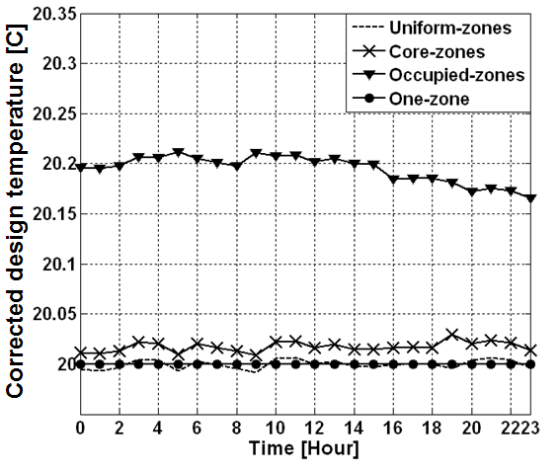

Figure 5.53 Corrected design temperatures of Case 1

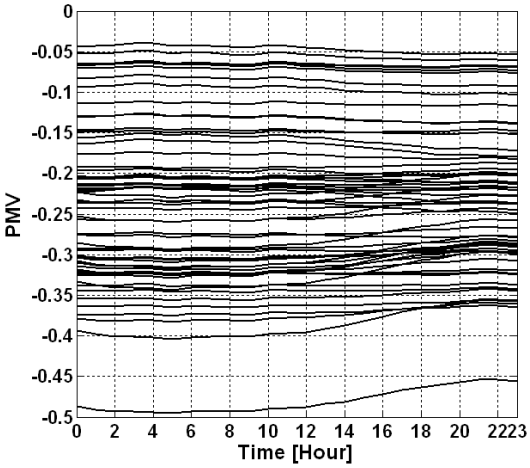

Figure 5.54 PMVs for "Uniform-zones" scheme of Case 1

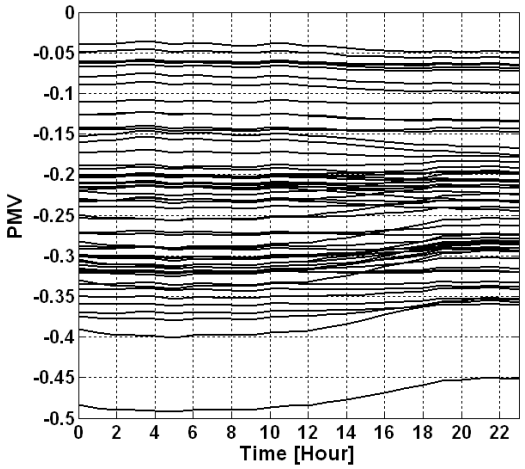

Figure 5.55 PMVs for "Core-zones" scheme of Case 1

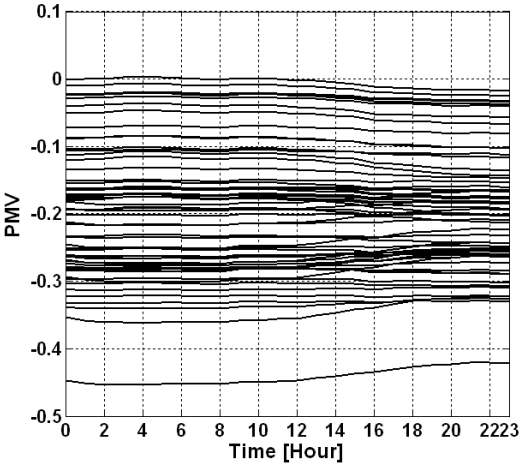

Figure 5.56 PMVs for "Occupied-zones" scheme of Case 1

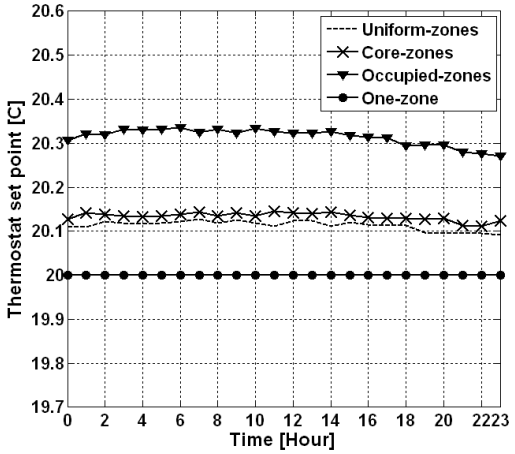

Figure 5.57 Thermostat set points of Case 2

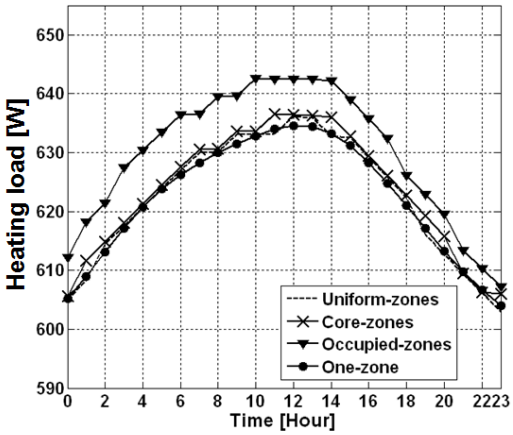

Figure 5.58 Heating loads of Case 2

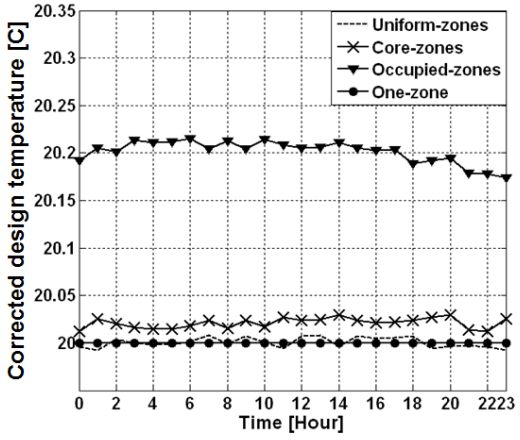

Figure 5.59 Corrected design temperatures of Case 2

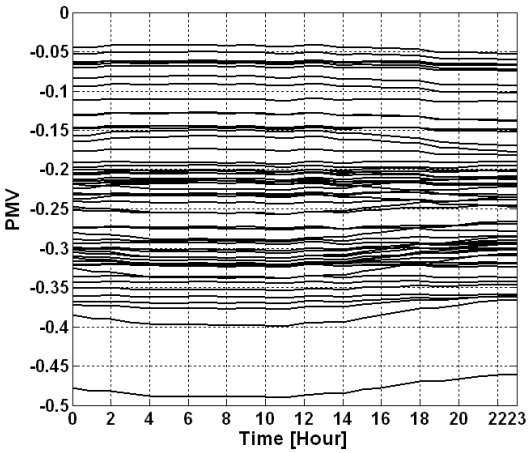

Figure 5.60 PMVs for "Uniform-zones" scheme of Case 2

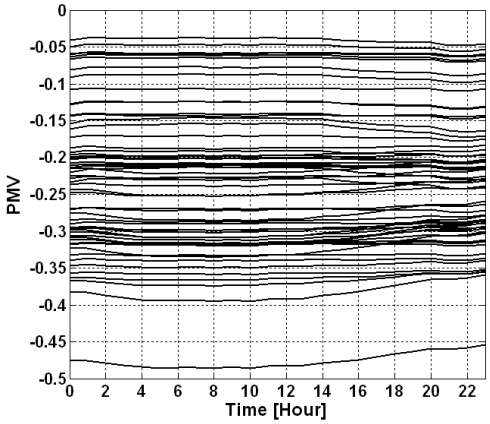

Figure 5.61 PMVs for "Core-zones" scheme of Case 2

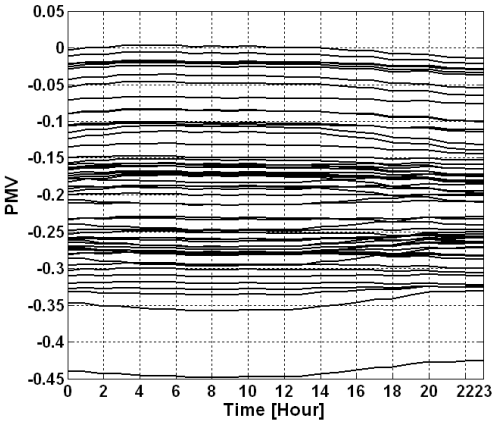

Figure 5.62 PMVs for "Occupied-zones" scheme of Case 2

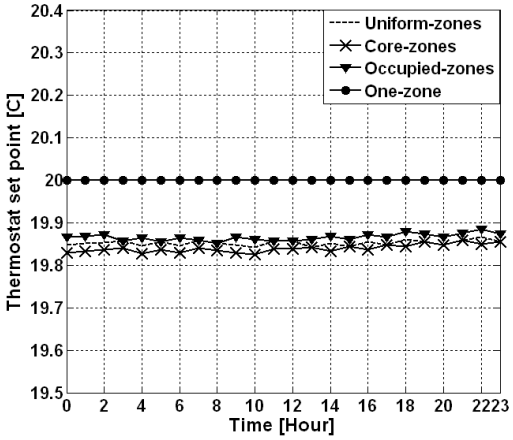

Figure 5.63 Thermostat set points of Case 3

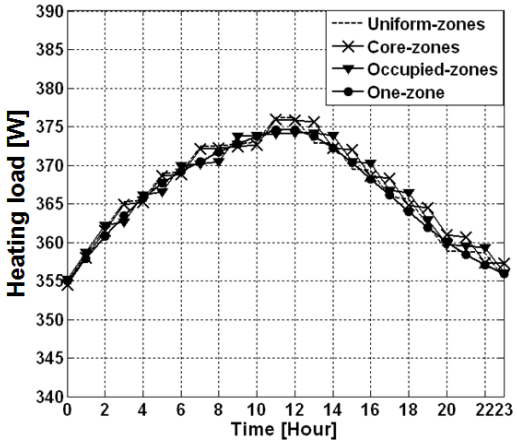

Figure 5.64 Heating loads of Case 3

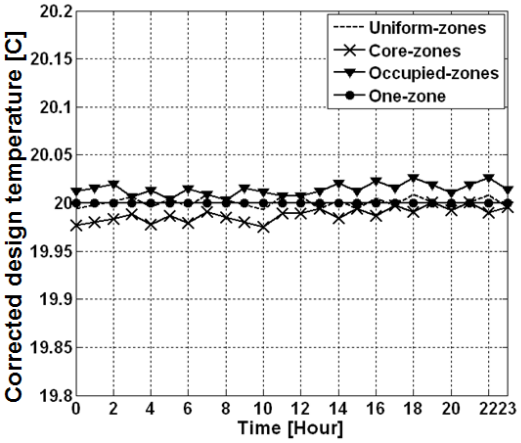

Figure 5.65 Corrected design temperatures of Case 3

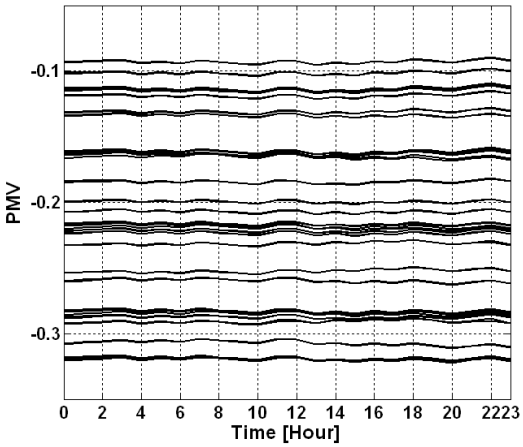

Figure 5.66 PMVs for "Uniform-zones" scheme of Case 3

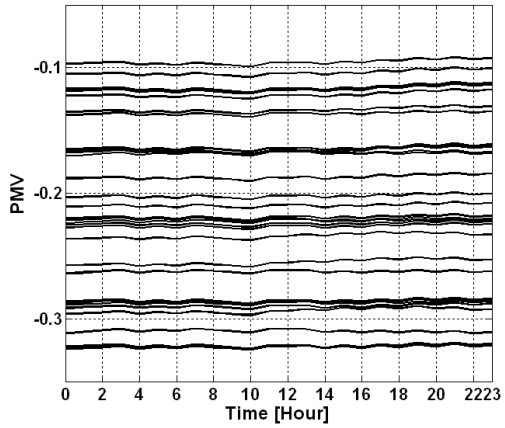

Figure 5.67 PMVs for "Core-zones" scheme of Case 3

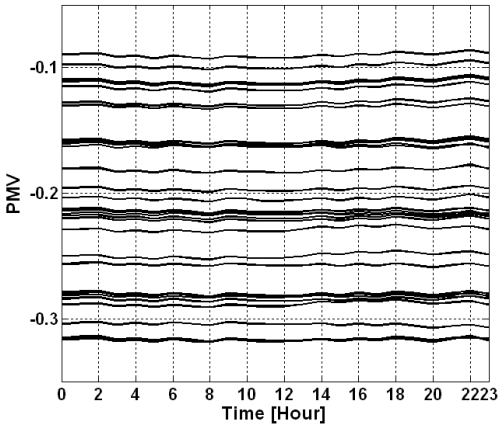

Figure 5.68 PMVs for "Occupied-zones" scheme of Case 3

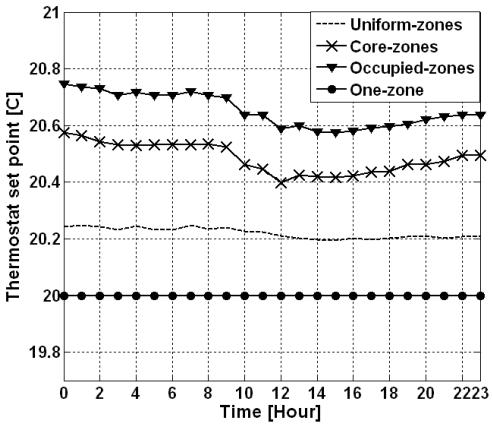

Figure 5.69 Thermostat set points of Case 4

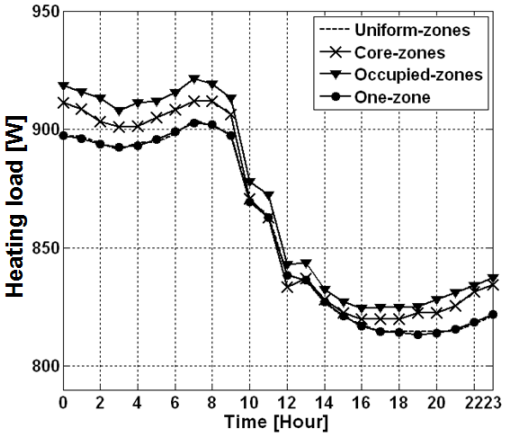

Figure 5.70 Heating loads of Case 4

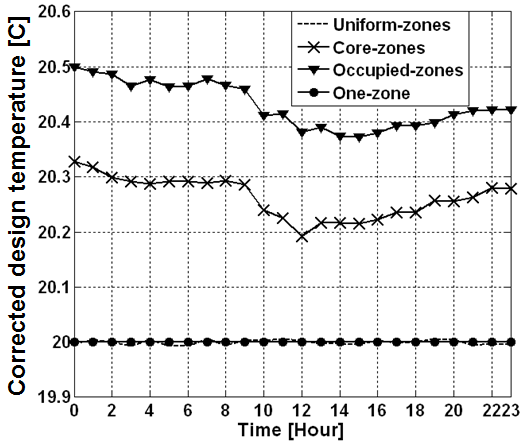

Figure 5.71 Corrected design temperatures of Case 4

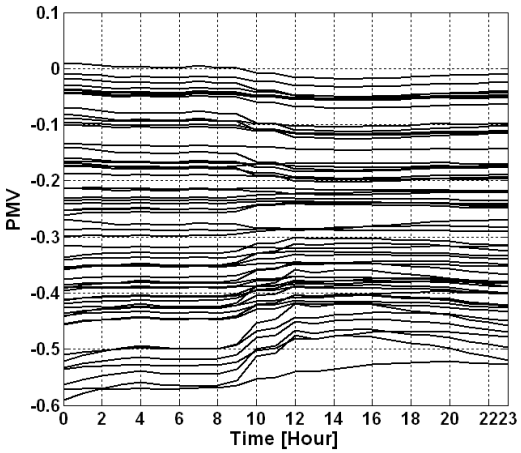

Figure 5.72 PMVs for "Uniform-zones" scheme of Case 4

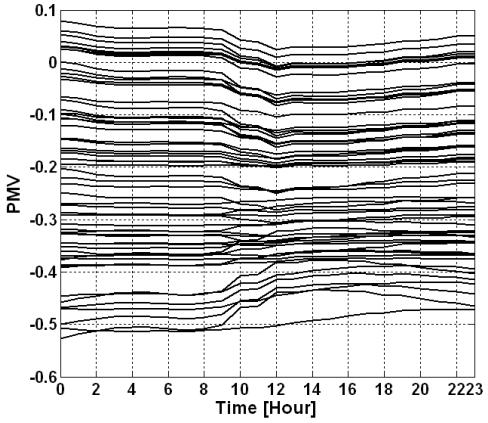

Figure 5.73 PMVs for "Core-zones" scheme of Case 4

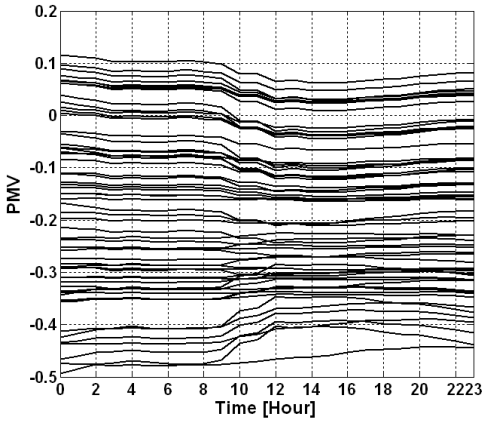

Figure 5.74 PMVs for "Occupied-zones" scheme of Case 4

As shown in the figures 5.51, 5.57, 5.63, 5.69, the different OST schemes and OT values account for different thermostat set point profiles. In the conventional single/multi-zone thermal model, constant set point temperatures are utilized, and thus there is no difference between the thermostat set point and the OT, as shown in the figures 5.75, 5.76, 5.77, and 5.78, which display the temperature differences between the OTs (various OST schemes) and the thermostat set points (the temperature at the location (5,6)) of the cases 1, 2, 3, and 4, respectively. In these figures, there is no significant difference observed between the results of the "Uniform-zones" and "Core-zones" schemes, except for the case 4, in which a relatively non-uniform temperature distribution is observed due to the presence of a window on the west wall. A more uniform temperature distribution exists in the case 3, which causes the insignificant temperature differences when the "Uniform-zones", "Core-zones", and "Occupied-zones" schemes are applied, as shown in the figure 5.77. The degree of the non-uniformity of the room temperature distribution determines the magnitude of the temperature difference between the thermostat set point and the OT. A non-uniform temperature distribution may result in significant temperature difference. No evident discrepancy is noticed between the figures 5.75 and 5.76. Consequently, whether the thermal mass of the building construction is light or heavy does not significantly

affect the thermostat design temperature and the inside temperature distribution, as long as the heat transfer coefficients of the building constructions at the surface levels are the same. However, these two thermal masses indeed account for different heating loads, as shown in the figures 5.52 and 5.58. A lower energy is required when the heavy thermal mass of building construction is applied.

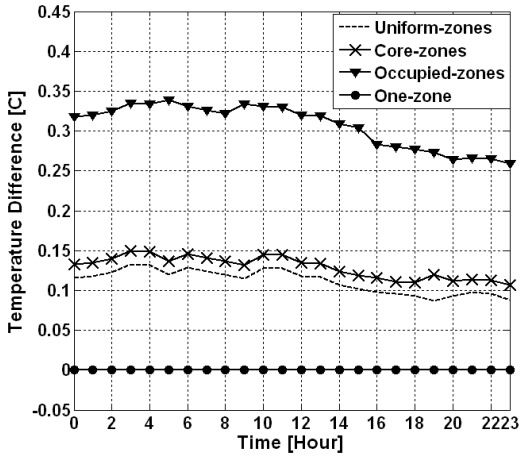

Figure 5.75 Temperature differences between the thermostat set points and the OTs of Case 1

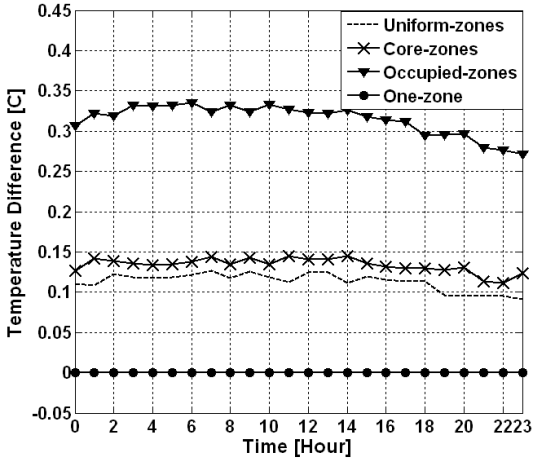

Figure 5.76 Temperature differences between the thermostat set points and the OTs of Case 2

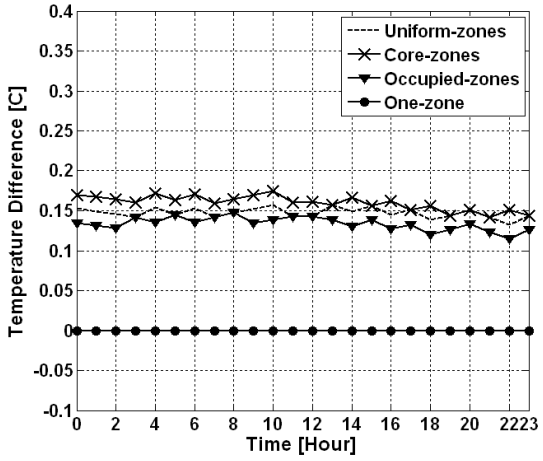

Figure 5.77 Temperature differences between the thermostat set points and the OTs of Case 3

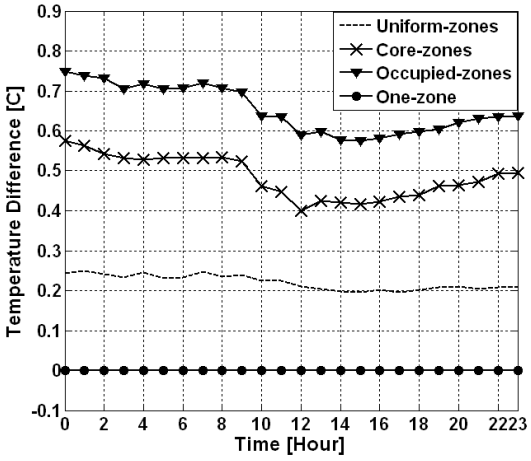

Figure 5.78 Temperature differences between the thermostat set points and the OTs of Case 4

The “Occupied-zones” scheme, as the strictest requirement for indoor thermal comfort among these three schemes, requires higher thermostat set point temperatures and more energy, as shown in the figures 5.51, 5.57, 5.63, 5.69, as well as the figures 5.52, 5.58, 5.64, 5.70. Nevertheless, noticeable improvements of indoor thermal comfort level are observed when the “Occupied-zones” scheme is used compared to the other two schemes, as shown from the figures 5.54, 5.55, and 5.56 for the case 1, the figures 5.60, 15.61, and 5.62 for the case 2, and the figures 5.72, 5.73, and 5.74 for the case 4. No significant difference was found from the figures 5.66, 5.67, and 5.68 for the case 3, owing to its nearly uniform temperature distribution within the room. After the comparison of the PMVs for both “Uniform-zones” and “Core-zones” schemes of these 4 cases, one may conclude that an improvement of the PMVs for the “Core-zones” scheme over the “Uniform-zones” scheme is only observed in the case 4. Therefore, the difference between these two schemes in terms of thermal comfort and energy consumption can be only distinguished when a significantly non-uniform temperature distribution exists within a room.

In fact, whether the room air temperature distribution is uniform or not plays a key role in the predictions of room thermostat set point and heating load. For a room characterized by a nearly uniform temperature distribution, the default design parameters of the conventional single/multi-zone thermal model, such as the IDT (Indoor Design Temperature) with 20^{o}C (68^{o}F), are still good to use, because of the small discrepancy of the results between the three OST schemes and the conventional single/multi-zone thermal model in terms of the thermostat set point, heating load, and corrected indoor design temperature, as shown in the figures 5.63, 5.64, and 5.65. Oppositely, for a room characterized by a significantly non-uniform temperature distribution, these default design parameters of the conventional single/multi-zone thermal

model, i.e. the IDT, are not acceptable; instead, a corrected design temperature, as shown in the figure 5.71, is needed, in order to improve the design accuracy of the conventional single/multi-zone thermal model.

5.2.3.1.4 Summary. In this application, a temperature control strategy, along with three different schemes, "Uniform-zones", "Core-zones", and "Occupied-zones", has been investigated through four case studies, in which different construction types of a one-room building have been considered, in order to determine the thermostat set points, heating loads, and thermal comfort indices (PMV).

After the comparisons and analysis, we conclude that:

For a space with a nearly uniform temperature distribution, such as the interior space of a building, the default design parameters of the conventional single/multi-zone thermal model, i.e. 20^{o}C (68^{o}F) for the indoor design temperature, are still acceptable to use in the energy/load estimations and even the determination of thermostat set points when the building is under operation. However, for a space with a significantly non-uniform temperature distribution, such as the space that has exterior walls within a building, the corrected indoor design temperatures for the single/multi-zone thermal model are needed in the estimation of energy/load. In addition, the thermostat set points, for operation purposes of the building, need to be updated by using the values that were obtained.

The "Occupied-zones" scheme gives a more comfortable environment, compared to the other two schemes, but requires more energy. This temperature control strategy gives the BMS more control options concerning either the energy saving or indoor thermal comfort, or even both.

5.2.3.2 The second application – the prediction of heating loads corresponding to different thermostat locations. In this application, the developed integrated thermal model has been used to estimate the hourly heating loads of the residential house and to quantify the impact of the different thermostat locations on the building heating load. The four cases described in the section 5.2.2 have been studied. The simulation procedure is described below.

5.2.3.2.1 Description of the simulation procedures

- Step 1: Selection of the set point temperature and position of the thermostat

Theoretically, the thermostat set point temperature is a temperature value at which the thermostat will transmit a signal to turn on/off the heating/cooling device (the differential or dead band is ignored). Unlike the IDT of the single/multi-zone thermal model, this set point temperature represents the local thermostat-position air temperature, rather than the average air temperature of this entire room. Therefore, even though there are standards (ASHRAE Standard 55, 2004) that provide the recommended IDT values based on thermal comfort considerations, these standards cannot be used directly to determine the thermostat set point temperature considering that this set point temperature is not able to reflect the temperature of the occupied space. Consequently, at the building design stage, investigating different thermostat set points is necessary in order to find the most appropriate value in consideration of energy saving and/or better thermal comfort. In this application, the thermostat set point is selected to be a constant, i.e. 20 ^{o}C (68 ^{o}F), for the following case studies, and different thermostat locations are considered depending on the mesh grid used in the zonal model.

- Step 2: Determination of the Design Temperature Distribution (DTD)

For the general heating system, the DTD is determined using room interior surface temperatures because of the characteristic of natural convection of this system. The first step is to

determine the interior surface temperatures that will be used to predict the room temperature distribution using the integrated thermal model. In fact, IDT is a special form of DTD, and it represents the uniform design temperature distribution. Using IDT in the integrated thermal model is equivalent to the direct usage of the conventional single-multi-zone thermal model. Therefore, the concept of IDT is needed in the determination of required interior surface temperatures. In the integrated thermal model, the change of IDT corresponds to a change of the room interior surface temperatures (T1, T2, T3, and T4 shown in the figure 5.79 a). In the integrated thermal model, the room air temperature distributions can be predicted using the room interior surface temperatures (Figure 5.79 b). Consequently, for each IDT, there is a corresponding room air temperature distribution profile. Then, the air temperature of the zone where the thermostat is located can be observed particularly. When this zone air temperature is equal to the thermostat set point temperature defined in Step 1, the current air temperature distribution profile can be regarded as the DTD for this time step (Figure 5.79 c). In fact, this DTD includes the effects of several factors, including the shape of the space in the house, the constructions, the outdoor weather conditions, etc., and thus this DTD is unique and exclusive to this space for this specified time step.

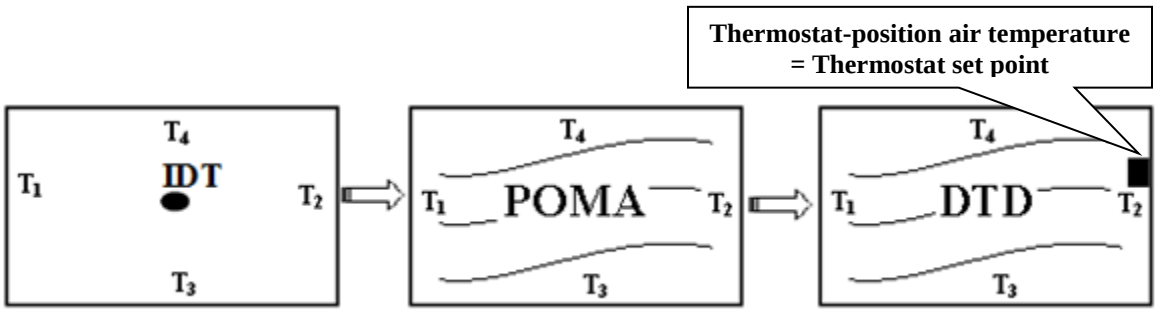

(a) (b) (c)

Figure 5.79 Demonstration of the procedure to determine the DTD

- Step 3: Calculation of the hourly heating load of this house

Once the DTD was obtained in Step 2, its corresponding room interior surface temperatures, i.e the surface temperatures that were used by the integrated thermal model to calculate the DTD in Step 2, are also known. Using these interior surface temperatures and the energy balance equation 5.16 (section 5.2.3.1.1), where $T_{New\ design\ Temperature}$ (°C or ^{o}F) is the corrected IDT for the integrated thermal model to predict the room heating loads. After the substitution of the corrected IDT into the integrated thermal model, the heating loads can be calculated. As a matter of fact, in the integrated thermal model, the introduction of the zonal model is for the sake of the determination of the $T_{New\ design\ Temperature}$ which can be regarded as the correction of IDT for the integrated thermal model. Although $T_{New\ design\ Temperature}$ is also a single average temperature value for the entire space, it is different from the original IDT that can be pre-determined by using standards (ASHRAE Standard 55, 2004), because the corrected IDT takes the thermostat position into account, but the original IDT does not. Consequently, for different thermostat positions, the $T_{New\ design\ Temperature}$ is distinct, and thus there will be different corresponding heating loads.

These steps for various thermostat locations and different time steps may be repeated, if necessary. The difference in the determination of energy/load between the single/multi-zone thermal model (Figure 5.80 a) and the integrated thermal model (Figure 5.80 b) is displayed. A complete flow chart demonstrating this simulation procedure is also provided in the figure 5.81.

(a)

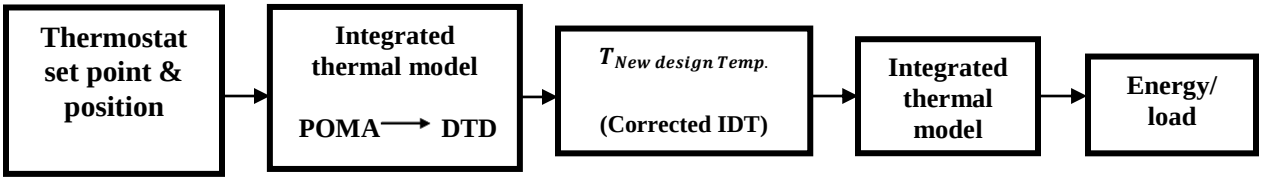

(b)

Figure 5.80 Different approaches in the determination of the energy/load
(a) Conventional approach; (b) Integration approach

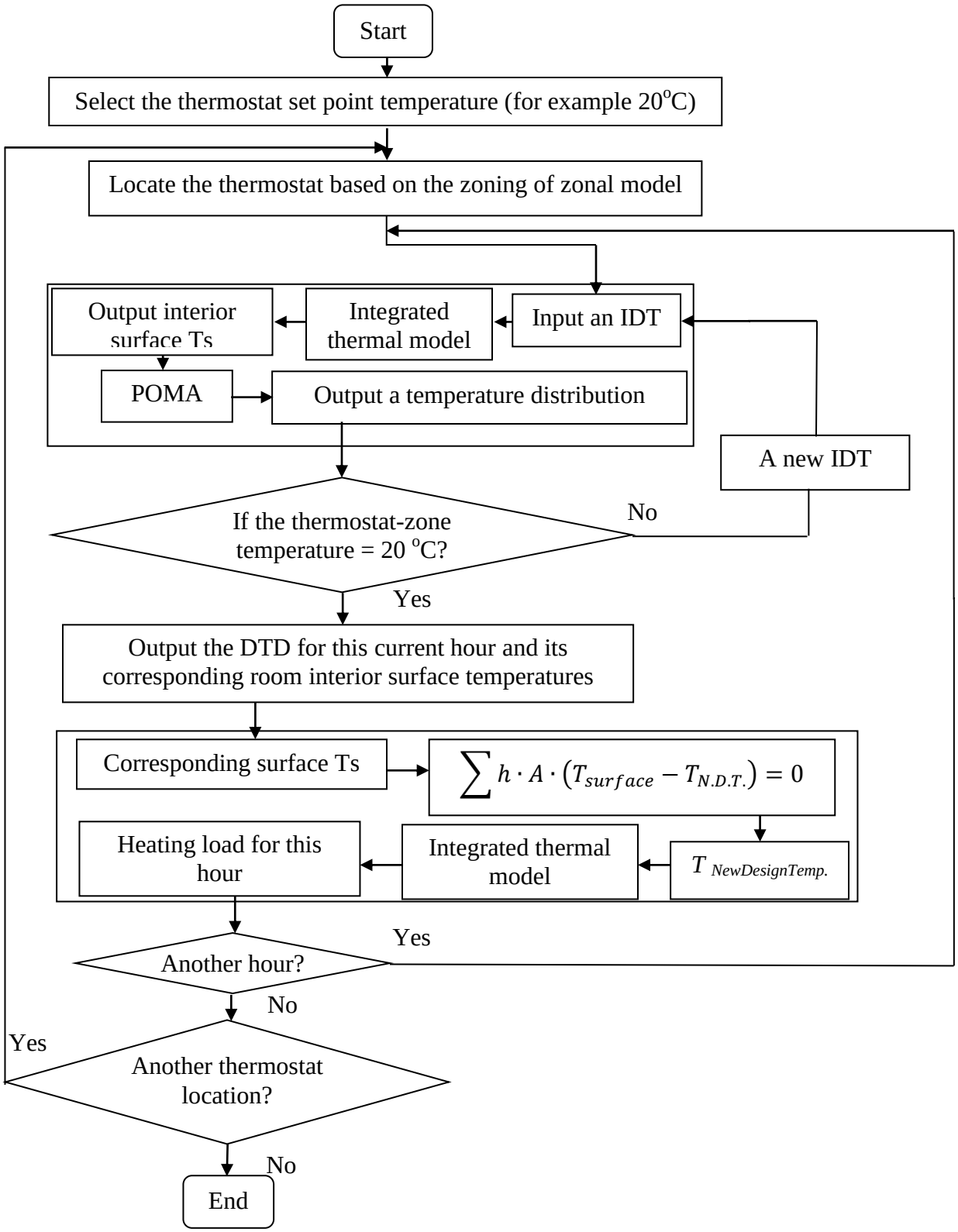

Figure 5.81 Structure of the integration simulation

5.2.3.2.2 Results and discussions. The figures 5.82, 5.87, 5.92, and 5.97 respectively display the heating load results corresponding to all the potential thermostat positions considering the different cases, i.e. the case 1 (Figure 5.82), the case 2 (Figure 5.87), the case 3 (Figure 5.92), and the case 4 (Figure 5.97). In these figures, each curve represents the heating loads associated with one thermostat position. The figures 5.83, 5.88, 5.93, and 5.98 respectively display the heating load comparison between the "one-zone" (single/multi-zone) thermal model and the integrated thermal model when the thermostat is located at the typical position (5,6) (Figure 5.42), considering the different cases, i.e. the case 1 (Figure 5.83), the case 2 (Figure 5.88), the case 3 (Figure 5.93), and the case 4 (Figure 5.98).

The figures 5.84, 5.85, and 5.86 display the zonal PMV and PPD profiles of the case 1, when the thermostat is located at (9,1), (1,4), and (5,6), respectively (see the figure 5.42). Similarly, the figures 5.89, 5.90, and 5.91 display the zonal PMV and PPD profiles of the case 2, when the thermostat is located at (9,1), (1,4), and (5,6), respectively. The zonal PMV and PPD profiles of the cases 3 and 4 are shown in the figures 5.94, 5.95, and 5.96 (Case 3) and in the figures 5.99, 5.100, and 5.101 (Case 4), respectively. In these PMV/PPD figures, each curve represents the PMV/PPD profile of each zone corresponding to the zone division of the zonal model. The 60 zones are used in the zonal model, and thus there are 60 curves in each PMV/PPD figure. For the cases 1, 2, and 3, when the thermostat is at the location (9,1), the house heating loads nearly reach the maximum values, and when the thermostat is at the location (1,4), the house heating loads mostly have the minimum values; whereas for the case 4, the maximum values of the house heating loads occur when the thermostat is located around the position (9,1), and the minimum values happen when the thermostat is around the position (1,3).

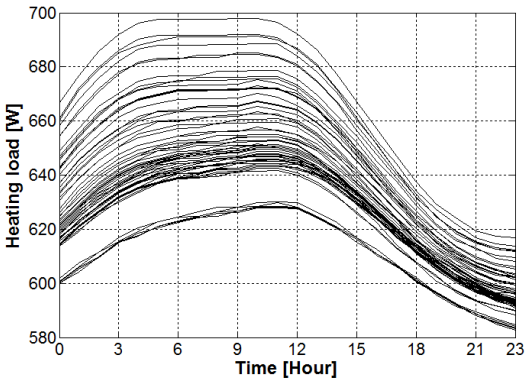

Figure 5.82 Heating loads with different thermostat locations (Case 1)

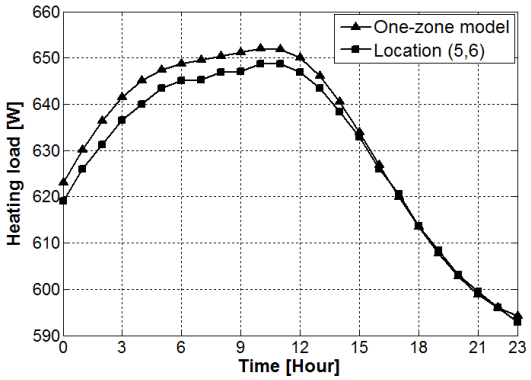

Figure 5.83 Heating loads of the original and integrated thermal models with the thermostat location (5,6) (Case 1)

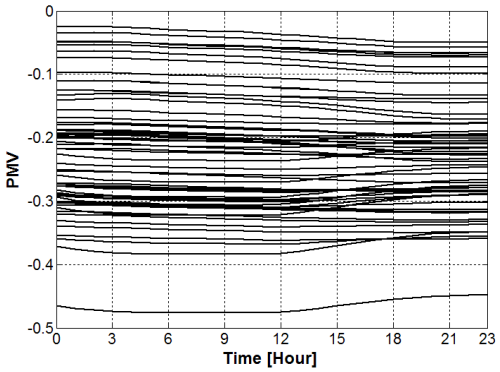

PMVs with the thermostat location (9,1)

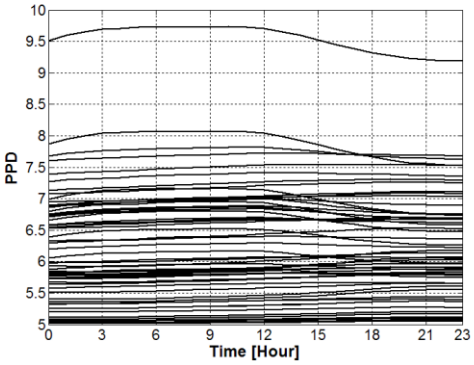

PPDs with the thermostat location (9,1)

Figure 5.84 Zonal PMV and PPD profiles with the thermostat location (9,1) (Case 1)

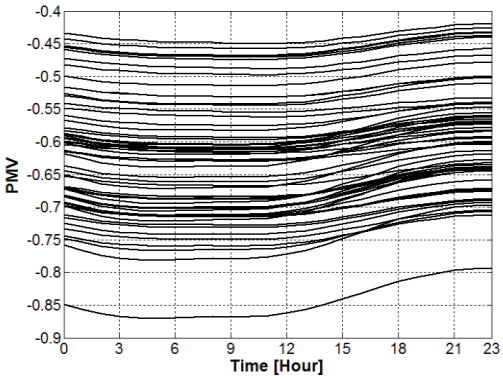

PMVs with the thermostat location (1,4)

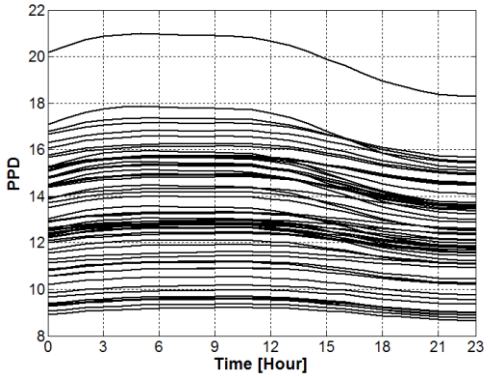

PPDs with the thermostat location (1,4)

Figure 5.85 Zonal PMV and PPD profiles with the thermostat location (1,4) (Case 1)

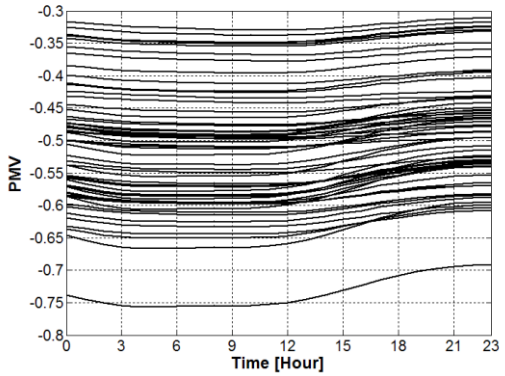

PMVs with the thermostat location (5,6)

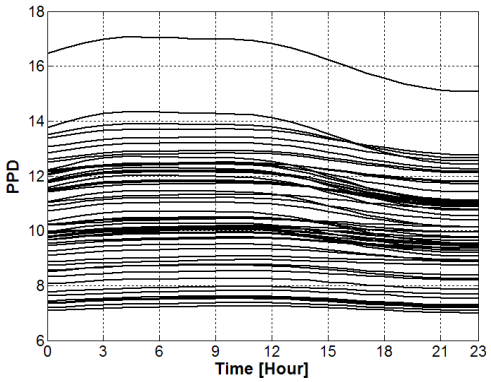

PPDs with the thermostat location (5,6)

Figure 5.86 Zonal PMV and PPD profiles with the thermostat location (5,6) (Case 1)

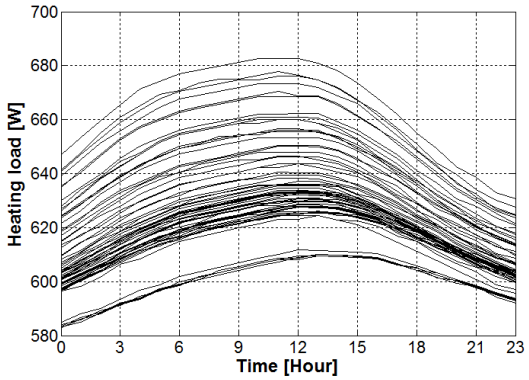

Figure 5.87 Heating loads with different thermostat locations (Case 2)

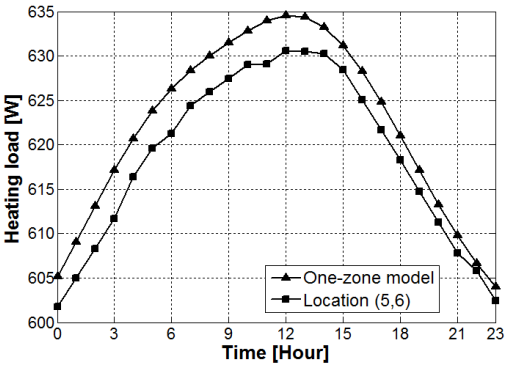

Figure 5.88 Heating loads of the original and integrated thermal models with the thermostat location (5,6) (Case 2)

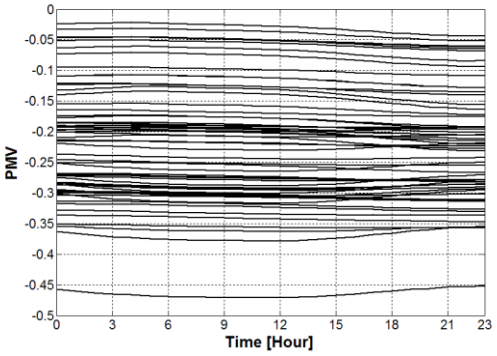

PMVs with the thermostat location (9,1)

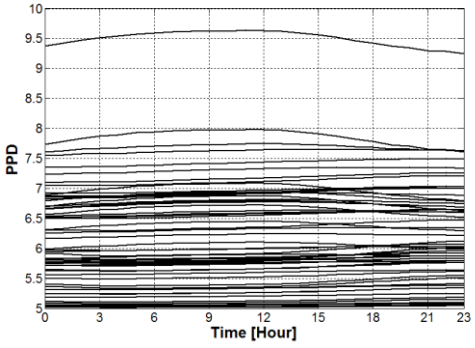

PPDs with the thermostat location (9,1)

Figure 5.89 Zonal PMV and PPD profiles with the thermostat location (9,1) (Case 2)

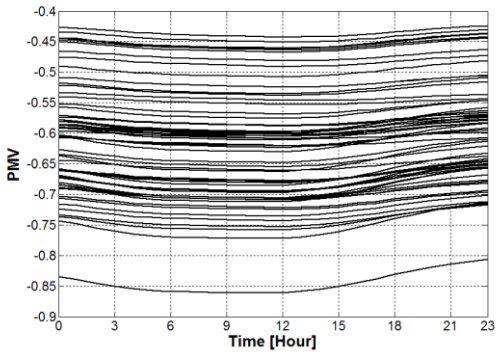

PMVs with the thermostat location (1,4)

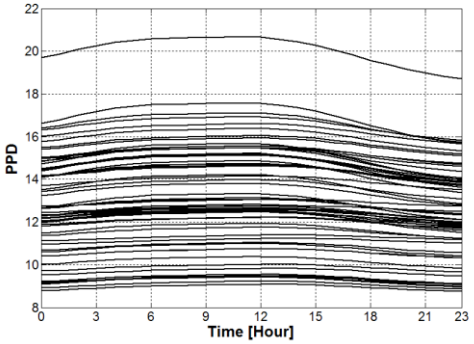

PPDs with the thermostat location (1,4)

Figure 5.90 Zonal PMV and PPD profiles with the thermostat location (1,4) (Case 2)

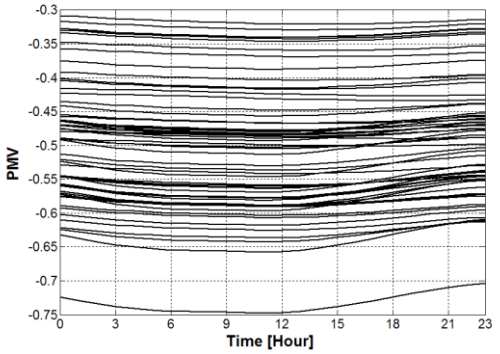

PMVs with the thermostat location (5,6)

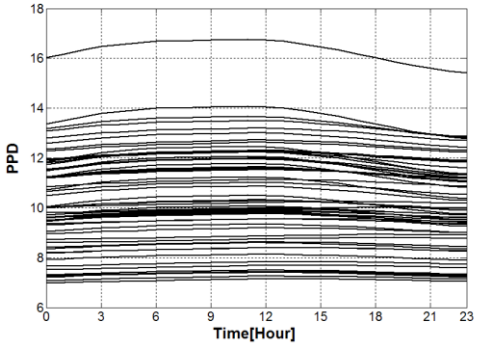

PPDs with the thermostat location (5,6)

Figure 5.91 Zonal PMV and PPD profiles with the thermostat location (5,6) (Case 2)

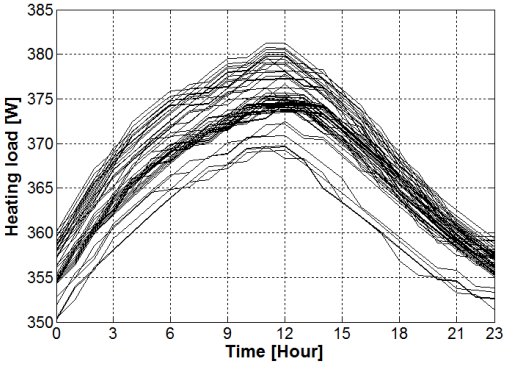

Figure 5.92 Heating loads with different thermostat locations (Case 3)

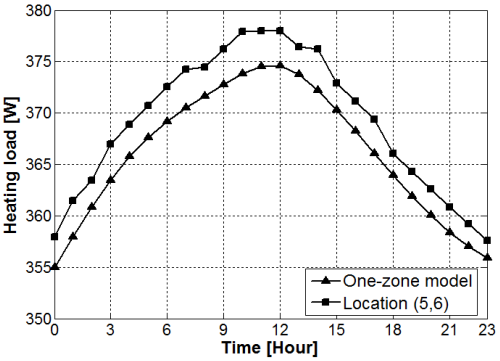

Figure 5.93 Heating loads of the original and integrated thermal models with the thermostat location (5,6) (Case 3)

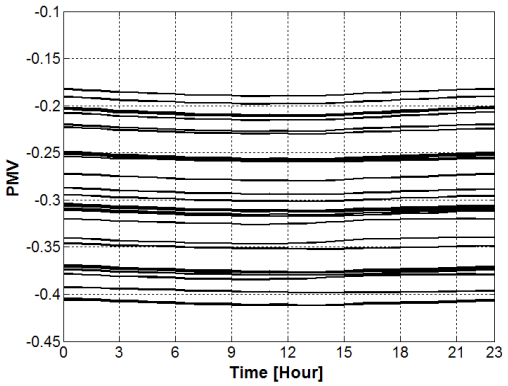

PMVs with the thermostat location (9,1)

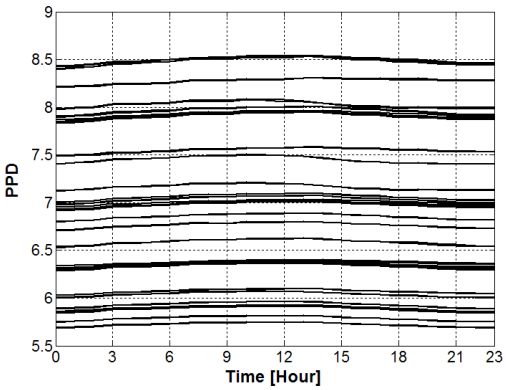

PPDs with the thermostat location (9,1)

Figure 5.94 Zonal PMV and PPD profiles with the thermostat location (9,1) (Case 3)

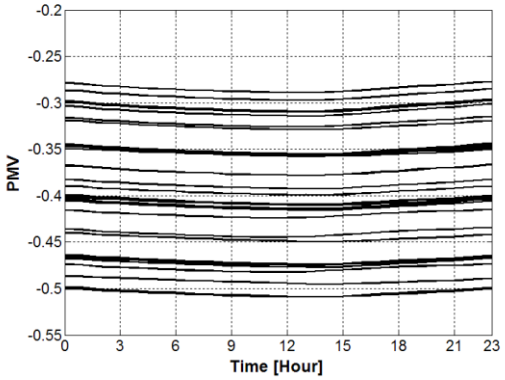

PMVs with the thermostat location (1,4)

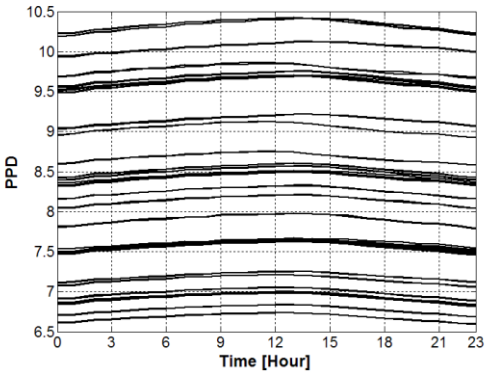

PPDs with the thermostat location (1,4)

Figure 5.95 Zonal PMV and PPD profiles with the thermostat location (1,4) (Case 3)

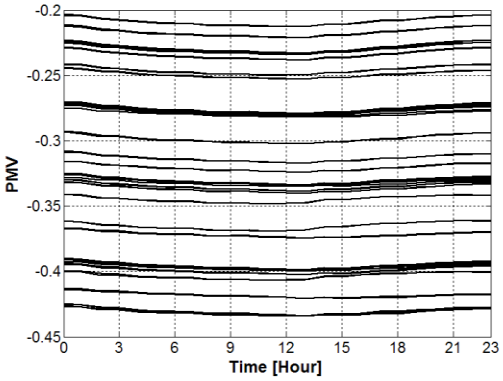

PMVs with the thermostat location (5,6)

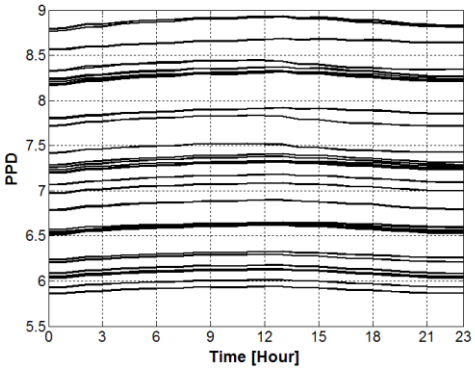

PPDs with the thermostat location (5,6)

Figure 5.96 Zonal PMV and PPD profiles with the thermostat location (5,6) (Case 3)

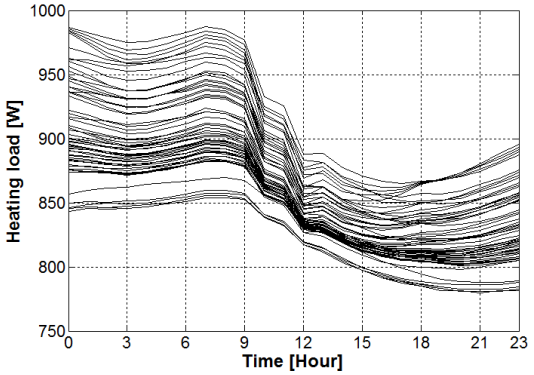

Figure 5.97 Heating loads with different thermostat locations (Case 4)

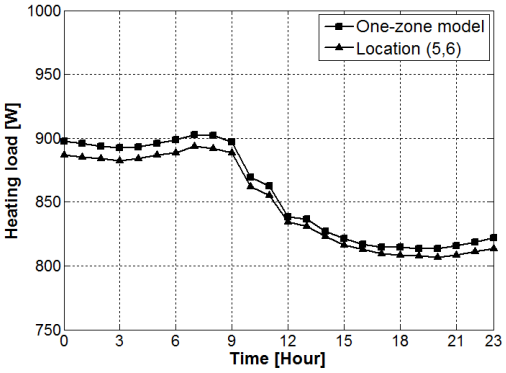

Figure 5.98 Heating loads of the original and integrated thermal models with the thermostat location (5,6) (Case 4)

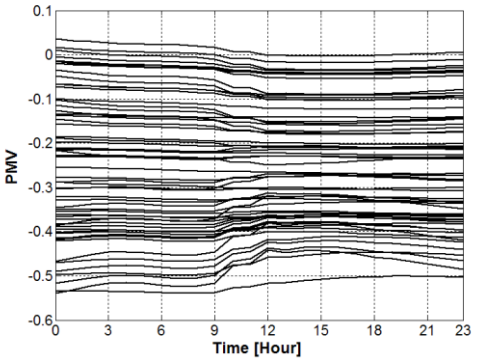

PMVs with the thermostat location (9,1)

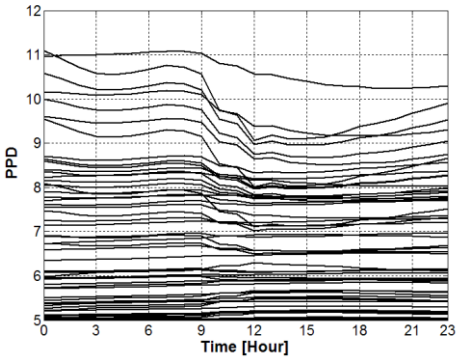

PPDs with the thermostat location (9,1)

Figure 5.99 Zonal PMV and PPD profiles with the thermostat location (9,1) (Case 4)

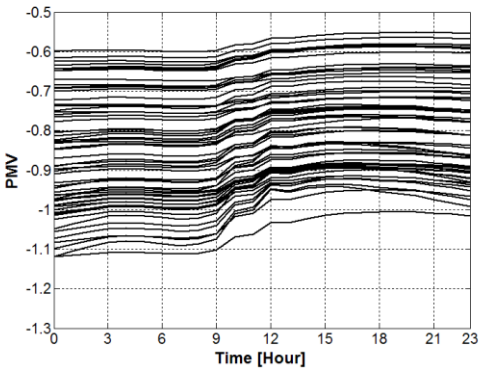

PMVs with the thermostat location (1,3)

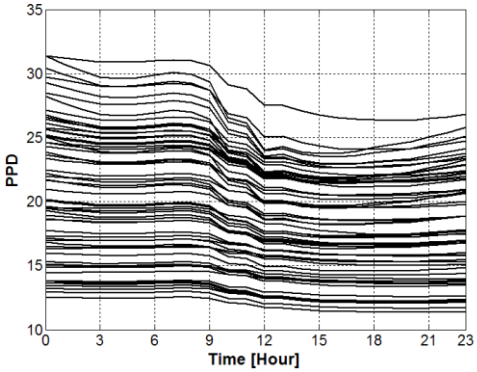

PPDs with the thermostat location (1,3)

Figure 5.100 Zonal PMV and PPD profiles with the thermostat location (1,3) (Case 4)

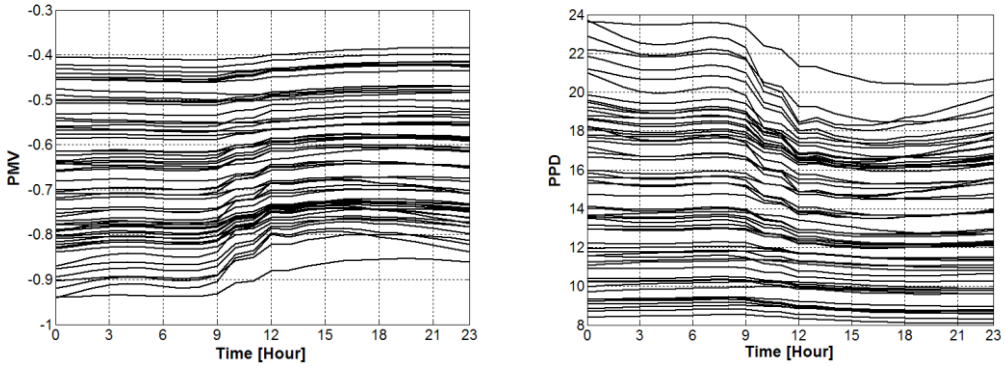

PMVs with the thermostat location (5,6) PPDs with the thermostat location (5,6)

Figure 5.101 Zonal PMV and PPD profiles with the thermostat location (5,6) (Case 4)

As shown in the results of the cases 1 and 2, different thermostat locations account for different heating load behaviors. Also, as the heating energy requirements go down (the declines of the heating load curves), the differences between the maximum and minimum values of the heating loads in both of the figures 5.82 and 5.87 diminish. This phenomenon can be also observed from the figures 5.83 and 5.88. In the figures 5.83 and 5.88, as the heating energy curves decline, the heating load values of the "one-zone" model (single/multi-zone thermal model) and the integrated thermal model are approaching to each other. This conclusion indicates that for the cases 1 and 2, the potential inaccuracies generated by the "one-zone" (single/multi-zone) model in building load calculations can be reduced, as the heating energy requirements are decreasing. In the PMV and PPD analysis of the cases 1 and 2, it is found that better indoor thermal comfort levels require higher heating energy. Moreover, compared to the light construction situation (case 1), no significant improvements are noticed in terms of human thermal comfort in the heavy construction situation (case 2), even though the structures of the heating loads of these two situations are distinct, as shown in the figures 5.82 and 5.87.

As shown in the results of the case 3, compared to the case 1 (Figure 5.82), when the west wall overall heat transfer coefficient U-value is reduced, the heating load decreases

significantly (around 45%), as shown in the figure 5.92. In the thermal comfort analysis, the lower U-value of the west wall accounts for a more uniform room temperature distribution. Consequently, compared to the case 1, a more comfortable environment is created in this room in the case 3, as displayed in the figures 5.94, 5.95, and 5.96.

As shown in the results of the case 4, higher heating loads (more than 25%) are observed (Figure 5.97) compared to the other cases, because of the addition of the high heat-transfer-coefficient window on the west wall. As displayed in the thermal comfort PMV/PPD figures 5.99, 5.100, and 5.101, better indoor thermal comfort levels require higher heating energy. Additionally, as shown in the figure 5.101, the PMV values are as low as -0.9 (PPD values are up to 24%) in some zones. Therefore, in comparison of the figure 5.101 with the figures 5.91 and 5.96, it is found that for the case 4, a slightly uncomfortable indoor environment for occupants would be created owing to the addition of the window on the west wall, when the thermostat is located at the typical position (5,6). Hence, for this case, in order to improve indoor comfort, a higher thermostat set point temperature should be applied instead of 20°C (68^{o}F), if the thermostat is located at (5,6). Alternatively, a new thermostat location can be investigated, if the thermostat set point temperature remains unchanged, i.e. 20°C (68^{o}F). In fact, this analysis procedure should be included at the building design stage in order to determine the appropriate selections for both the set point temperature and position of thermostat within a space.

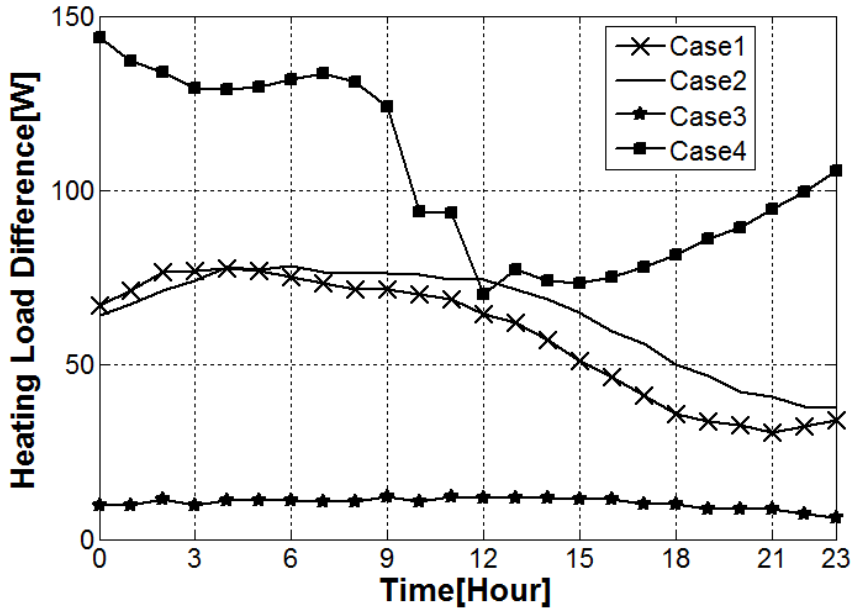

Figure 5.102 Heating load differences between the maximum and minimum values of these four cases

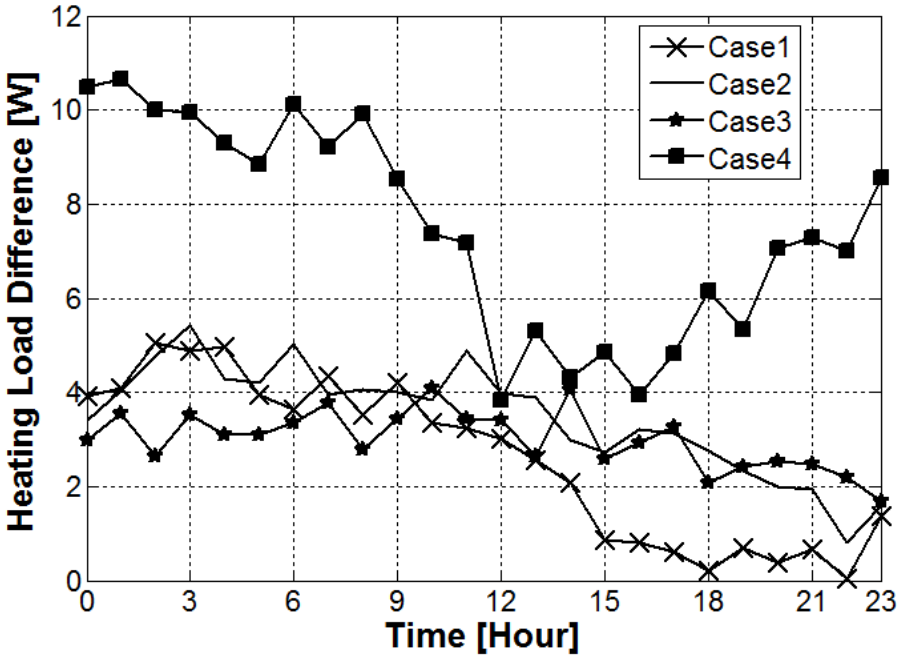

Figure 5.103 Heating load differences between the original and integrated thermal models with the thermostat location (5,6)

The figure 5.102 shows the differences between the maximum and minimum values of the heating load results that are displayed in the figures 5.82, 5.87, 5.92, and 5.97. As the room temperature distribution tends to be uniform, the heating load differences decline, and thus the corresponding potential inaccuracies the single/multi-zone thermal model generates can be reduced. In other words, the single/multi-zone thermal model is acceptable for use in building energy/load calculations, if a relatively uniform temperature distribution can be created in a room or building.

The figure 5.103 demonstrates the heating load differences between the single/multi-zone thermal model and the integrated thermal model with the thermostat location (5,6), corresponding to the heating load results shown in the figures 5.83, 5.88, 5.93, and 5.98. In consideration of the small discrepancy values shown in this figure, the performance of the single/multi-zone thermal model in the building energy/load predictions is desirable. Therefore, for this one-room residential house, if the thermostat would be placed at the typical position (5,6), the conventional thermal model is acceptable for use in the energy estimations.

5.2.3.2.3 Summary. In this application, the case studies using the integrated thermal model have not only revealed the importance of detailed room air models, such as zonal models, for predicting building energy/loads, but also demonstrated the optional analysis procedures at the building design stage in consideration of different thermostat set points and positions. Some suggestions regarding building energy prediction are given below.

- The different thermostat locations indeed affect the building energy consumption/load. As shown in these cases, the building heating load difference caused by the different thermostat locations may be as high as almost 150 W (511.8 Btu/hr) (the case 4 in the

figure 5.102), which is about 15% of the total heating energy. Therefore, an appropriate design of the thermostat location within a space is indispensable.

- The thermostat set point, 20°C (68^{o}F), is an appropriate value for the cases 1, 2 and 3, when the thermostat is located at the typical position. However, for the case 4, a slightly uncomfortable indoor environment would be created with 20°C (68^{o}F) as the thermostat set point, and thus a higher value, such as 21°C (69.8^{o}F) or 22°C (71.6^{o}F), is preferred.

- Although the construction thermal mass does not significantly impact the indoor thermal comfort behavior in an air-conditioned building, it indeed changes the structure of room heating load, according to the results shown in the cases 1 and 2. A large amount of thermal mass, such as the heavy construction situation of the case 2, contributes to the decrease of the building energy consumption and the shift of the peak loads.

CHAPTER 6

Conclusions and Recommendations

In modern buildings, HVAC systems control the indoor conditions, such as temperature and humidity. Besides the judicious design of HVAC systems and the appropriate selection of air conditioning equipment, the efficient control and operation of a BMS are essential to avoid waste of energy. As a part of the BMS, a room thermostat measures the local air temperature and then transmits it to a controller to take the appropriate decision regarding room temperature control.

Very often, the room thermostat is located outside the occupied space and usually on the wall near a front door or in a hallway that is subject to warm and cold drafts. These drafts can cause the HVAC system to cycle on or off at improper times, when the actual room temperature is still different from the set point temperature. Actually, the thermostat feedback temperature cannot reflect the actual room temperature, since a thermostat is always attached to a wall rather than to the center of the room. Consequently, the temperature of the thermostat is usually not representative of the room temperature and a discrepancy exists between the temperature at the thermostat location and the occupied space.

Most of the current available commercial software packages, such as eQUEST, EnergyPlus, Trace700, etc., which were developed for the prediction and simulation of energy consumption of residential and commercial buildings, are based on the simple single/multi-zone modeling approach, in which a room or even an entire building is treated as a whole with the assumption that the air in this room or building is well mixed and the indoor air temperature is uniformly distributed. In reality, indoor air temperature distribution is usually not uniform, and temperature differences exist which affect not only the energy consumption of the building, but also the occupants' thermal comfort levels and indoor air quality, especially in large room spaces,

such as ballroom, theater, auditorium, conference room, and so on. Therefore, the usage of the simple single/multi-zone model in these energy simulation software packages may cause pronounced flaws in building energy simulation and prediction. In order to avoid the flaws and improve the accuracy and applicability of the energy simulation models, the single/multi-zone model needs to be substituted with an advanced detailed model, such as zonal model.

In this dissertation, a new comprehensive energy simulation model has been developed, which consists of the zonal model POMA and a multi-zone thermal model, both of which are integrated together in order to estimate the energy consumption of various air conditioning systems and to optimize the appropriate set point and location of a room thermostat in consideration of maximizing the energy saving and/or improving the indoor thermal comfort. Several applications of this integrated thermal model have been carried out, in which two air conditioning systems have been considered, including an UFAD system and a general heating system. For the general heating system that stands for the non-specified air-conditioning system, the zonal model POMA has been validated with the assistance of a reliable CFD model prior to being integrated with the multi-zone thermal model. For the UFAD system, a new zonal model has been developed by coupling the zonal model POMA with a vertical thermal jet model in order to simulate the thermal characteristics of the UFAD system. After the evaluation by comparing its results with those obtained from a CFD model in terms of indoor air temperature distribution, this coupled zonal model has been integrated with a multi-zone thermal model.

In the first application, an UFAD system has been considered as the heating system in a one-zone residential house. The developed thermal model has been used to predict the appropriate thermostat set point subject to improving indoor thermal comfort and/or increasing energy savings. A temperature control strategy, along with three different schemes, “Uniform-

zones", "Core-zones", and Occupied-zones", has been investigated through three case studies considering the different OT values. The results have quantitatively proved the existence of the temperature difference between the occupied space and the thermostat position, and have demonstrated the characteristics of these three control schemes in improving indoor thermal comfort and/or optimizing building energy consumption.

In the second application, two cases associated with the UFAD system used under heating operation have been studied considering the different slab-on-grade floor constructions. The results show that the conventional well-mixed single-zone (multi-zone) method in building energy predictions is not appropriate to use for UFAD systems. Instead, a zonal model is more preferred. In addition, an UFAD system applied under heating operation in a residential house is not only able to save energy but also to provide a more comfortable environment, compared to a traditional overhead air distribution system. The importance of thermostat location in building energy design/simulation has been demonstrated, as well.

In the third application, the general heating system has been applied to a one-room residential house in winter with the three control schemes, "Uniform-zones", "Core-zones", and Occupied-zones". Four cases have been studied considering different construction thermal characteristics. The results of this application include the determined appropriate thermostat set points, corresponding heating loads and thermal comfort indices (PMV). From these results, it is concluded that, for a space with a nearly uniform temperature distribution, such as the interior space of a building, the conventional single/multi-zone thermal model are still acceptable to use in the energy estimations. Nevertheless, for a space with a significantly non-uniform temperature distribution, such as the exterior space of a building, the integrated thermal model is needed in the estimation of energy. In addition, these determined appropriate thermostat set points provide

the BMS more control options concerning either energy savings or indoor thermal comfort, or even both.

In the last application, the general heating system has been still used in the four cases considering different constructions thermal characteristics. The thermostat locations accounting for the maximum and minimum heating loads have been investigated, as well. Some suggestions for building energy calculations at the design stage have been proposed. For example, a large amount of thermal mass in building construction contributes to the decrease of the building energy consumption and the shift of the peak loads.

In general, the results and discussions of these four applications show the interest of integrating the zonal model POMA into the multi-zone thermal model in order to improve its prediction of building energy consumption. Additionally, unlike the traditional energy simulation model, this integrated thermal model can provide a detailed description regarding the indoor thermal behavior and airflow pattern. As a result, an accurate energy simulation can be established based on this detailed room thermal description, in which more factors that are able to impact the building energy consumption can be considered, such as the dynamic thermostat location, which is difficult to simulate in the traditional energy simulation model. The parameter, thermostat location, is of significance in building load and energy prediction. This parameter not only affects the building energy consumption, but also determines the indoor thermal comfort. Therefore, studying the thermostat location is necessary in the building energy/load prediction.

The final goal of my research involves the commercialization and wide application of this new energy simulation model in industry. Therefore, the perspective of my future work includes more experimental studies and further analysis of this new simulation model for diverse building types as well as mechanical systems. Additionally, in order to further improve the performance

of this model in yearly hour-by-hour energy simulation and to reduce the computational time, the optimization of the algorithm and the usage of parallel computing technique (MPI, OpenMP, GPU) contribute to the achievement of the goal of this research. Specifically, the recommendations for the future work include:

- The further development of this integrated thermal model for various HVAC systems in the applications of energy saving/indoor air quality in buildings;
- The experimental studies and validations of this integrated thermal model in terms of temperature distribution and energy/load for different building types and air conditioning systems, such as chilled beam system, displacement ventilation system, etc.;
- The detailed practicability analysis of this integrated thermal model in terms of computational time, complexity, and accuracy for yearly energy simulation in building environment;
- The development of an optimization model based on this integration approach in order to optimize building energy consumption;
- The application of parallel computing technique at the programming level in order to reduce the computational time of simulations involving complicated geometrical structures of buildings.

References

Alajmi, A., & El-Amer, W. (2010). Saving energy by using underfloor-air-distribution (UFAD) system in commercial buildings. Energy Conversion and Management, 51 (8), 1637-42.

Allard, F., Dorer, V.B., Feustel, H.F., Garcia, E.R., Gross, M., Herrlin, M.K., Mingsheng, L., Phaff, J.C., Utsumi, Y., & Yoshino, H. (1990). Fundamentals of multizone airflow model—COMIS. Technical Note AIVC 29, Air Infiltration and Ventilation Center, Coventry, UK.

ASHRAE Standard 55. (2004). Thermal Environmental Conditions for Human Occupancy. Atlanta, GA.

ASHRAE Fundamentals. (2005). ASHRAE Handbook-Fundamentals, American Society of Heating, Refrigeration, and Air-Conditioning Engineers, Inc., Atlanta.

Axley, J.W. (2001). Surface-drag flow relation for zonal modeling. Building and Environment, 36(7), 843–50.

Axley, J., & Chung, D. H. (2007). Embedded detail microscopic models of rooms within macroscopic models of whole building systems. International journal of ventilation, 6(3), 257-273.

Bastide, A., Lauret, P., Carde, F., & Boyer, H. (2006). Building energy efficiency and thermal comfort in tropical climates presentation of a numerical approach for predicting the percentage of well-ventilated living spaces in buildings using natural ventilation. Energy and Buildings, 38, 1093-1103.

Bauman, F.S., Jin, H. & Webster, T. (2006). Heat transfer pathways in underfloor air distribution (UFAD) systems. ASHRAE Transactions, 112(2), 567-580.

Beiza, M., Ramos, J.C., Rivas, A., Anton, R., Larraona, G.S., Gastelurrutia, J. & Miguel, I. (2014). Zonal thermal model of the ventilation of underground transformer substations: Development and parametric study. Applied Thermal Engineering, 62(1), 215-228.

Bellivier, A. (2004). Modélisation numérique de la thermoaéraulique du bâtiment: des modèles CFD à une approche hybride volumes finis/zonale. Thèse de doctorat, Université de La Rochelle, France.

Beltaos, S. (1976). Oblique impingement of circular turbulent jets. Journal of Hydraulic Research, 14(1).

Blandin, D., Caccavelli, D., Krauss, G., & Bouia, H. (2007). A zonal approach for modeling stratified solar. Proceedings: Building Simulation, 678-683.

Boukhris, Y., Gharbi, L., & Ghrab-Morcos, N. (2009). Modleing coupled heat transfer and air flow in a partitioned building with a zonal model: Application to the winter thermal comfort. Building Simulation, 2(1), 67-74.

Bouia, H. (1993). Modélisation simplifiée d'écoulements de convection mixte interne: application aux échanges thermo-aérauliques dans les locaux. Thèse de doctorat, Université de Poitiers, France.

Bouia, H. (1998). Intégration du calcul de couche limite turbulente de convection naturelle et des échanges thermiques par rayonnement grandes et courtes longueurs d'onde dans le modèle venda de ventilation par déplacement d'air. Rapport EDF/INSAVALOR No. T31 L396 A2933 RNE 658, INSA-CETHIL-TB.

Bozonnet, E., Belarbi, R., & Allard, F. (2005). Modelling solar effects on the heat and mass transfer in a street canyon, a simplified approach. Solar Energy, 79(1), 10-24.

Cannistraro, G., Franzitta G., & Giaconia C. (1992). Algorithms for the calculation of the view factors between human body and rectangular surfaces in parallelepiped environments. Energy and Buildings, 19, 51-60.

Clarke, J. A., Hensen, J. L. M., & Negrao, C. O. R. (1995). Predicting indoor airflow by combining CFD and thermal simulation. Proceedings of the 16th AIVC Conference on Implementing Results of Ventilation Research, Palm Springs, CA, 145–54.

CODYBA. (1992). CODYBA – Cahier des algorithmes. ADEME Editions, Paris, February 1992, 59 p.

COMSOL. (2010). COMSOL Multiphysics User's Guide 4.1. COMSOL AB.

Daoud, A., Galanis, N., & Bellache, O. (2008). Calculation of refrigeration loads by convection, radiation and condensation in ice rinks using a transient 3D zonal model. Applied Thermal Engineering, 28, 1782–1790.

Diasty, R. EL., Fazio, P., & Budaiwi, I. (1993). The dynamic modeling of air humidity behavior in a multi-zone space. Building and Environment, 28(1), 33-51.

Dols, W.S., & Walton, G.N. (2002). CONTAMW 2.0 User Manual. National Institute of Science and Technology (NIST), Technology Administration, US Department of Commerce.

During, H. (1994). Consommations énergétiques et confort thermique des locaux chauffés: Approche par les modèles zonaux. Thèse de doctorat, INSA de Lyon, Villeurbanne, France.

EnergyPlus. (2011). EnergyPlus Energy Simulation Software. Energy Efficiency & Renewable Energy, US Department of Energ.

eQUEST. (2010). Introductory Tutorial, Version 3.64, James J. Hirsch & Associates, December, 2010.

ESP-r. (2002). Energy Systems Research Unit. The ESP-r System for Building Energy Simulation, User Guide Version 10 Series. University of Strathclyde.

Feustel, H. E. (1998). COMIS – An International Multizone Air-Flow and Contaminant Transport Model. the Assistant Secretary for Energy Efficiency and Renewable Energy, Office of Building Technology, of the U.S. Department of Energy under Contract No. DE-AC03-76F00098.

FLOVENT. (2011). Optimizing airflow design with simulation. Mentor Graphics Corporation.

FLUENT. (2001). FLUENT 6 user's guide. Fluent Inc.

Gagneau, S., & Allard, F. (2001). About the construction of autonomous zonal models. Energy and Buildings, 33, 245-250.

Gao, J., Zhang, X., Zhao, J. N., & Gao, F. S. (2010). A heat transfer parameter at air interfaces in the BLOCK model for building thermal environment. International Journal of Thermal Sciences, 49, 463-470.

Gastelurrutia, J., Ramos, J. C., Rivas, A., Larraona, G. S., Izagirre, J., & Rio, Luis del. (2011). Zonal thermal model of distribution transformer cooling. Applied Thermal Engineering, 31(17-18), 4024-35.

Gharbi, N., Ghrab-Morcos, N., & Roux, J. J. (2004). ZAER: a zonal model for heat transfer and airflow in unconditioned buildings – an experimental validation. International Journal of Ventilation, 3(1), 11-20.

Griffith, B., & Chen, Q. (2003). A momentum-zonal model for predicting zone airflow and temperature distributions to enhance building load and energy simulations. HVAC&R Research, 9(3), 309-325.

Griffith, B., & Chen, Q. (2004). Framework for coupling room air models to heat balance model load and energy. HVAC&R Research, 10(2), 91–111.

Grimitlin, M. (1970). Zuluftverteilung in räumen, Luft-und Kältetechnik. No. 5.

Grundwald, J., & Kikkawa, Y. (2011). An integral building simulation method for evaluation of indoor climate applied to model risk inside a library building. HVAC&R Research, 17(4), 577-590.

Gschwind, M., Fonzes, G., Loiseau, P.H., Bezian, J.J., Hasebe, T., Fujita, S., & Takeda, I. (1995). A zonal model to simulate a room heated by a gas heat pump (GHP). Proceedings of the 5th International Conference on Air Distribution in Rooms (Roomvent), Yokohama, Japan, 61–68.

Guthrie, A. (1996). Designing for climate control in large volumes. Proceedings of ROOMVENT'96, 5th Int. Conf. on Air Distribution in Rooms, Yokohama, 1, 1-8.

Guthrie, A., Ikezawa, H., Otaka, K., & Yau, R. (1992). Air flow studies in larger spaces: A case study of Kansai international airport passenger terminal building, Osaka, Japan. Proceedings of the International Symposium on Room Air Convection and Ventilation Effectiveness (ISRACVE). Soc. Heat. Air Cond. Sanitary Engs. Of Japan (SHASE), Tokyo, Japan. July, 22-24, 674-680.

Haghighat, F., Lin, Y., & Megri, A.C. (2001). Development and validation of a zonal model—POMA. Building and Environment, 36(9), 1039–47.

Haghighat, F., & Li, H. (2004). Building airflow movement – validation of three airflow models. Journal of Architectural and planning research, 21(4), 331-348.

Heiselberg, P., Murakami, S., & Roulet, C.-A. (1998). Ventilation of large spaces in Buildings analysis and prediction techniques. IEA Energy conservation in buildings and community systems, Annex 26: Energy efficient ventilation of large enclosures, Aalborg University, Aalborg, Denmark, ISSN 1395-7953 R9803.

Hestad, T. (1976). Dimensioning of supply openings, cold downdraught (in Norwegian). Norsk VVS, No. 6.

Hiyama, K., Kato, S., Takahashi, T., Huang, H., Kobayashi, S., & Iwase, S. (2005). Building design utilizing natural ventilation based on CFD and ventilation network analysis and its performance evaluation by field measurement. International Journal of Ventilation, 4(1), 13-23.

Hiyama, K., & Kato, S. (2011). Integration of three-dimensional CFD results into energy simulations utilizing an advection-diffusion response factor. Energy and Buildings, 43, 2752-2759.

Holmes, M.J. & Sachariewicz, E. (1973). The effect of ceiling beams and light fittings on ventilating jets. Laboratory Report No. 79, HVRA.

Howarth, A.T. (1985). The prediction of air temperature variations in naturally ventilated rooms with convective heating. Building Service Engineering Research and Technology, 6(4), 169–75.

Huang, H. (2003). Modeling of volatile organic compounds emissions and sinks from building materials. Ph.D. Thesis, Concordia University, Canada.

Huang, H., & Haghighat, F. (2005). An integrated zonal model for predicting indoor airflow, temperature, and VOC distributions. ASHRAE Transactions, 111(1), 601–11.

Huang, H., Haghighat F., and Wurtz, E. (2002). An integrated zonal model for predicting transient VOC distribution in ventilated room. Proceedings of Esim 2002, Montreal, Canada, 78-83.

Huang, L., Liao, Z., Ge, H., & Zhao, L. (2012). Physical rules based adaptive neuro-fuzzy inferential sensor model design and analysis in predicting the indoor temperature in heating system. Advanced Materials Research, 516-517, 370-379.

Inard, C., Meslem, A., & Depecker, P. (1996a). Use of a zonal model for the prediction of air temperature distribution in large enclosures. 5th International Conference on Air Distribution in Rooms: ROOMVENT '96 : Yokohama, Japan, July 17-19, 1996.

Inard, C., & Molle, N. (1989). Le chauffage par corps de chauffe: Efficacité en confort et en consommation. Revue Générale de Thermique, 28(335–336 [November–December]), 650–56.

Inard, C., & Buty, D. (1991). Simulation and thermal coupling between a radiator and a room with zonal models. Proceedings of Building Simulation ‘91, Nice, France, 113–17.

Inard, C., Bouia, H., & Dalicieux, P. (1996b). Prediction of air temperature distribution in buildings with a zonal model. Energy and Buildings, 24(2), 125–32.

Inard, C., Depecker, P., & Roux, J.J. (1997a). Un modèle simplifié pour la prédiction du champ de temperature dans les bâtiments. Revue Générale de Thermique, 36, 113–23.

Inard, C., Meslem, A., Depecker, P., & Barles, P. (1997b). Structure moyenne et analyse intégrale du panache thermique des convecteurs électriques. Revue Générale de Thermique, 36, 495–509.

Jackman, P. J. (1970). Air movement in rooms with sidewall mounted grilles – A design procedure. Laboratory Report No. 65, HVRA.

Jiru, T.E. (2006). A new generation of zonal models: development, verification and application, Ph.D. thesis, Department of Building, civil and environmental engineering, Concordia University, Montreal, Quebec, Canada, April, 2006.

Jiru, T.E., & Haghighat, F. (2004). Zonal models for indoor air flow—A critical review. International Journal of Ventilation, 3(2), 119–29.

Jiru, T.E., & Haghighat, F. (2006). A new generation of zonal models. ASHRAE Transactions, 112(2), 163–174.

Jiru, T.E., & Haghighat, F. (2008). Modeling ventilated double skin fac¸ade—A zonal approach. Energy and Buildings, 40 (2008), 1567–1576.

Kofoed, P., & Nielsen, P. V. (1990). Thermal plumes in ventilated rooms. Proc. Of the International Conference on Engineering Aero- and Thermodynamics of Ventilated room. ROOMVENT'90, Oslo.

Lam, J.C. (2000). Energy analysis of commercial buildings in subtropical climates. Building and Environment, 35 (1), 19-26.

Laret, L. (1980). Contribution au development de modeles mathematiques du comportement thermique transitoire de structures d'habitation. These de doctorat, Universite de Liège, France.

Lebrun, J. (1970). Exigences physiologiques et modalités physiques de la climatisation par source statique concentrée. Doctoral thesis, University of Liège, France.

Lebrun, J., & Ngendakumana, P. (1987). Air circulation induced by heating emitters and corresponding heat exchanges along the walls: Test-room results and modeling. Proceedings of Roomvent ‘87, Stockholm, Sweden, pp. 15.

Lin, Y., Megri, A.C., & Haghighat, F. (1999). Zonal model—a new generation of combined airflow and thermal model. Proceedings of Indoor Air ‘99, Edinburgh, Scotland.

MacCarty, N. A. (2013). A zonal model to aid in the design of household biomass cookstoves, Master thesis, Department of Mechanical Engineering, Iowa State University, USA.

Madsen, T.L., Schmidt, T.P., & Helk, U. (1990). How important is the location of the room thermostat. ASHRAE Trans., 96(1), American Society of Heating, Refrigeration, and Air-Conditioning Engineers, Inc., Atlanta.

Majali, V., Prasad, B. N., & Bhat, A. K. (2005). Development of an analytical tool in modeling of non-air-conditioned multi-zone buildings. Journal of the Institution of Engineers (India). Architectural Engineering Division, 86, 15-19.

Matlab. (2011). Matlab 7 Getting Started Guide. The MathWorks, Inc.

Megri, A.C. (1993). Air flow modeling in multizone buildings equipped with a ventilation system. Prediction of pollutant transport. Doctoral thesis, Thermal Engineering Center, Department of Civil Engineering and Building, INSA, Lyon, France.

Megri, A.C., Achard, G., & Haghighat, F. (1999). Etude de la faisabilité de la ventilation accélérée pour le rafraîchissement des bâtiments tertiaires. Proceedings of the CIFQ, Montreal, Canada, pages 255-260.

Megri, A.C., Snyder, M., & Musy, M. (2005). Building zonal thermal and airflow—A review. International Journal of Ventilation, 4(2), 177–88.

Megri, A. C. (2007). Building load and energy simulation programs and the design process. International Journal of Ventilation, 6(2), 177-192.

Megri, A.C., & Haghighat, F. (2007). Zonal Modeling for Simulating Indoor Environment of Buildings: Review, Recent Developments, and Applications. HVAC&R Research, 13(6), 887-905.

Megri, A.C., & Yu, Y. (2010). New calibrated zonal model for temperature, pressure and airflow predictions. 10th REHVA WORLD CONGRESS Sustainable Energy Use in Buildings (Clima 2010), May 9-12, Antalya, Turkey.

Megri, A.C. (2010). An alternative procedure to recycling plastic waste for basement underground thermal insulation in cold climate buildings. The Journal of Solid Waste Technology and Management, 36(1), 44-53.

Megri, A.C., & Yu, Y. (2011). Prediction of Water Temperature of a Mantle Tank for Solar Domestic Hot Water Systems Using a New Zonal Model. 12th International conference on air distribution in rooms (ROOMVENT 2011), June 19-22, 2011, Trondheim, Norway.

Megri, A.C., Yu, Y., Zhang, Q., Denzer, A., & Puckett, J. (2011). Thermal comfort and energy analysis for the slab-on-grade floor and basement of a building. 12th International conference on air distribution in rooms (ROOMVENT 2011), June 19-22, 2011, Trondheim, Norway.

Megri, A.C., & Yu, Y. (2014). Energy Prediction of Electric Floor Radiation Systems Using a New Integrated Modeling Approach. ASHRAE Transactions, 120(1).

Milke, J. A. & Mowrer, F.W. (1995). Computer aided design for smoke management. ASHRAE Journal, 1995.

Moon, J.W., & Han, S.-H. (2011). Thermostat strategies impact on energy consumption in residential buildings. Energy and Buildings, 43 (2-3), 338-346.

Moore, T.C., & Ouzts, P. J. (2012). Zonal approach to modeling thermally stratified atria. Fifth National conference of IBPSA-USA, August 1-3, Madison, Wisconsin.

Mora, L. (2003). Prédiction des performances thermo-aérauliques des bâtiments par association de modèles de différents niveaux de finesse au sein d'un environnement orienté objet. Thèse de doctorat, Université de La Rochelle, La Rochelle, France.

Mora, L., Mendonça, K.C., Wurtz, E., & Inard, C. (2003a). Simspark: An object-oriented environment to predict coupled heat and mass transfers in buildings. Proceedings of the Building Simulation '03 Conference, Eindhoven, the Netherlands, pp. 903–10.

Mora, L., Gadgil, A.J., & Wurtz, E. (2003b). Comparing zonal and CFD model predictions of isothermal indoor airflows to experimental data. Indoor Air, 13(2), 77-85.

Mundt, E. (1992). Convection flows in rooms with temperature gradients – theory and measurements. Proc. Of the 3rd Internatinal conference on Air Distribution in Rooms. ROOMVENT’92, Aalborg.

Mundt, E. (1996). The performance of displacement ventilation systems—Experimental and theoretical studies. Doctoral thesis, Royal Institute of technology, Stockholm, Sweden.

Murakami, S., Kato, S., & Nakagawa, H. (1991). Numerical prediction of horizontal nonisothermal 3-d jet in room based on the k-ε model. ASHRAE Transaction, 97(1), 96-105.

Musy, M. (1999). Génération automatique de modeles zonaux pour l’étude du comportement thermo-aéraulique des baatiments. Doctoral thesis, University of La Rochelle, France.

Musy, M., Wurtz, E., Winkelmann, F., & Allard, F. (2001). Generation of a zonal model to simulate natural convection in a room with a radiative/convective heater. Building and Environment, 36(5), 589–96.

Musy, M., Winkelmann, F., Wurtz, E., & Sergent, A. (2002). Automatically generated zonal models for building airflow simulation: principles and applications. Building and Environment, 37, 873-881.

Ngendakumana, P. (1988). Modélisation simplifiés du comportement thermique d'un batiment et verification expérimantle. Thèse de doctorat, Université de Liège, France.

Nicol, F., & Roaf, S. (1996). Pioneering new indoor temperature standards: the Pakistan project. Energy and Buildings, 23, 169-174.

Nielsen, P. V. (1976). Flow in air conditioned rooms – Model experiments and numerical solution of the flow equations. English translation of Ph.D. Thesis, Technical University of Denmark, Copenhagen.

Nielsen, P. V. (1980). The influence of ceiling-mounted obstacles on the air flow pattern in air-conditioned rooms at different heat loads. Building Service Engineering Research & Technology, 1(4).

Nielsen, P.V. (1983). Air diffusion in rooms with ceiling-mounted obstacles and two-dimensional isothermal flow. 16th International Congress of Refrigeration, Commission E1, Paris.

Nielsen, P. V., Evensen, L., Grabau, P., & Thulesen-Dahl, J. H. (1987). Air distribution in rooms with ceiling-mounted obstacles and three-dimensional isothermal flow. ROOMVENT'87, International Conference on Air Distribution in Ventilated Spaces, Stockholm.

Nielsen, P. V., & Moller, A.T.A. (1985). Measurements of the three-dimensional wall jet from different types of air diffusers. Clima 2000, Copenhagen.

Nielsen, P.V., & Moller, A.T.A. (1987). Measurements on buoyant wall jet flows in air-conditioned rooms. ROOMVENT'87, International Conference on Air Distribution in Ventilated Spaces, Stockholm.

Nielsen, P.V., & Moller, A.T.A. (1988). Measurements on buoyant jet flows from a ceiling mounted slot diffuser. Proc. Of the 3rd Seminar on Application of Fluid Mechanics in Environmental Protection – 88, Silesian Technical University.

Norrefeldt, V., Grun, G., & Sedlbauer, K. (2012). VEPZO – Velocity propagating zonal model for the estimation of the airflow pattern and temperature distribution in a confined space. Building and Environment, 48, 183-194.

Pan, Y., Li, Y., Huang, Z., & Wu, G. (2010). Study on simulation methods of atrium building cooling load in hot and humid regions, Energy and Buildings, 42(10), 1654-1660.

Phoenics. (2010). Phoenics-VR Reference Guide. CHAM.

Popiolek, Z. (1996). Air volume flux in buoyant plumes. Silesian Technical University, Gliwice, Poland.

Press, W.H., Teukolsky, S. A., Vetterling, W. T. and Flannery, B. P. (2007). Numerical Recipes, the art of scientific computing. Third edition. Cambridge Uni-versity Press.

Rajaratnam, N. (1976). Turbulent jets. Elsevier, Amsterdam.

Rees, S.J. (1998). Modeling of displacement ventilation and chilled ceiling systems using nodal models. Doctoral thesis, Loughborough University, Leicestershire, UK.

Rees S.J., & Haves, P. (1999). A nodal model for displacement ventilation and chilled ceiling systems. Proceedings of Building Simulation '99, Kyoto, Japan, pp. 433–40.

Ren, Z., & Stewart, J. (2003). Simulating air flow and temperature distribution inside buildings using a modified version of COMIS with sub-zonal divisions. Energy and Buildings, 35, 257–71.

Ren, Z., & Stewart, J. (2005). Prediction of personal exposure to contaminant sources in industrial buildings using a sub-zonal model. Environmental modeling and software, 20(5), 623-638.

Riederer, P., Marchio, D., Visier, J.C., Husaunndee, A. & Lahrech, R. (2002). Room thermal modelling adapted to the test of HVAC control systems. Building and Environment, 37(8-9), 777-790.

Riederer, P., & Dexter, A. L. (2003). Effect of room modeling and sensor position on performance assessment of variable air volume control systems, Building Serv. Eng. Technol., 24(1), 9-24.

Schiavon, S., Lee, K.H., Bauman, F., & Webster, T. (2010). Influence of raised floor on zone design cooling load in commercial buildings. Energy and Buildings, 42 (8), 1182-91.

Schiavon, S., Lee, K. H., Bauman, F., & Webster, T. (2011). Simplified calculation method for design cooling loads in underfloor air distribution (UFAD) systems. Energy and Building, 43, 517–528.

Seem, J.E. (1987). Modeling of heat in buildings. Ph. D. thesis, Solar Energy Laboratory, University of Wisconsin Madison.

Skåret, E. (1976). Air movement in ventilated rooms (in Norwegian). Institute for VVS, Technical University of Norway, Trondheim.

Skåret, E. (1986). Ventilation by displacement – Characterization and design implications. Ventilatin'85, edited by H. D. Goodfellow, Elsevier Science Publishers B.V., Amsterdam.

Song, Z., Murray, B.T., & Sammakia, Bahgat (2013). A compact thermal model for data center analysis using the zonal method. Numerical Heat Transfer, Part A: Applications: An International Journal of Computation and Methodologh, 64(5), 361-377.

Star-CD. (2005). Star-CD User Guide version 3.26. Star-CD adapco.

Steskens, P.W.M.H., Janssen, H., & Rode, C. (2013). Evaluation of sub zonal air flow models for the prediction of local interior boundary conditions natural and forced convection cases. Indoor and Built Environment, 22(2), 395-409.

Stewart, J., & Ren, Z. (2003). Prediction of indoor gaseous pollutant dispersion by nesting sub-zones within a multizone model. Building and Environment. 38(5), 635–43.

Stewart, J., & Ren, Z. (2006). COwZ—A sub-zonal indoor airflow, temperature and contaminant dispersion model. Building and Environment, 41(12), 1631–48.

Tan, G., and Glicksman, L. R. (2005). Application of integrating multi-zone model with CFD simulation to natural ventilation prediction. Energy and Buildings, 37, 1049-1057.

Togari, S., Arai, Y., & Miura, K. (1993). A simplified model for predicting vertical temperature distribution in a large space, ASHRAE Transactions, 99 (1), 84 – 99.

Trace 700. (2010). Building energy and Economic Analysis User's Manual, Version 6.2. Trane.

TRNSYS. (2000). A transient system simulation program, Software manual, Solar Energy Laboratory, University of Wisconsin-Madison.

U.S. Department of Energy (DOE). (2012). 2011 Buildings Energy Data Book. Prepared for the Building Technologies Program of Energy Efficiency and Renewable Energy by D&R International, Ltd., March, 2012.

Vialle, P., & Blay, D. (1996). Decay laws in the case of 3D vertical free jets with positive buoyancy. ROOMVENT'96, Yokohama, July 17-19, Japan.

Wan, J.W., Yang, K., Zhang, W.J., & Zhang, J.L. (2009). A new method of determination of indoor temperature and relative humidity with consideration of human thermal comfort. Building and Environment, 44 (2), 411-417.

Watkins, D. S. (2010). Fundamentals of Matrix Computations. Third edition. A John Wiley & Sons, Inc.

Wurtz, E. (1995). Modélisation tridimensionnelle des transferts thermiques et aérauliques dans le bâtiment en environnement oriente objet. Doctoral thesis, Ecole Nationale des Ponts et Chausses, Marne-la-Vallée, France.

Wurtz, E., Musy, M., & Mora, L. (1999a). Description des écoulements d'air dans un local a l'aide de la méthode zonale: Influence de panache, jets d'air et couches limite. Proceedings of the IV Colloque Inter-Universitaire Franco-Québécois, Montréal, Canada.

Wurtz, E., Nataf, J. M., & Winkelmann, F. (1999b). Two-and three-dimensional natural and mixed convection simulation using modular zonal models in building. Int. J. Heat and mass transfer, 42, 923-940.

Wurtz, E., Mora, L., & Inard, C. (2006a). An equation-based simulation environment to investigate fast building simulation. Building and Environment, 41(11), 1571–83.

Wurtz, E., Haghighat, F., Mora, L. Mendonca, K.C., Zhao, H., Maalouf, C., & Bourdoukan, P. (2006b). An integrated zonal model to predict transient indoor humidity distribution. ASHRAE Transactions, 12(2), 175-186.

Yang, L., Xu, P., & Li, Y. (2006). Nonlinear dynamic analysis of natural ventilation in a two-zone building part A – theoretical analysis. HVAC&R, 12(2), 231-255.

Yu, Y. (2012). Zonal modeling approach and its applications in buildings, Master thesis, Department of Civil and Architectural engineering, University of Wyoming, USA, December, 2012.

Yu, Y. & Megri, A.C. (2011). Development and Application of a new Dynamic Zonal model (POMA+). 12th International conference on air distribution in rooms (ROOMVENT 2011), June 19-22, Trondheim, Norway.

Zhai, Z., Chen, Q., Haves, P., & Klems, J. H. (2002). On approaches to couple energy simulation and computational fluid dynamics programs. Building and Environment, 37(8-9), 857-864.

Zhai, Z., & Chen, Q. (2003). Solution characters of iterative coupling between energy simulation and CFD programs. Energy and Buildings, 35(5), 493-505.

Zhai, Z., & Chen, Q. (2005). Performance of coupled building energy and CFD simulations. Building and Environment, 37, 333-344.

Zhai, Z., & Chen, Q. (2006). Sensitivity analysis and application guides for integrated building energy and CFD simulation. Energy and Buildings, 38, 1060-1068.

Zhang, L., Zhang, C., & Martinuzzi, R. (2007). Numerical modeling of energy consumption in a typical residential building, Computational in modern science and engineering,

proceedings of the international conference on computational methods in science and engineering 2007, 2(B), 1417-1420.